The influence of sea ice on Antarctic ice core sulfur chemistry and on the future evolution of Arctic snow depth: Investigations using global models

Paul J. Hezel

A dissertation
submitted in partial fulfillment of the
requirements for the degree of

Doctor of Philosophy

University of Washington

2012

Reading Committee:

Cecilia M. Bitz, Chair

Becky Alexander, Chair

Eric J. Steig

Program Authorized to Offer Degree:
Department of Atmospheric Sciences

University of Washington

Abstract

The influence of sea ice
on Antarctic ice core sulfur chemistry and
on the future evolution of Arctic snow depth:
Investigations using global models

Paul J. Hezel

Co-Chairs of the Supervisory Committee:
Associate Professor Cecilia M. Bitz
Department of Atmospheric Sciences

Assistant Professor Becky Alexander
Department of Atmospheric Sciences

Observational studies have examined the relationship between methanesulfonic acid (MSA) measured in Antarctic ice cores and sea ice extent measured by satellites with the aim of producing a proxy for past sea ice extent. MSA is an oxidation product of dimethylsulfide (DMS) and is potentially linked to sea ice based on observations of very high surface seawater DMS in the sea ice zone. Using a global chemical transport model, we present the first modeling study that specifically examines this relationship on interannual and on glacial-interglacial time scales. On interannual time scales, the model shows no robust relationship between MSA deposited in Antarctica and sea ice extent. We show that lifetimes of MSA and DMS are longer in the high latitudes than in the global mean, interannual variability of sea ice is small (<25%) as a fraction of sea ice area, and sea ice determines only a fraction of the variability (<30%) of DMS emissions from the ocean surface. A potentially larger fraction of the variability in DMS emissions is determined by surface wind speed (up to 46%) via the parameterization for ocean-to-atmosphere gas exchange. Furthermore, we find that a significant fraction (up to 74%) of MSA deposited in Antarctica originates from north of 60°S, north of the seasonal sea ice zone.

We then examine the deposition of MSA and non-sea-salt sulfate ($\mathrm{nssSO_4^{2-}}$) on glacial-

interglacial time scales. Ice core observations on the East Antarctic Plateau suggest that MSA increases much more than nssSO_4^{2-} during the last glacial maximum (LGM) compared to the modern period. It has been suggested that high MSA during the LGM is indicative of higher primary productivity and DMS emissions in the LGM compared to the modern day. Studies have also shown that MSA is subject to post-depositional volatilization, especially during the modern period. Using the same chemical transport model driven by meteorology from a global climate model, we examine the sensitivity of MSA and nssSO_4^{2-} deposition to differences between the modern and LGM climates, including sea ice extent, sea surface temperatures, oxidant concentrations, and meteorological conditions. We are unable to find a mechanism whereby MSA deposition fluxes are higher than nssSO_4^{2-} deposition fluxes on the East Antarctic Plateau in the LGM compared the modern period. We conclude that the observed differences between MSA and nssSO_4^{2-} on glacial-interglacial time scales are due to post-depositional processes that affect the ice core MSA concentrations. We can not rule out the possibility of increased DMS emissions in the LGM compared to the modern day. If oceanic DMS production and ocean-to-air fluxes in the sea ice zone are significantly enhanced by the presence of sea ice as indicated by observations, we suggest that the potentially larger amplitude of the seasonal cycle in sea ice extent in the LGM implies a more important role for sea ice in modulating the sulfur cycle during the LGM compared to the modern period.

We then shift our focus to study the evolution of snow depth on sea ice in global climate model simulations of the 20th and 21st centuries from the Coupled Model Intercomparison Project 5 (CMIP5). Two competing processes, decreasing sea ice extent and increasing precipitation, will affect snow accumulation on sea ice in the future, and it is not known *a priori* which will dominate. The decline in Arctic sea ice extent is a well-studied problem in future scenarios of climate change. Moisture convergence into the Arctic is also expected to increase in a warmer world, which may result in increasing snowfall rates. We show that the accumulated snow depth on sea ice in the spring declines as a result of decreased ice extent in the early autumn, in spite of increased winter snowfall rates. The ringed seal

(*Phoca hispida*) depends on accumulated snow in the spring to build subnivean birth lairs, and provides one of the motivations for this study. Using an empirical threshold of 20 cm of snow depth on level sea ice for ringed seal lair success, we estimate a decline of potential ringed seal habitat of nearly 70%.

TABLE OF CONTENTS

Page

List of Figures iii

List of Tables v

Chapter 1: Introduction 1
1.1 Investigations of MSA and non-sea-salt sulfate deposition in Antarctica on multiple time scales 1
1.2 Snow depth on Arctic sea ice 4
1.3 Summary of published work 5

Chapter 2: Modeled methanesulfonic acid (MSA) deposition in Antarctica and its relationship to sea ice 6
2.1 Introduction 7
2.2 Model Description and Methods 9
2.3 Model evaluation 20
2.4 Results 29
2.5 Conclusions 42

Chapter 3: Modeled modern versus LGM non-sea-salt sulfate and methanesulfonic acid (MSA) deposition in Antarctica 45
3.1 Introduction 46
3.2 Model description and methods 47
3.3 Results and Discussion 50
3.4 Conclusions 58

Chapter 4: Projected decline in spring snow depth on Arctic sea ice caused by progressively later autumn open ocean freeze-up this century 60
4.1 Introduction 61
4.2 Methods and Validation 62
4.3 Results 65

4.4 Discussion and Conclusions 70
4.5 Auxiliary Figures 73

Chapter 5: Conclusions 77
5.1 DMS emissions from the sea ice 77
5.2 DMS oxidation and influence of halogens 80
5.3 Wet and dry deposition in the polar regions 80
5.4 Snow depths on sea ice 81

LIST OF FIGURES

Figure Number Page

2.1 January surface DMS concentrations and January climotological DMS emissions fluxes. . . . 12
2.2 Mean annual precipitation rate in Antarctica. . . . 16
2.3 Illustration of seawater DMS concentrations applied in the sea ice zone. . . . 17
2.4 Annual cycle of atmospheric MSA, nssSO_4^{2-} and DMS concentrations at DDU. 24
2.5 Annual cycle of DMS concentrations at the surface at Cape Grim and Amsterdam Island. . . . 26
2.6 Mean MSA deposition flux in Antarctica. . . . 27
2.7 Mean MSA snow concentration in Antarctica. . . . 28
2.8 Correlation coefficients between sea ice extent for each point around the Antarctic continent and MSA snow concentration and deposition fluxes. . . . 30
2.9 DMS emissions and sulfur deposition by latitude from the difference between uncapped and capped runs. . . . 33
2.10 MSA snow concentration from DMS emissions in the sea ice zone. . . . 34
2.11 Correlation of DMS emissions to sea ice extent and wind speeds in the capped runs. . . . 38
2.12 Correlation of DMS emissions to sea ice extent and wind speeds for the difference between the uncapped and capped runs. . . . 38

3.1 MSA and nssSO_4^{2-} snow concentrations in observations and models on the East Antarctic Plateau. . . . 51
3.2 MSA and nssSO_4^{2-} deposition fluxes in observations and models on the East Antarctic Plateau. . . . 52
3.3 Precipitation on the East Antarctic Plateau. . . . 53

4.1 Multi-model mean April snow depth on sea ice. . . . 65
4.2 Time series of April snow depth averaged north of 70°N on sea ice and PDF of snow depth distributions. . . . 66
4.3 Time series of multi-model mean November-March total precipitation and snowfall. . . . 68
4.4 Multi-model mean climatology of snowfall, snow depth and sea ice area. . . . 69

4.5 Time series of multi-model mean snow depth for all models. 73
4.6 Mean April snow depth versus global annual mean temperature and mean april snow depth versus sea ice area, for each model. 74
4.7 Mean snow depth on sea ice (1981-2000) for each model. 75
4.8 Mean snow depth on sea ice (2081-2100) for each model. 76
4.9 Climatology of snowfall and rainfall, snow depth, and ice area for each model. 78

LIST OF TABLES

Table Number Page

2.1 Summary of simulations and sensitivity simulations discussed in the text. . . 19

2.2 Annual global sulfur budget for Simó and Dachs capped run compared to global sulfur budgets summarized in other studies. 22

2.3 Total DMS emissions for south of 60°S and total MSA deposition to Antarctica. 32

3.1 Climate scenarios and boundary conditions used in this study. 48

4.1 Models used in snow depth on sea ice study. 63

ACKNOWLEDGMENTS

I would especially like to thank my advisors, Cecilia Bitz, Becky Alexander, and Eric Steig. Cecilia first took me on board as staff and then as a student, never wavered in her confidence in my abilities, and has taught me to ask solid scientific questions. I appreciate her attention to details, especially with respect to writing and communication. Becky sets a great example of how to focus on the important questions, and is a model of efficiency in getting things completed. Eric stands out as a wellspring of ideas and enthusiasm. I consider myself extremely lucky to have had their scientific guidance, support, and friendship right from the original conception of this project. I would also like to thank Tom Ackerman for his support on my committee, and Rebecca Woodgate for her support and encouragement throughout as well as for serving as my GSR.

I owe thanks to many colleagues and friends at the UW. I would especially like to thank Kelly McCusker, Kyle Armour, Eric Sofen, Maria Zatko, Louise Leahy, Brian Smoliak and Jimmy Booth as well as the rest of the Bitz and Alexander groups. It has been a pleasure and a very humbling experience to be a part of the research community here.

My family deserves many thanks for their support throughout this endeavor. I would also like to recognize my extended family in Seattle – they are too many to list here. Ben and Jenny and Laura and Drew have given me a place to call home over the last several years, and to them I am deeply indebted. Finally, I am grateful for the kids on 21st Avenue, Oscar, Andy, Aubin, and Mateo, who have made it impossible to arrive home without a smile on my face.

DEDICATION

This work is dedicated to my mom, who has asked me
when I would be getting a Ph.D. for as long as I can remember.

Chapter 1

INTRODUCTION

Sea ice plays a significant role in the climate system, especially with respect to its albedo and associated radiative properties. The presence or absence of ice in the high latitudes provides an important feedback to the climate system on multiple time scales, from seasonal and interannual to glacial-interglacial time scales. Our understanding of the magnitude of these feedbacks is generally derived from global climate model (GCM) simulations. In glacial climate states, simulations of sea ice extent vary substantially, especially in the summer months [*Braconnot et al.*, 2007a; *Otto-Bliesner et al.*, 2007]. Given the importance of sea ice in the modern climate and the uncertainty about how it will change in the 21st century, we look to proxies for sea ice to better understand and constrain its role in the climate system on multiple time scales. Of several proxies that have been investigated for sea ice — methanesulfonic acid (MSA) [e.g., *Curran et al.*, 2003], sea salt [*Wolff et al.*, 2003], and sediment cores of diatoms and foraminifera [*de Vernal et al.*, 2005; *Gersonde et al.*, 2005] — a reliable indicator of ice extent on large spatial scales has thus far proven elusive.

1.1 Investigations of MSA and non-sea-salt sulfate deposition in Antarctica on multiple time scales

Methanesulfonic acid (MSA) is one of the potential sea ice proxies and is the subject of the first part of this dissertation. MSA in ice cores from Antarctica has been investigated for its potential as an indicator of sea ice extent over the past several decades. MSA is an oxidation product of dimethylsulfide (DMS), which is produced by phytoplankton throughout the worlds oceans, but with high seawater concentrations in or near the sea ice zone [e.g., *Trevena and Jones*, 2006]. *Curran et al.* [2003] showed a convincing correlation of winter ice exent in coastal East Antarctica with MSA concentrations at Law Dome (66°46'S 112°48'E 1370 m ASL) using satellite observations of ice extent. They conclude that ice extent has declined in this region since the 1950s. Other studies, however, do not agree

on the sign of the relationship between MSA and sea ice extent on interannual time scales [*Pasteur et al.*, 1995; *Sun et al.*, 2002; *Abram et al.*, 2007, 2010]. On longer timescales, it has been suggested that high MSA concentrations from the East Antarctic Plateau are indicative of greater dimethylsulfide (DMS) and/or primary productivity during the last glacial maximaum (LGM) compared to the modern day [*Legrand et al.*, 1991]. It has since been shown that post-depositional effects likely modify MSA deposition [*Wagnon et al.*, 1999; *Weller et al.*, 2004].

In the first part of this dissertation (Chapters 2 and 3), we investigate the relationships between DMS emissions, MSA and non-sea-salt sulfate ($\mathrm{nssSO_4^{2-}}$) deposition, and sea ice extent in a global chemical transport model to better understand the relationships shown in the observational literature. In Chapter 2, we investigate the variability of MSA deposition on interannual timescales for the modern period. Using meteorology from the GEOS Data Assimilation System (DAS) to force the GEOS-Chem chemical transport model over the period 1985-2003, we are unable to find a robust relationship in the model between MSA and sea ice extent similar to that characterized in the observational literature. The interannual variability in sea ice extent is small as a percentage of the total ice area, and the lifetimes of DMS and MSA in the high latitudes are longer than the global mean lifetimes. We also find that the net transport of DMS-derived sulfur species is northward from the sea ice zone. The model does produce correlations of MSA with sea ice extent of the magnitude found in the observational literature, though these correlations are not governed by the association of DMS emissions and sea ice.

In Chapter 3, we investigate the deposition of MSA and $\mathrm{nssSO_4^{2-}}$ in Antarctica on glacial-interglacial time scales. It had been suggested that the large glacial-interglacial variation in MSA was indicative of increased primary productivity (and hence DMS production) in the glacial periods [*Legrand et al.*, 1991]. The observations also suggest that the glacial-interglacial variation of MSA on the East Antarctic Plateau was of the the opposite sign of ice core sites closer to the coast. It has since been shown, however, that MSA deposition in low accumulation environments such as the East Antarctic Plateau ($\sim$25-30 kg $\mathrm{m^{-2}y^{-1}}$) are subject to the post-depositional loss through volatility [*Wagnon et al.*, 1999; *Weller et al.*, 2004]. This process does not affect $\mathrm{nssSO_4^{2-}}$[*Silvente and Legrand*, 1993]. Dust fluxes to the

East Antarctic Plateau in the LGM (∼25-30 times higher in the LGM than modern day [*Fischer et al.*, 2007]) likely reduces the volatility of MSA during this period.

In a series of GEOS-Chem experiments forced with meteorology from the GISS-ModelE global climate model (GCM), we explore both MSA and nssSO_4^{2-} deposition to the East Antarctic Plateau in comparison to ice core observations. We seek to understand two primary questions: (1) How does the glacial–interglacial variation in MSA and nssSO_4^{2-} depend on the assumed DMS emissions from the sea ice zone, especially if the LGM summer sea ice extent is much larger than the modern day? (2) How strongly do climate variations between modern day and LGM affect the deposition of MSA and nssSO_4^{2-}? We search in particular for a mechanism in the model that contributes to a different glacial-interglacial response in MSA than in nssSO_4^{2-}, namely one which causes higher MSA deposition flux in the glacial period than the modern day, while keeping nssSO_4^{2-} deposition flux to remain similar to the modern day.

We explore the first question in a series of capped and uncapped DMS emissions scenarios, where the DMS emissions are restricted and unrestricted respectively by the presence of sea ice for the duration of the austral summer (October through March). On the East Antarctic Plateau, we can only reproduce the sign of the glacial-interglacial variation in snow concentration of either MSA or nssSO_4^{2-} when we allow DMS emissions from within the sea ice itself. This result is consistent with more recent sea ice and SST reconstructions that indicate the Southern Ocean sea ice extent is lower than in the sea ice and SST reconstructions used in the GCM simulations [*Gersonde et al.*, 2005].

For the second question, we assume that DMS emissions are roughly the same in the glacial and interglacial periods. We examine the response in MSA and nssSO_4^{2-} deposition fluxes as a response to glacial-interglacial differences in ocean surface wind speeds and sea surface temperatures (SSTs) (both of which affect DMS emissions), temperature of DMS oxidation, cloudwater pH, precipitation, and oxidation mechanism. We find no mechanism in the model that causes the observed differences in MSA and nss$SO_4^{2-}$from the glacial to the interglacial climates. With small variation, both MSA and nssSO_4^{2-} have nearly the same response in the model to our imposed climate scenarios. We conclude that the observed glacial-interglacial variations in MSA are primarily the result of the post-depositional

processes that occur on the East Antarctic Plateau in the modern period. The differences in post-depositional loss of MSA between the glacial and interglacial periods make it difficult if not impossible to interpret MSA as an indicator of changes in sea ice or in biological activity on these time scales.

1.2 Snow depth on Arctic sea ice

Snow on sea ice plays a fundamental role in the seasonal evolution of the sea ice and its sensitivity to climate change. Accumulated snow on sea ice also represents an important habitat for ringed seal (*Phoca hispida*) in the Arctic. The National Marine Fisheries Service (NMFS), under the National Oceanic and Atmospheric Administration (NOAA), prepared an assessment [*Kelly et al.*, 2010] of the present and future habitat of the ringed seal in response to a petition for listing ringed seals under the Endangered Species Act (ESA, 16 U.S.C. §1531 et seq. (1973)). NMFS proposed to list the species as threatened in December 2010 (75 FR 77476, December 10, 2010), and a final decision is pending as of the publication of this thesis in August 2012. The fate of snow on sea ice in the 21st century, with a specific focus on how it could influence ringed seal habitat, is the subject of Chapter 4.

Since the release of the NMFS status report on the ringed seal, the Coupled Model Intercomparison Project 5 (CMIP5) [*Taylor et al.*, 2012a] data have become available, which for the first time includes snow depth accumulated on sea ice as one of the archived variables. We use CMIP5 data to examine the change in snow depth over the course of the 20th and 21st century in the historical simulations combined with Representative Concentration Pathway (RCP) 2.6, 4.5, and 8.5 simulations for 10 of the models. Atmospheric specific humidity increases with warming temperatures according to the Clausius-Clapeyron equation. There is net convergence of moisture into the Arctic [*Cullather et al.*, 2000; *Bengtsson et al.*, 2011] and hence precipitation is expected to increase with global warming.

At the same time, sea ice extent in the Arctic is declining rapidly [*Kwok and Rothrock*, 2009; *Comiso et al.*, 2008]. It is not known *a priori* whether the decline in sea ice or the increase in precipitation and snowfall will be the dominant driver of changes in snow accumulation by the end of the 21st century. The CMIP5 models demonstrate that it is the decline in sea ice, specifically later autumn freeze-up and the reduction in area that

accumulates autumn and early winter snow, that drives the decline in snow depth at the end of the boreal winter before the onset of spring ice melt.

1.3 Summary of published work

Chapters 2 and 4 have been published in the *Journal of Geophysical Research-Atmospheres* [*Hezel et al.*, 2011] and *Geophysical Research Letters* [*Hezel et al.*, 2012], respectively, and should be referenced directly. Chapter 3 is in preparation for submission to *Geophysical Research Letters*. Chapter 5 summarizes the open questions related to this dissertation.

Chapter 2

MODELED METHANESULFONIC ACID (MSA) DEPOSITION IN ANTARCTICA AND ITS RELATIONSHIP TO SEA ICE

This chapter is published as an article in the *Journal of Geophysical Research-Atmospheres*, and is reproduced here by permission of the American Geophysical Union.

Hezel, P. J., B. Alexander, C. M. Bitz, E. J. Steig, C. D. Holmes, X. Yang, and J. Sciare (2011), Modeled methanesulfonic acid (MSA) deposition in Antarctica and its relationship to sea ice, *J. Geophys. Res.*, 116, D23214, doi:10.1029/2011JD016383.

Abstract

Methanesulfonic acid (MSA) has previously been measured in ice cores in Antarctica as a proxy for sea ice extent and Southern Hemisphere circulation. In a series of chemical transport model (GEOS-Chem) sensitivity experiments, we identify mechanisms that control the MSA concentrations recorded in ice cores. Sea ice is linked to MSA via dimethylsulfide (DMS), which is produced biologically in the surface ocean and known to be particularly concentrated in the sea ice zone. Given existing ocean surface DMS concentration datasets, the model does not demonstrate a strong relationship between sea ice and MSA deposition in Antarctica. The variability of DMS emissions associated with sea ice extent is small (11-30%) due to the small interannual variability of sea ice extent. Wind plays a role in the variability in DMS emissions, but its contribution relative to that of sea ice is strongly dependent on the assumed DMS concentrations in the sea ice zone. Atmospheric sulfur emitted as DMS from the sea ice undergoes net transport northward. Our model runs suggest that DMS emissions from the sea ice zone may account for 26-62% of MSA deposition at the Antarctic coast and 36-95% in inland Antarctica. Though our results are sensitive to model assumptions, it is clear that an improved understanding of both DMS concentrations and emissions from the sea ice zone are required to better assess the impact of sea ice variability on MSA deposition to Antarctica.

2.1 Introduction

Methanesulfonic acid (MSA) concentrations in Antarctic ice cores are thought to be influenced by the distribution of nearby sea ice and have therefore been investigated with the goal of producing a proxy for sea ice cover in past climates [*Saigne and Legrand*, 1987; *Legrand and Feniet-Saigne*, 1991; *Welch et al.*, 1993; *Curran et al.*, 2003; *Abram et al.*, 2007; *Mayewski et al.*, 2009]. MSA is one of several oxidation products of dimethylsulfide (DMS), which originates in the atmosphere from biological production in the surface ocean. Observations demonstrate particularly high DMS concentrations in surface seawater in the seasonal sea ice zone around Antarctica throughout the austral spring and summer [e.g., *Kettle et al.*, 1999; *Tortell and Long*, 2009; *Gabric et al.*, 2005; *Jones et al.*, 2010]. This observed relationship constitutes the basis of the proposed link between sea ice and MSA deposition on the Antarctic continent.

MSA concentrations in ice cores from various locations in Antarctica have shown inconsistent relationships with satellite observations of sea ice extent. Positive correlations of MSA with nearby sea ice extent have been reported by *Welch et al.* [1993], *Curran et al.* [2003], *Foster et al.* [2006], and *Abram et al.* [2010], with years of greater sea ice extent inducing larger areas of high DMS production and thereby increasing MSA concentrations in the ice core record. Using three ice cores from the Weddell Sea region, *Abram et al.* [2007] found negative correlations of MSA with sea ice extent in the Weddell Sea and positive correlations of MSA with sea ice extent to the west in the Bellingshausen Sea. *Pasteur et al.* [1995] and *Sun et al.* [2002] found negative correlations of MSA with sea ice extent at Dolleman Island and on the Lambert Glacier respectively.

The observational literature has not yet established which processes govern MSA deposition in Antarctica and the spatial extent over which such relationships hold. In addition to sea ice, MSA concentrations have also been linked to changes in atmospheric circulation [e.g., *Becagli et al.*, 2009; *Fundel et al.*, 2006]. The extent to which MSA is influenced by sea ice compared to atmospheric circulation may be regionally dependent. Recent studies have questioned whether sea ice plays a significant role in measured atmospheric MSA concentrations at all. *Preunkert et al.* [2007] found that atmospheric concentrations of high

DMS coincided with high MSA at Dumont D'Urville (DDU) (140°1'E, 66°40'S) on short timescales (days) and was related to simultaneous high regional chlorophyll-*a* measured by satellite, though they concluded that a relationship to sea ice was not straightforward. *Weller et al.* [2011] compared atmospheric measurements of MSA and non-sea-salt sulfate ($\mathrm{nssSO_4^{2-}}$) at Neumayer station (8°15'W, 70°39'S) and found no significant relationship between these and sea ice extent or any other other climate indicators.

Nearly all of the MSA-sea ice proxy studies have compared observed MSA concentrations in ice cores from point locations in Antarctica to satellite observations of sea ice extent around the continent. In this study, we use a chemical transport model to examine some of the spatial characteristics of the link between MSA and sea ice extent. The experiments were designed to understand the impact of DMS emissions from the sea ice zone on MSA deposition patterns in Antarctica, since modeling studies of the sulfur cycle have neglected this important regional source [e.g., *Cosme et al.*, 2002]. Though this sulfur source is important to understand, more fundamental characteristics of DMS emissions and MSA deposition in the high latitudes also emerge as a compelling story. In a series of model simulations with the chemical transport model GEOS-Chem [*Bey et al.*, 2001] (http://geos-chem.org), we explore the sensitivity of MSA deposition in Antarctica to modification of DMS emissions from the sea ice itself. We find that the estimates of seawater DMS emissions play a prominent role in determining whether Antarctic sulfur deposition is dominated by DMS emissions from the sea ice zone or by southward transport of sulfur emissions from lower latitudes. We fail to find credible correlations between sea ice extent and MSA deposition in Antarctica within the model given reasonable estimates of the influence of sea ice on DMS surface concentrations. Interannual variability of DMS emissions in the model, and hence interannual variability of MSA deposition, is not strongly influenced by variability in sea ice extent.

2.2 Model Description and Methods

2.2.1 Background to model simulations

Previous global sulfur cycle modeling studies 'cap' DMS emissions in the presence of sea ice [e.g., *Chin et al.*, 2000; *Cosme et al.*, 2002], which assumes that sea ice prevents gas exchange from the ocean, even from water among sea ice floes. Though these studies broadly capture features of the Antarctic regional sulfur cycle including atmospheric concentrations, seasonal cycles, and spatial gradients in deposition fluxes [*Chin et al.*, 2000; *Cosme et al.*, 2002, 2005; *Gondwe et al.*, 2004; *Castebrunet et al.*, 2006], estimates of MSA and nssSO_4^{2-} deposition to the Antarctic continent miss this important regional source. Surface seawater DMS concentrations are typically prescribed from a climatology [e.g., *Kettle et al.*, 1999; *Simo and Dachs*, 2002; *Lana et al.*, 2011], with ocean-to-air gas exchange fluxes parameterized based on empirical relationships with wind speed and SST [e.g., *Liss and Merlivat*, 1986; *Wanninkhof*, 1992; *Nightingale et al.*, 2000; *Huebert et al.*, 2010].

Current understanding of both sea ice biology and gas exchange processes suggests that there may be multiple ways in which the DMS source to the atmosphere is enhanced by the presence of sea ice [*Levasseur et al.*, 1994]. Certain high DMS-producing species, including *Phaeocystis sp.*, are prevalent in Southern Ocean waters, including the sea ice zone [*Malin and Kirst*, 1997]. Melting sea ice is thought to release nutrients that stimulate a phytoplankton bloom near the ice edge [*Curran et al.*, 2003, and references therein]. Algal communities within sea ice brine pockets [*Delille et al.*, 2007] may release dimethylsulfoniopropionate (DMSP), a DMS precursor, to the water column; DMSP is then converted to DMS by enzymatic cleavage of DMSP via bacterial consumption. DMS has also been measured in pore spaces among snow crystals on sea ice [*Zemmelink et al.*, 2008], suggesting DMS may pass from ice to the atmosphere, and possibly from the water column through the ice as a result of direct gas exchange [*Gosink et al.*, 1976; *Semiletov et al.*, 2004]. Measurements of gas exchange of oxygen and sulfur hexafluoride through laboratory sea ice suggest that diffusion of gases through sea ice is much smaller than gas transfer to the atmosphere through open water leads, even when the fraction of open water is less than 1% of the ice area [*Loose et al.*, 2011].

We use the GEOS-Chem model version v8-01-03 for our study, at a horizontal resolution of 2° latitude by 2.5° longitude and vertical resolution of 30 hybrid pressure-sigma levels. GEOS-Chem is a global 3-D chemical transport model [*Bey et al.*, 2001], driven by GEOS-4 meteorological fields from the Goddard Earth Observing System of the NASA Global Modeling and Assimilation Office [*Bloom et al.*, 2005]. The input meteorological fields are 3-hour averages for surface fields, 6-hour averages for upper level fields, and 6-hour instantaneous fields for sea level and surface pressures and ice extent. Meteorological fields are originally computed at a resolution of 1° latitude x 1.25° longitude, 55 vertical hybrid sigma levels, and degraded to the GEOS-Chem model resolution. We use the offline-aerosol version of GEOS-Chem, described in *Park et al.* [2004], which uses monthly mean oxidant concentrations from a full-chemistry simulation. The set of simulations are described at the end of this section, and each was begun after a 1.5 year spinup of the chemistry model.

2.2.2 Sea ice and sea surface temperature

Sea ice extent and sea surface temperatures (SSTs) are specified from NOAA Optimum Interpolation (OI v.2) weekly fields [*Reynolds et al.*, 2002], interpolated to 6-hour instantaneous fields at 1°x1° resolution. Sea ice in GEOS-Chem is a binary field (the ocean fraction of a grid cell is either all ice or ice free) on the model grid. When the OI v.2 is degraded to 2°x2.5° resolution, a grid cell is designated 'ice' if more than 50% of the area is covered with ice concentration of 15% or greater.

2.2.3 Ocean-to-air DMS emissions and surface seawater DMS concentrations

Atmospheric DMS emissions from seawater are parameterized using a climatology of surface seawater DMS concentrations [*Simo and Dachs*, 2002; *Kettle et al.*, 1999; *Lana et al.*, 2011] combined with a sea-to-air transfer velocity computed as a function of instantaneous 10-meter wind speed and SST [*Nightingale et al.*, 2000; *Huebert et al.*, 2010].

The *Nightingale et al.* [2000] parameterization is used primarily in our simulations and specifies a quadratic dependence on wind speed, which implies more efficient gas transfer at higher wind speeds than the linear dependence specified in the widely-used *Liss and*

Merlivat [1986] parameterization. Recent measurements, however, suggest that the DMS sea-to-air transfer velocity at medium wind speeds (4-12 m s^{-1}) is at best described by a linear dependence on wind speeds [*Huebert et al.*, 2010]. A sensitivity test using the *Huebert et al.* [2010] parameterization shows that our results are not strongly dependent on the difference between these parameterizations.

The three DMS climatologies used in this study are from *Simo and Dachs* [2002], *Kettle et al.* [1999], and *Lana et al.* [2011]. All three originate from a compilation of *in situ* surface seawater DMS concentration measurements in the Global Surface Seawater DMS Database (GSSDD, http://saga.pmel.noaa.gov/dms) begun following the publication of the climatology by *Kettle et al.* [1999]. We primarily use DMS concentrations from a monthly climatology following *Simo and Dachs* [2002], and present results using the other two (*Kettle et al.* [1999] and *Lana et al.* [2011]) in sensitivity studies. *Simo and Dachs* [2002] determined an empirical relationship between the seawater DMS concentrations in the GSSDD and simultaneous measurements of chlorophyll-a (Chl-a) concentrations at the surface and the mixed layer depth (MLD). A global DMS dataset is then derived from global datasets of Chl-*a* and MLD. We use a *Simo and Dachs* [2002] DMS climatology derived from Chl-*a* estimates from the Sea-viewing Wide Field-of-view Sensor (SeaWiFS) monthly climatological data from 2001-2006 and ocean MLD monthly climatology from *de Boyer-Montegut et al.* [2004]. The widely-used *Kettle et al.* [1999] DMS dataset interpolates the GSSDD measurements into a monthly climatology. The *Lana et al.* [2011] DMS climatology was constructed using the three-fold increase in GSSDD measurements over *Kettle et al.* [1999] projected onto biogeographic provinces and processed with objective techniques to obtain monthly fields.

Since SeaWiFS data do not provide reliable Chl-*a* estimates in areas with sea ice, persistent cloud cover or during the polar night, the *Simo and Dachs* [2002] DMS dataset does not report high latitude DMS concentrations under extensive ice or cloud conditions. We replace missing DMS concentrations in the Southern Ocean using an average of concentrations immediately to the north of the missing data. This simple fix enables the spatial continuity of DMS emissions in the Southern Ocean without the additional impact of missing concentration values in the sea ice zone. High latitude DMS concentrations in the *Simo and Dachs* [2002] DMS dataset are are below the peak *in situ* measurements in the GSSDD

and hence are likely a lower bound on the true concentration fields in the sea ice zone under extensive ice coverage.

Figure 2.1 shows the January surface seawater DMS concentrations from the *Simo and Dachs* [2002], *Kettle et al.* [1999], and *Lana et al.* [2011] DMS datasets and the corresponding mean DMS emission fluxes to the atmosphere from our simulations using the *Nightingale et al.* [2000] parameterization. The interpolation of sparse spatial and temporal *in situ* DMS measurements in the *Kettle et al.* [1999] dataset results in extensive hot-spots and strong zonal gradients in DMS concentrations and emissions within the sea ice zone. We use the *Simo and Dachs* [2002] DMS climatology in our primary simulations because it lacks this strong zonal asymmetry in DMS concentrations.

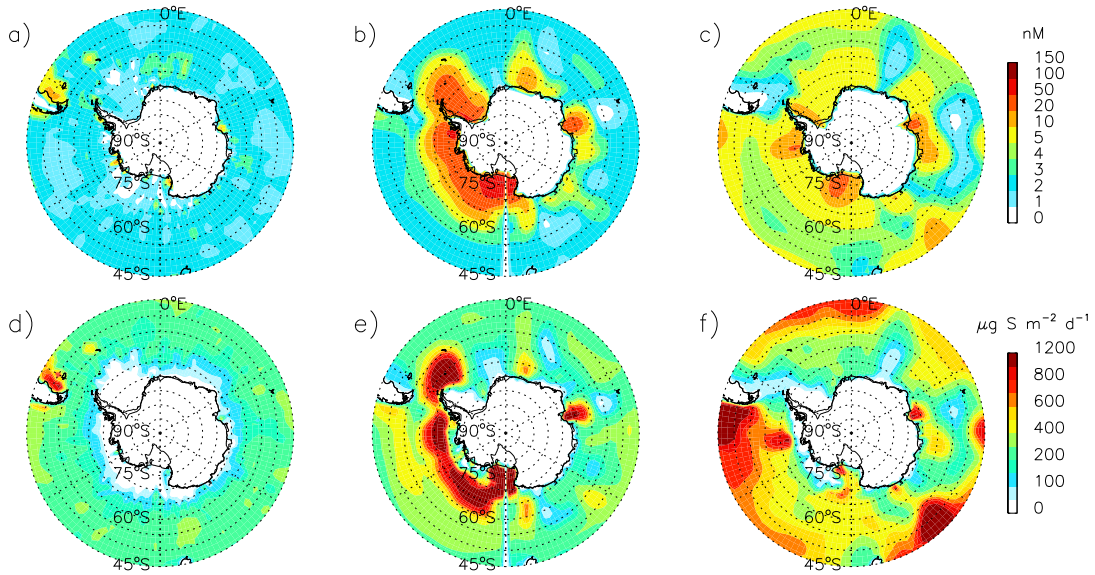

Figure 2.1: January surface DMS concentrations (nM) from (a) *Simo and Dachs* [2002], (b)*Kettle et al.* [1999], and (c) *Lana et al.* [2011] DMS datasets. January climotological DMS emissions fluxes (μg m^{-2} d^{-1}) in the (d) Simó and Dachs 'capped', (e) Kettle1999 'capped', and (f) Lana 2011 'capped' simulations, where DMS emissions fluxes are zero in the presence of sea ice. Scales are not linear. See Section 2.8 and Table 2.1 for the description of the simulations.

Global DMS surface concentrations are difficult to estimate from present measurements, as seen in the wide variation of DMS concentrations and resulting emissions in Figure

2.1. Ecological and biogeochemical dynamics within planktonic communities also play a significant role in determining DMS production and hence DMS emissions [*Elliott*, 2009; *Cameron-Smith et al.*, 2011]; these dynamics are not represented in the DMS seawater climatologies used in our model simulations. The use of a surface seawater DMS concentration climatology in the model neglects any interannual variability in surface DMS concentrations, though the interannual variability of DMS emissions is approximated to some extent via the interannual variability in SSTs and winds that govern the DMS ocean-to-air flux parameterizations.

2.2.4 Other sulfur emissions

Natural (except DMS), anthropogenic, and biomass burning sulfur emissions are from the Global Emissions Inventory Activity (GEIA v.1) database (http://www.geiacenter.org/). Non-DMS emissions in all simulation years are prescribed at 1995 magnitudes to restrict interannual sulfur cycle variability to processes associated with DMS. Volcanic emissions are included in the GEIA as part of the natural source emissions, and include an average of continuous volcanic emissions over 25 years plus eruptive volcanic emissions. Ship SO_2 emissions follow *Corbett et al.* [1999]. The model does not include sea-salt sulfate emissions, and therefore all sulfate in the model is non-sea-salt sulfate ($\mathrm{nssSO_4^{2-}}$).

2.2.5 DMS chemistry

The oxidative pathways of DMS are complex and not completely understood [*von Glasow and Crutzen*, 2004; *Lucas and Prinn*, 2005] and typically are simplified in large scale models. [e.g., *Chin et al.*, 1996; *Cosme et al.*, 2002]. DMS is thought to be oxidized in the atmosphere to SO_2 and MSA primarily by the hydroxyl radical (OH) and the nitrate radical (NO_3). Measurements of BrO have been shown to be high in the presence of first-year sea ice [*Wagner et al.*, 2007; *Alvarez-Aviles et al.*, 2008; *Simpson et al.*, 2007], and halogen (BrO) chemistry is also known to play a role in DMS oxidation [*Boucher et al.*, 2003; *Read et al.*, 2008]. The magnitude, variability, and relative importance of BrO is not yet well understood. SO_2 is further oxidized to sulfate and contributes the dominant fraction of

nssSO_4^{2-} aerosols in remote marine locations. Sulfate has other natural and anthropogenic origins which confound its relationship to DMS, but it is thought that MSA is a product only of DMS oxidation. In a study of seven DMS oxidation schemes, *Karl et al.* [2007] showed that the relatively simple DMS chemistry used by *Chin et al.* [1996] (and used in this study) reproduced observed features of the sulfur cycle extremely well compared to more complicated mechanisms.

The DMS-MSA chemistry in GEOS-Chem is simplified as described by *Chin et al.* [1996, 2000]. Yields for DMS oxidation via gas-phase reaction with OH are 100% SO_2 (abstraction channel) and 75% SO_2 and 25% MSA (addition channel). The fraction of DMS oxidized to MSA is larger in the high latitudes than globally, due to the temperature dependence of the OH reaction. DMS reaction with NO_3 in the gas phase also yields 100% SO_2, however reaction with NO_3 is limited to periods of no solar insolation. Globally, 26% of DMS oxidation occurs via reaction with NO_3.

Gas phase DMS oxidation by BrO produces dimethylsulfoxide (DMSO) which is further oxidized in the gas phase to MSA [*Breider et al.*, 2010]. A simplified BrO oxidation mechanism was added in a sensitivity study as:

$$\mathrm{DMS} + \mathrm{BrO} \rightarrow 0.6 \cdot \mathrm{SO_2} + 0.4 \cdot \mathrm{MSA} \tag{2.1}$$

[*Pham et al.*, 1995; *Boucher et al.*, 2002; *Chatfield and Crutzen*, 1990; *Breider et al.*, 2010] using a pseudo-first order rate constant of $k = 1.5 \times 10^{-14} \exp(1000/T)$ [BrO] [*IUPAC*, 2007]. This reaction assumes all DMS is oxidized to SO_2 and MSA and neglects the intermediate product dimethylsulfoxide (DMSO) and its deposition, since DMSO is not explicitly included in the current model. This simplified chemistry will lead to an overestimate of MSA produced via DMS oxidation by BrO. A simple diurnal cycle was imposed by setting the rate constant to zero in the absence of sunlight.

2.2.6 Aerosol deposition

Wet deposition of aerosols is described by *Liu et al.* [2001] and includes contributions from scavenging in convective updrafts, rainout and washout from convective anvils and large

scale precipitation, and return to the atmosphere following re-evaporation. Dry deposition velocities are computed with a standard resistance-in-series scheme based on *Wesely* [1989] as described by *Wang et al.* [1998]. Since deposition processes on Antarctica occur primarily on snow surfaces for both dry and wet deposition, sulfate deposition is calculated as the sum of both SO_2 and sulfate for both wet and dry processes. Snow concentrations of MSA and other species are computed as $\frac{F_i}{p}$, where F_i is the monthly mean deposition flux of chemical tracer i (kg m^{-2} d^{-1}), and p is the monthly mean precipitation (mm d^{-1}). Seasonal and yearly averages of MSA snow concentration are computed as precipitation-weighted means.

2.2.7 Meteorology

Figure 2.2 shows GEOS-4 annual precipitation (mm yr^{-1} water equivalent) in Antarctica with maximum values (400-1000 mm yr^{-1}) at the coast decreasing inland (10-100 mm yr^{-1}). Comparison of GEOS-4 precipitation rates for Antarctica with those from *Monaghan et al.* [2006] reveal no significant bias. *Monaghan et al.* [2006] derived a 50-year time series of snowfall accumulation over Antarctica by combining model simulations and observations primarily from ice cores. *Bloom et al.* [2005] evaluated the GEOS-4 analysis data set compared to observations and other reanalysis products and note an underestimation by up to a factor of two in precipitation of the Southern Hemisphere extratropics (30-60°S) and a high bias in zonal austral summer winds in the Southern Ocean (40-60°S).

We also conduct a sensitivity study with GEOS-5 meteorology data, which has higher boundary layer resolution than GEOS-4. We examine whether the reduced boundary layer resolution of GEOS-4 overestimates transport out of the boundary layer into the free troposphere. GEOS-5 also corrects some of the low bias in precipitation in the Southern Ocean, with increases of 25-100% over GEOS-4 precipitation in the 30-60°S region. Antarctic continental precipitation, however, is lower in GEOS-5 compared to GEOS-4. In most locations in Antarctica precipitation is within 25% of GEOS-4 values, though in some sections of West Antarctica precipitation is lower by 50% in the GEOS-5 data. The effects of the GEOS-5 meteorology on our simulations are discussed in detail in Section 4.7, but the sensitivity study indicates that the choice of meteorological input does not change our conclusions.

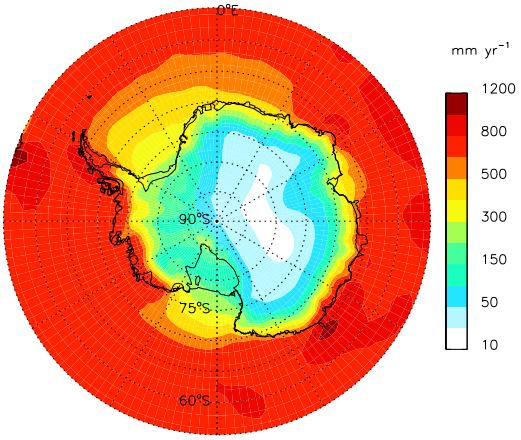

Figure 2.2: Mean annual precipitation rate (mm yr^{-1} water equivalent) from GEOS-4 meteorological fields.

We use the GEOS-4 meteorology for our primary simulations because of the longer time period over which meteorological data is available for GEOS-Chem (1985-2006 for GEOS-4, compared to 2004-present for GEOS-5).

2.2.8 Simulations

As in most sulfur models, GEOS-Chem implements a 'cap' associated with gas exchange through the sea ice, and therefore assumes that DMS emissions are zero within the sea ice by default. We experiment with relaxing this condition in our scenarios, whereby we use the same gas transfer parameterization over sea ice as over open ocean. We assume that the gas transfer parameterization over sea ice is appropriate for the sea ice fraction as well as open water among sea ice floes, which may not be realistic [e.g., *Loose et al.*, 2011]. This is, however, useful as a first order determination of the influence of DMS emissions from within the sea ice itself. In three model scenarios we vary the DMS concentrations in the presence of sea ice from October through March. The 'capped' scenario uses this default cap on DMS emissions in the presence of sea ice in all months. The 'uncapped' scenario removes the cap from October through March, effectively removing the influence of sea ice on DMS fluxes from the ocean except via the influence of sea ice on SST. A third scenario is an 'enhanced' run where the surface DMS concentration is set to 6 nM wherever sea ice is present from

October through March. Figure 2.3 illustrates the DMS concentrations imposed in the sea ice in each of these scenarios. We also examine the difference between the uncapped and capped runs to examine the impact of DMS emissions only from within the sea ice.

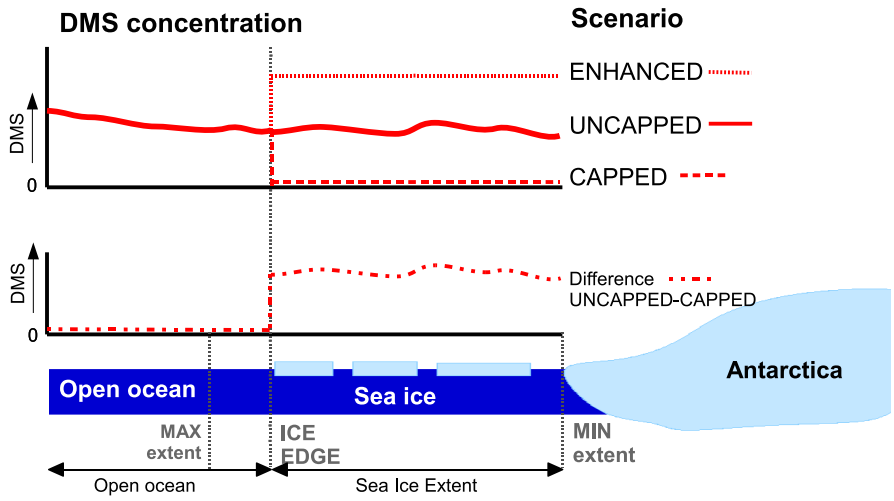

Figure 2.3: Illustration of seawater DMS concentrations applied in the sea ice zone for each of the scenarios. (Top) DMS concentrations for the DMS dataset are applied to the open ocean and the sea ice in the UNCAPPED scenario (solid red), with no influence of sea ice. For the CAPPED scenario, DMS concentrations are set to 0 (dash red). In the ENHANCED scenario, DMS concentrations are set to a scalar value above the mean DMS concentrations of the ice extent (fine dash red). (Bottom) The difference (UNCAPPED minus CAPPED) between two scenarios allows evaluation of effect of DMS concentrations of the DMS dataset from within sea ice only (red dot-dot-dash). In all simulations, the sea ice expands and retreats through its seasonal cycle (between maximum and minimum ice extent). Each scenario is applied for the to the sea ice extent at each point in time for the months October-March. All simulations have a 'capped' scenario for April-September.

Table 2.1 summarizes all simulations discussed in the paper. Our primary simulations use the *Simo and Dachs* [2002] DMS climatology with the *Nightingale et al.* [2000] gas transfer parameterization under the capped, uncapped, and enhanced scenarios as described above.

These are referred to in the text below as 'Simó and Dachs capped', 'Simó and Dachs uncapped', etc. The *Simo and Dachs* [2002] DMS dataset has a mean DMS concentration from October-March over the climatological sea ice area of 1.2 nM, with a peak concentration of 2.0 nM in January. The 6 nM concentration is thus 5 times larger than the October-March mean of the uncapped run. We compute the difference between the uncapped and capped and the enhanced and capped model scenarios to isolate the effect of DMS emissions from within sea ice itself. The Simó and Dachs capped, uncapped, and enhanced simulations are run for 17 years from July 1985 through June 2004 after a 1.5 year spin up, excluding the period July 1997 through June 1999. This overlaps the period of satellite observations of sea ice as well as several ice core records of MSA concentrations.

To determine appropriate DMS concentrations to use in sea ice in the enhanced simulation, we consulted DMS surface concentration measurements from the Global Surface Seawater DMS Database. When averaged into monthly 5° zonal bands between 60°S and 75°S, monthly median concentrations in each band range between 1-7 nM over the course of the austral summer. Regions of very high median DMS concentration (>10 nM) in the Weddell and Ross Seas near their respective ice shelves were excluded. Though the observed monthly median values exhibit a seasonal cycle, a constant value of 6 nM was prescribed in the enhanced simulation for October through March. These prescribed concentrations are low compared to the range of DMS seawater measurements associated with the seasonal sea ice zone [e.g., *Jones et al.*, 2010], but they are enhanced compared to the mean values contained in the *Simo and Dachs* [2002] DMS dataset as noted above, and are therefore useful in evaluating the sensitivity of MSA deposition to DMS emissions from the sea ice itself. In the capped run, over 56% and up to 90% of the annual MSA deposited at each spatial location in Antarctica occurs between October and March, forming the basis of the seasonality in modified DMS concentrations.

In addition to the 17-year Simó and Dachs simulations described above, several other sensitivity runs were completed to examine our results with different DMS concentrations and gas flux parameterizations (See Table 2.1). Simulations using the *Kettle et al.* [1999] DMS dataset and the *Nightingale et al.* [2000] emissions parameterization were each run for six years to understand the sensitivity of our results to the specific DMS concentration

Table 2.1: Summary of simulations and sensitivity simulations discussed in the text.

Simulation name	DMS conc in ice	DMS dataset[a]	DMS emissions parameterization[a]	Simulation length	Sensitivity test of
Simó and Dachs capped	0	SD2002	N2000	17 years (7/1985-6/2004)[b]	
Simó and Dachs uncapped	Oct-Mar: Dataset; Apr-Sep: 0	SD2002	N2000	17 years (7/1985-6/2004)[b]	
Simó and Dachs enhanced	Oct-Mar: 6 nM; Apr-Sep: 0	SD2002	N2000	17 years (7/1985-6/2004)[b]	
Huebert2010 capped	0	SD2002	H2010	3 yrs (7/1985-6/1988)	Emissions linear with windspeed
Huebert2010 uncapped	Oct-Mar: Dataset; Apr-Sep: 0	SD2002	H2010	3 yrs (7/1985-6/1988)	Emissions linear with windspeed
BrO capped	0	SD2002	N2000	3 yrs (7/1985-6/1988)	BrO oxidation mechanism
BrO uncapped	Oct-Mar: Dataset; Apr-Sep: 0	SD2002	N2000	3 yrs (7/1985-6/1988)	BrO oxidation mechanism
GEOS-5 capped	0	SD2002	N2000	2 yrs (7/2005-6/2007)	GEOS-5 meteorological dataset
GEOS-5 uncapped	Oct-Mar: Dataset; Apr-Sep: 0	SD2002	N2000	2 yrs (7/2005-6/2007)	GEOS-5 meteorological dataset
Kettle1999 capped	0	K1999	N2000	6 yrs (7/1985-6/1991)	Alternate DMS dataset
Kettle1999 uncapped	Nov-Mar: Dataset; Apr-Oct: 0	K1999	N2000	6 yrs (7/1985-6/1991)	Alternate DMS dataset
Lana2011 capped	0	L2011	N2000	3 yrs (7/1985-6/1988)	Alt. DMS dataset emissions only
Lana2011 uncapped	Oct-Mar: Dataset; Apr-Sept: 0	L2011	N2000	3 yrs (7/1985-6/1988)	Alt. DMS dataset emissions only

[a] Abbreviations as SD2002: *Simo and Dachs* [2002]; N2000: *Nightingale et al.* [2000]; H2010: *Huebert et al.* [2010]; K1999:*Kettle et al.* [1999]; L2011: *Lana et al.* [2011].

[b] Data from July 1997-June 1999 was excluded from the analysis because an error in regridding GEOS-4 surface precipitation and specific humidity tendency fields for GEOS-Chem.

dataset (Kettle1999 capped and Kettle1999 uncapped). The sensitivity of our results to the DMS flux parameterization was investigated using the *Huebert et al.* [2010] parameterization, which describes a linear function of DMS emissions with wind speed (Huebert2010 capped and Huebert2010 uncapped). A BrO sensitivity study was conducted by implementing a simplified BrO oxidation mechanism (described in Section 2.2.5) and utilizing monthly mean BrO fields from *Holmes et al.* [2010] and *Yang et al.* [2005] (BrO capped and BrO uncapped). The BrO sensitivity study includes capped and uncapped simulations using the *Simo and Dachs* [2002] surface ocean DMS concentrations and the *Nightingale et al.* [2000] gas transfer parameterization. A sensitivity experiment was performed using the GEOS-5 meteorological data in order to investigate the dependence of our results on the boundary layer resolution and other meteorological input fields (GEOS-5 capped and GEOS-5 uncapped). Finally, the *Lana et al.* [2011] DMS surface seawater climatology was used to estimate the set of both capped and uncapped DMS emissions using the *Nightingale et al.* [2000] gas transfer parameterization and the GEOS-4 meteorology fields (Lana2011 capped and Lana2011 uncapped). We find that emissions using the *Simo and Dachs* [2002] and *Kettle et al.* [1999] DMS datasets bracket DMS emissions obtained using *Lana et al.* [2011], and results of a chemistry simulation with the *Lana et al.* [2011] DMS climatology would yield little new information to our analysis here.

2.3 Model evaluation

2.3.1 Global sulfur budget

Table 2.2 compares the annual global sulfur budget for the capped simulation with other published estimates of the global sulfur cycle. Annual DMS emissions of 23.6 Tg S yr^{-1} using the *Simo and Dachs* [2002] DMS dataset and the *Nightingale et al.* [2000] emissions parameterization are within the range of estimates of 10-40 Tg S y^{-1} summarized in *Penner et al.* [2001]. We note that the *Simo and Dachs* [2002] DMS dataset results in larger global DMS emissions than both the *Kettle et al.* [1999] DMS dataset (19.6 Tg S y^{-1}) and the *Lana et al.* [2011] DMS dataset (22.2 Tg S y^{-1}) under a capped sea ice emissions scenario. Global DMS emissions are larger in our simulations than estimates made with the widely-

used *Liss and Merlivat* [1986] parameterization for sea-to-air flux [*Kettle and Andreae*, 2000; *Nightingale et al.*, 2000], as a result of the greater sensitivity to higher wind speeds in the Nightingale parameterization. Lifetimes are calculated as mean burden divided by the sum of the loss processes (i.e., chemical loss for lifetimes of DMS, and deposition for MSA). Global annual lifetimes of DMS and MSA are 1.8 and 6.7 days for the capped run. These estimates are comparable to other published estimates of the lifetime of both MSA and DMS [e.g., *Faloona*, 2009; *Spracklen et al.*, 2005; *Berglen et al.*, 2004; *Chin et al.*, 2000]. Global budgets of SO_2 and SO_4^{2-} also compare well to previously published estimates.

Emissions of DMS from within sea ice have only a modest effect on the global sulfur budget, and 'capping' emissions in the presence of sea ice has likely been appropriate in studies of the global sulfur cycle. The increases in global sulfur emissions in the Simó and Dachs uncapped and enhanced DMS runs over the capped run are 0.05 Tg S y^{-1} (<1%) and 0.31 Tg S y^{-1} (1.4%) respectively; these increases are less than the magnitude of interannual variability of global DMS emissions (∼1 Tg S y^{-1}) caused by variability in wind speeds and SSTs. The increase in global DMS emissions in the Kettle1999 uncapped run compared to the capped run is also small (0.36 Tg S y^{-1}, or 1.8%).

2.3.2 Comparison of modeled and observed atmospheric concentrations

We compared the modeled atmospheric concentrations of MSA, nssSO_4^{2-}, and DMS at Antarctic locations where observational data exist. Figure 2.4 shows modeled monthly mean concentrations of MSA, nssSO_4^{2-} and DMS at Dumont D'Urville (DDU) (140°1'E, 66°40'S) compared to observations [*Minikin et al.*, 1998; *Preunkert et al.*, 2008]. The modeled and observed high-latitude atmospheric MSA and nssSO_4^{2-} concentrations at the surface exhibit a maximum in austral summer and minimum in austral winter (Figure 2.4a and 2.4b). The seasonal maximum in MSA is broad in both observations and the model, showing high MSA values (16-18 ppt) lasting from late summer through autumn. The winter minimum (2-3 ppt), however, is shorter in the model than in observations, with modeled concentrations increasing earlier (in August) than observations after the winter minimum. The Kettle1999 capped simulation overestimates the summer MSA maximum by a factor of 3 and does not

Table 2.2: Annual global sulfur budget for Simó and Dachs capped run compared to global sulfur budgets summarized in other studies. Uncertainties are one standard deviation of annual global means over 17 years of simulation.

	Capped run Mean ± 1σ	Published range Min - Max
Total Sulfur Emissions (Tg S y^{-1})	97.3 ± 0.8	83 - 124.6[a]
DMS oceanic emissions	23.6 ± 0.9	10.7 - 27.9[b]
Total Sulfur Deposition (Tg S y^{-1})	95.2 ± 0.7	82.3 - 95.6[c]
SO_2 dry deposition	30.7 ± 0.4	23 - 55[a]
SO_2 wet deposition	14.9 ± 0.3	0.2 - 19.9[a]
Sulfate dry deposition	6.0 ± 0.1	3.2 - 17[b]
Sulfate wet deposition	41.5 ± 0.8	24.7 - 74.1[b]
MSA dry deposition	0.2 ± 0.0	
MSA wet deposition	1.9 ± 0.1	
Burden (Tg S)		
SO_2	0.36 ± 0.00	0.2 - 0.68[a]
Sulfate	0.60 ± 0.01	0.5 - 0.96[c]
DMS	0.11 ± 0.00	0.02 - 0.15[a]
MSA	0.04 ± 0.00	0.02 - 0.03[a]
Lifetime (days)		
SO_2	1.46 ± 0.02	0.6 - 5.3[a]
Sulfate	4.66 ± 0.12	3.4 - 7.2[b]
DMS	1.77 ± 0.04	0.5 - 3[a]
MSA	6.71 ± 0.35	5.6 - 18.5[a]

[a] Summarized in *Faloona* [2009].
[b] Summarized in *Spracklen et al.* [2005].
[c] Summarized in *Berglen et al.* [2004].

capture the late summer peak, but better simulates the timing of the rise in concentrations after summer and into the spring season than the Simó and Dachs capped simulation. Modeled nssSO_4^{2-} concentrations match the observations at DDU well, capturing both the magnitude and timing of the seasonal cycle through both the summer and winter (Figure 2.4b). The Kettle1999 capped simulation overestimates the magnitude of the nssSO_4^{2-} summer peak but captures the winter minimum quite well. *Kettle and Andreae* [2000] corrected some of the errors associated with the DMS concentrations at high latitudes in the *Kettle et al.* [1999] DMS dataset that lead to the very large austral summer peaks in MSA and nssSO_4^{2-}.

Similar characteristics are found in comparisons of modeled MSA and nssSO_4^{2-} to station observations for Halley (26°19'W, 75°35'S), Mawson (62°30'E, 67°36'S), Neumayer (8°15'W, 70°39'S), and Palmer stations (64°03'W, 64°46'S) (not shown) [*Minikin et al.*, 1998; *Savoie et al.*, 1993]. In all cases, the comparison of modeled MSA and nssSO_4^{2-} to observations is similar to that at DDU. Modeled MSA concentrations increase earlier in springtime (August) than in observations, reach summer maxima in February-March, and overestimate winter minima.

Figure 2.4c shows surface DMS concentrations at DDU in the model compared to observations [*Preunkert et al.*, 2008]. Modeled summer values at DDU show reasonable agreement with observations (within a factor of 3), but winter values are substantially overestimated. The buildup of DMS in the high latitudes in the austral winter is related to the lack of a chemical sink in the model, due to the lack of a local source of NO_x (leading to low NO_3) and the lack of available sunlight (leading to low OH). Owing to the low solubility of DMS, its depositional sink is insignificant, even in winter.

Gas- and aqueous-phase oxidation of DMS by O_3, not included in GEOS-Chem, has been shown by *Boucher et al.* [2003] to be important in the high latitudes. Aqueous and gas phase oxidation of DMS by O_3 has been estimated to account for 30-40% of the annual DMS oxidation over the Southern Ocean and Antarctica though it contributes only up to 6% of oxidation of DMS globally. Though no seasonal figures are shown in *Boucher et al.* [2003], gas- and aqueous-phase DMS oxidation by O_3 contributes little to DMS oxidation at low and mid latitudes, and therefore likely contributes little in the high latitude austral

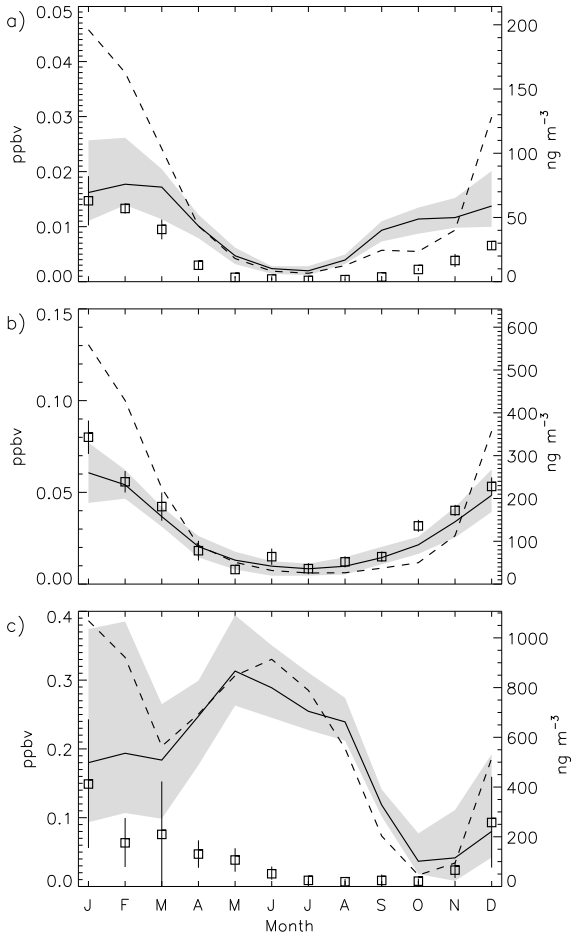

Figure 2.4: Annual cycle of (a) MSA concentrations (ppb) (b) nssSO_4^{2-} concentrations (ppb) and (c) DMS concentrations (ppb) at the surface at Dumont D'Urville (140°1'E, 66°40'S). The monthly mean (solid line) and minima/maxima (shaded) for the Simó and Dachs capped simulation from the 17 year run are shown with the Kettle1999 capped monthly mean for the 6 year run (dashed line). Observations are shown as open squares with the standard deviation as reported by *Preunkert et al.* [2008]; *Minikin et al.* [1998].

summer when OH and NO_3 dominate DMS oxidation. This suggests that oxidation by gas- and aqueous- phase O_3 dominates in the high latitude austral winter due to the lack of other oxidants. *Barnes et al.* [2006] outlines an argument for the importance of this oxidation pathway in global sulfur models, and its absence likely explains the discrepancy in the modeled seasonality of atmospheric DMS concentrations at high southern latitudes.

Our analysis of model results is restricted to the austral spring and summer months of October-March, and therefore the high winter bias in atmospheric concentrations of both DMS and MSA at high latitude stations has little impact on our results. The lifetimes of both DMS and MSA are relatively short (4.7 and 10.9 days for DMS and MSA calculated for September-November) in the early spring south of 60°S, and therefore the high winter DMS concentrations have little effect on October-March MSA deposition. Modeled October-March DMS and MSA atmospheric concentrations agree with the observations within a factor of 2 and 3 respectively.

We also compared the model to observations of atmospheric DMS at the lower-latitude stations of Cape Grim (144°41'E, 40°41'S) and Amsterdam Island (77°30'E, 37°50'S), shown in Figure 2.5 [*Ayers et al.*, 1995; *Sciare et al.*, 2000]. Observations at both of these sites show a clear austral summer maximum and winter minimum. There is no clear seasonal cycle in the model at Cape Grim in the Simo and Dachs capped simulation owing to the lack of seasonal cycle in the DMS emissions from the *Simo and Dachs* [2002] DMS dataset. The Kettle1999 capped simulation captures the observed seasonal cycle reasonably well, which reflects the seasonal cycle in modeled DMS emissions in that region. At Amsterdam Island, neither DMS climatology results in the capture of the observed seasonal cycle, which again reflects local model DMS emissions. This comparison of Cape Grim and Amsterdam Island illustrates that the atmospheric DMS concentrations depend strongly on the seawater DMS climatology. A comprehensive set of measurements of DMS seawater concentration, DMS emissions, and DMS and MSA surface air concentration would be extremely valuable for further assessing the model, even if only at a few locations.

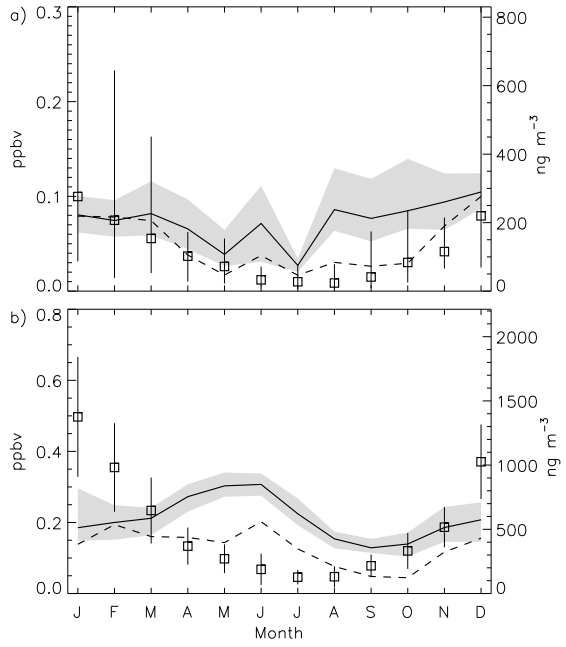

Figure 2.5: Annual cycle of DMS concentrations (ppb) at the surface at (a) Cape Grim (144°41'E, 40°41'S) and (b) Amsterdam Island (77°30'E, 37°50'S). Lines and symbols are the same as in figure 2.4. Observations for Cape Grim are from *Ayers et al.* [1995]; error bars indicate the spread of measurements in *Ayers et al.* [1995], Fig 3. Observations from Amsterdam Island cover the period 1987-2010 following the protocols reported by *Sciare et al.* [2000]. Error bars indicate the standard deviation in monthly means.

2.3.3 Mean MSA deposition fluxes and snow concentrations

Figure 2.6 shows the 17-year mean MSA deposition flux from October-March near Antarctica for the Simo and Dachs capped run. Modeled mean MSA deposition fluxes exhibit a strong gradient from the coast decreasing inland in Antarctica, similar to the gradient shown in the mean annual precipitation in Figure 2.2. MSA deposition fluxes are dominated by wet deposition processes at locations covering 82% of the Antarctic land area, and MSA deposition fluxes are strongly correlated with precipitation (r^2=0.78) in the Simó and Dachs capped run in Antarctica.

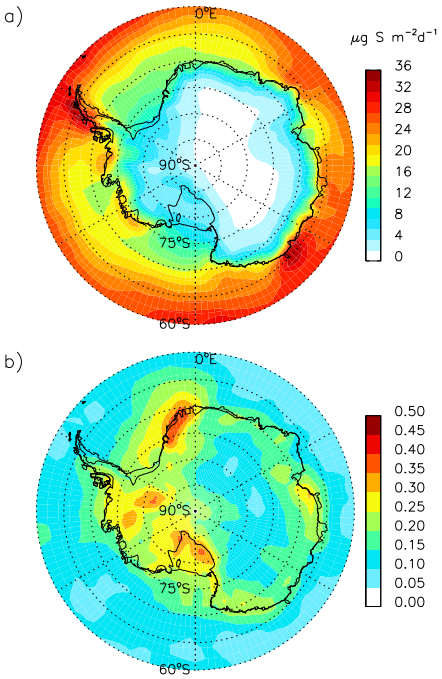

Figure 2.6: (a) Mean MSA deposition flux (μg S m^{-2} d^{-1}) for October-March from the capped run. (b) Standard deviation (unitless) of MSA deposition flux, normalized by (a).

Figure 2.7 shows the 17-year mean MSA snow concentration from October-March in Antarctica, compared to spring, summer, and annual measurements of MSA concentrations in ice cores and snow pits compiled from 520 sites by *Bertler et al.* [2005]. Modeled snow concentrations of MSA are of the same order of magnitude as measured snow pit and ice core measurements, though on average they are overestimated in the model by up to a

factor of 5 at the coasts in the modeled annual mean concentrations. Snow concentration measurements exhibit an increasing gradient from the coast toward the interior of the East Antarctic Plateau, due to a decreasing snow accumulation gradient inland from the coast in the same region (Figure 2.2). This increasing gradient is captured by the model. The lower precipitation rate causes a shift toward an increased fraction of MSA loss via dry deposition in inland Antarctica. Post-depositional processes such as surface snow redistribution and intra-seasonal diffusion of MSA peaks within firn [*Weller et al.*, 2004; *Wagnon et al.*, 1999] are not incorporated into the model. The observations in Figure 2.7 include both surface snow and ice core concentrations and may be influenced by post-depositional processes. In general these processes need to be understood well enough to interpret longer ice core records, but they are not relevant for the idealized analysis in our study.

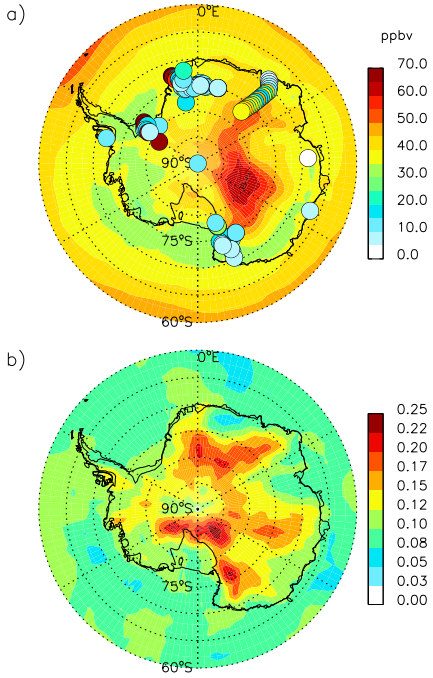

Figure 2.7: (a) Mean MSA snow concentration (ppb) for October-March from the capped run. Filled circles are MSA concentration measurements compiled from snow and ice chemistry at 520 sites across Antarctica by *Bertler et al.* [2005]. (b) Normalized standard deviation of MSA snow concentration (unitless). Values are displayed over the ocean as well as land to understand the spatial patterns, even though rainfall/snowfall does not accumulate over the ocean.

2.4 Results

2.4.1 Relationship between sea ice extent and MSA snow concentrations and MSA deposition flux

To mimic the analysis that is frequently done with MSA concentrations recorded in ice cores to find patterns of correlation with nearby sea ice extent, we create two MSA-sea ice metrics – correlation of each of the time series of MSA snow concentration and MSA deposition flux at one location in the model with sea ice extent around the continent. We correlate each MSA time series with the time series of the latitude of sea ice extent averaged in 15° longitudinal sectors around the continent. If the sea ice exerts sufficient influence on DMS emissions, we expect negative correlation coefficients in both MSA-sea ice metrics for nearby sea ice extent in the Simó and Dachs capped run. We isolate the effect of DMS emissions from the sea ice itself and also compute the MSA-sea ice metrics for the difference between the Simó and Dachs uncapped and capped scenarios, for which we expect positive correlation coefficients for nearby sea ice extent given that this isolates DMS emissions from the sea ice.

Figure 2.8a presents the MSA-sea ice metrics for a coastal area between 20°E and 35°E as an example of a location in the model that demonstrates relatively strong correlation coefficients compared to other locations. In the Simó and Dachs capped run, we find correlation coefficients for MSA snow concentration with sea ice in 15° sectors in the range of r=–0.75 to +0.75, and for MSA deposition flux with sea ice in the same sectors in the range of r=–0.4 to +0.4, as shown in Figure 2.8a. The magnitude of the modeled correlation coefficients are similar to the observations [e.g., *Curran et al.*, 2003; *Abram et al.*, 2007]. We expect the strongest negative correlation coefficients between the model MSA deposition flux/snow concentration and sea ice extent in adjacent sectors and/or upwind given the prevailing Southern Ocean westerlies and southeastward-moving storm tracks [e.g., *Yuan et al.*, 2009]. However, we find no consistency in the pattern or sign of correlation coefficients for this location in the Simó and Dachs capped run. The same MSA-sea ice metrics computed for the Simó and Dachs uncapped run (not shown) are similar in sign and magnitude, yet the Simó and Dachs uncapped runs by design eliminate any mechanistic relationship between

sea ice extent and MSA in Antarctica.

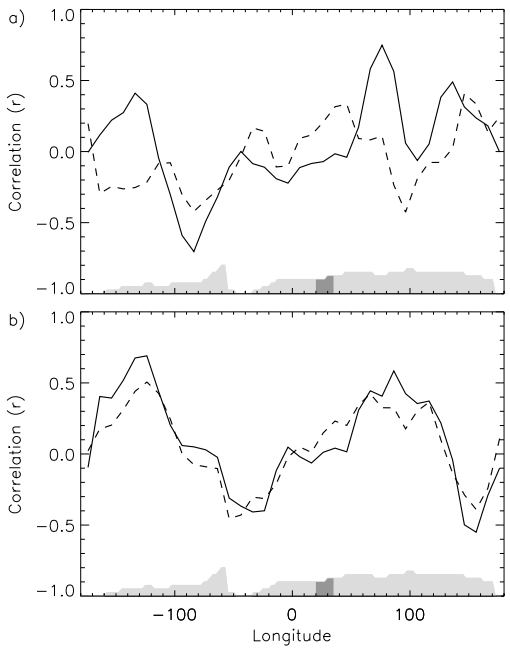

Figure 2.8: Correlation coefficients between sea ice extent for each point around the Antarctic continent and MSA snow concentration (solid line) and MSA deposition flux (dashed line) at a single location for the capped run (a) and difference between the uncapped and capped runs (b). Antarctica is shown as a shaded region along the x-axis for reference. Sea ice extent was averaged over 15° sectors, and MSA snow concentration / deposition flux was averaged over the region 20°E-35°E, between the coast and 74°S (dark shading).

Figure 2.8b shows same MSA-sea ice metrics for the difference between the Simó and Dachs uncapped and capped runs. The correlation coefficients are of magnitudes similar to those found for the Simó and Dachs capped run, yet again the pattern is inconsistent with our expectations. The correlation coefficients are near zero between MSA deposition flux / snow concentration and the adjacent sea ice extent. Positive correlation coefficients occur too far to the west of the selected location to indicate significant influence of sea ice on MSA.

Examination of the same MSA-sea ice metrics from other locations on Antarctica yield similar magnitudes of correlation coefficients between MSA deposition flux / snow concentration and sea ice extent, but no physically credible explanations. In the remainder of the

paper, we seek to understand why no sea ice-MSA relationship is apparent in the model, and focus on the relationship between sea ice extent and DMS emissions. We discuss fundamental differences between the global and high-latitude sulfur budgets that lead to longer DMS and MSA lifetimes, determine the zonal deposition pattern of sulfur species (SO_2, nssSO_4^{2-}, MSA) originating from the sea ice (from the difference between the uncapped and capped runs), and estimate the fraction of Antarctic MSA that originates in the Southern Ocean south of 60°S. We also estimate the relative contribution of the variability in sea ice extent and wind speed to variability in DMS emissions.

2.4.2 Regional sulfur budget

We consider the regional sulfur budget for October-March to examine how the southern high-latitudes deviate from global averages. Table 2.3 shows the October-March DMS emissions south of 60°S and MSA deposition on the Antarctic continent for all simulations. We find that DMS emissions in the region south of 60°S increase by 13% and 79% in the Simó and Dachs uncapped and enhanced runs over the capped run, respectively. MSA deposition to Antarctica, however, increases by only 4% and 19% respectively. DMS emissions from sea ice have a large effect on regional sulfur emissions; however, the MSA deposition to the Antarctic continent does not increase proportionally.

In the capped simulation, the October-March DMS lifetime south of 60°S (4.0 days) is about three times greater than the global mean (1.3 days) due to lower oxidant concentrations in the high latitudes. The October-March lifetime of MSA south of 60°S is 9.2 days compared to 6.7 days for the global mean. The lower scavenging efficiency at colder temperatures and lower precipitation rates on Antarctica lead to the longer MSA lifetime. The lengthening of both the MSA and DMS lifetimes in the high southern latitudes implies an increased potential for long range transport of chemical species in the region and smoothing of any local DMS signal in MSA deposition patterns. The lengthening of DMS and MSA lifetimes at high latitudes is not present in the BrO sensitivity simulations (See Section 4.6), suggesting that this is dependent on our understanding of the high-latitude oxidation mechanism of DMS. Lifetimes for the Simó and Dachs uncapped and enhanced

Table 2.3: Total DMS emissions for south of 60°S and total MSA deposition to Antarctica. All values represent the total for October-March.

Simulation	DMS dataset[a]	Emissions[a] parameterization	DMS emissions (Gg S)[b]	Antarctica MSA deposition (Gg S)[b]
Simó and Dachs capped	SD2002	N2000	361 ± 26	15.3 ± 1.5
Simó and Dachs uncapped	SD2002	N2000	409 ± 29	16.0 ± 1.6
Simó and Dachs enhanced	SD2002	N2000	646 ± 44	19.1 ± 1.7
Sensitivity simulations				
Huebert2010 capped	SD2002	H2010	281 ± 20[c]	9.8 ± 1.0[c]
Huebert2010 uncapped	SD2002	H2010	328 ± 23[c]	10.4 ± 1.0[c]
BrO capped	SD2002	N2000	366 ± 26[c]	19.6 ± 2.3
BrO uncapped	SD2002	N2000	417 ± 29[c]	21.0 ± 2.2
GEOS-5 capped	SD2002	N2000	333 ± 24[c]	4.9 ± 0.5[c]
GEOS-5 uncapped	SD2002	N2000	396 ± 28[c]	5.3 ± 0.5[c]
Kettle1999 capped	K1999	N2000	1026 ± 38	24.0 ± 2.8
Kettle1999 uncapped	K1999	N2000	1351 ± 72	29.5 ± 3.3
Lana2011 capped	L2011	N2000	769 ± 54[c]	—[d]
Lana2011 uncapped	L2011	N2000	976 ± 68[c]	—[d]

[a] Abbreviations as SD2002:*Simo and Dachs* [2002]; N2000: *Nightingale et al.* [2000]; H2010:*Huebert et al.* [2010]; K1999:*Kettle et al.* [1999]; L2011:*Lana et al.* [2011].

[b] Emissions fluxes and deposition fluxes are time and spatially integrated over the 6 month period October-March.

[c] Uncertainties estimated at same percentage as capped run.

[d] Lana2011 simulations were conducted to estimate DMS emissions in GEOS-Chem only.

runs are not significantly different in the southern high latitudes from those of the Simó and Dachs capped run. Regional lifetimes in the GEOS-5 sensitivity simulations are different from the GEOS-4 simulations and are discussed in more detail below, but lead to the same conclusions.

2.4.3 Distribution of MSA deposition from DMS emissions in sea ice

Figure 2.9 shows the zonal distributions of DMS emissions from the sea ice and sulfur deposition (sum of SO_2, nssSO_4^{2-}, and MSA) calculated from the difference between the Simó and Dachs uncapped and capped runs. Net transport of sulfur species from the sea ice zone is northward. The DMS emissions distribution peaks at 66°S, but sulfur deposition peaks at 60°S, with roughly half of the deposition to the north of 60°S. Of the sulfur emitted from the sea ice (i.e., in the difference between the Simó and Dachs uncapped and capped simulations), only 7.7% is deposited on the Antarctic continent. This ranges from as low as 4.1% for the GEOS-5 sensitivity simulations to as high as 9.6% in the Kettle1999 sensitivity simulations.

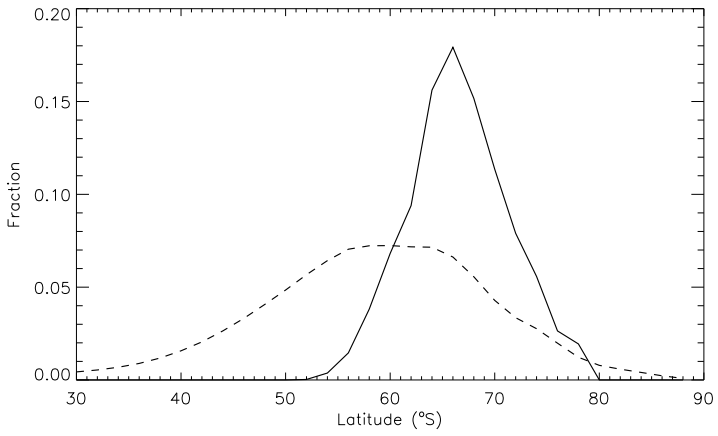

Figure 2.9: The fraction of DMS emitted at each latitude relative to the total DMS emissions for October through March from the difference between the Simó and Dachs uncapped and capped runs (solid line). The fraction of sulfur deposition at each latitude relative to the total sulfur deposition (dashed line). Sulfur deposition includes the sum of SO_2, nssSO_4^{2-}, and MSA, and is conserved with respect to DMS emissions in the difference between the uncapped and capped runs.

Figure 2.10 shows the mean October-March MSA snow concentrations resulting from DMS emissions only from the sea ice (uncapped minus capped) and the fraction this contributes to the uncapped simulation ([uncapped – capped]/uncapped) in both the Simó and Dachs and the Kettle1999 simulations. In the Simó and Dachs uncapped run, DMS emissions from the sea ice zone are small, so only a small fraction of the MSA deposited on Antarctica comes from DMS emitted in the sea ice at any given continental location (Figure 2.10a and 2.10b). The hot-spots of DMS concentration in the Kettle99 uncapped run (See Figure 2.1b) translate to a greater contribution from sea ice to MSA deposition in Antarctica, especially in the Ross Sea sector (Figure 2.10c and 2.10d). The relative importance of MSA derived from DMS in sea ice to total MSA snow concentrations is highly dependent upon seawater DMS concentrations within the sea ice zone, but in all simulations represents <25% of total MSA deposition throughout most of Antarctica.

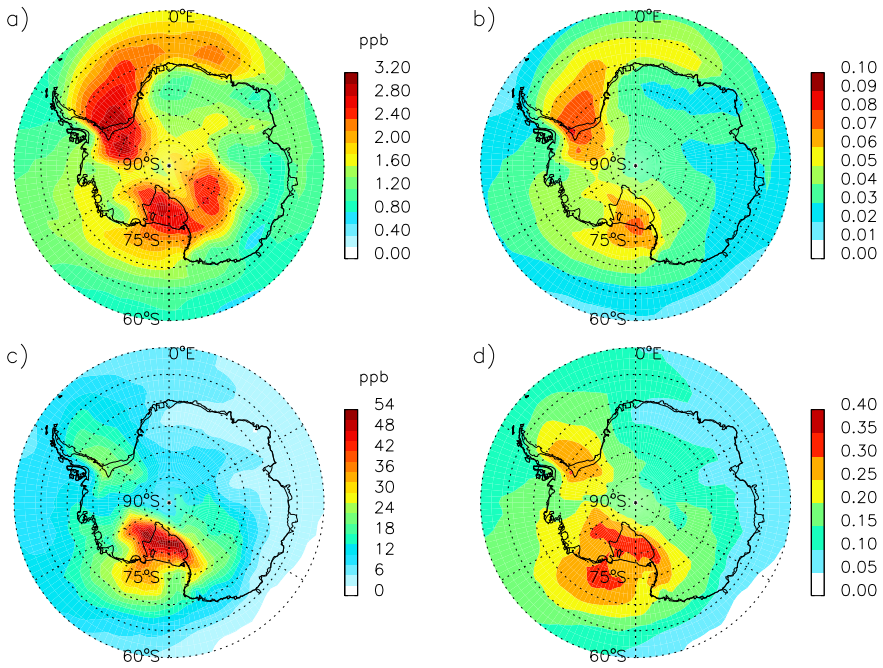

Figure 2.10: (a) MSA snow concentration (ppb) from DMS emissions in the sea ice zone (difference between the Simó and Dachs uncapped and capped runs), and (b) fraction of MSA deposition originating from the sea ice in the Simó and Dachs uncapped run. (c) and (d) are the same as (a) and (b) for the Kettle1999 uncapped and capped simulations.

Interannual variability in circumpolar sea ice extent in the Southern Ocean has been shown by *Zwally et al.* [2002] to be on the order of 8% (1%) of the summer (winter) mean areal extent, with maximum variability by sector of 25% in the summer extent in the Ross Sea (160°E-60°W) and 11% in winter in the Bellingshausen/Amundsen Seas (130°-60°W). Absent a mechanism whereby the interannual signal of sea ice on DMS emissions is amplified, we would expect interannual variation in DMS emissions associated with the variation in sea ice to be commensurate with interannual variation in sea ice extent. Given the relatively small fractional contribution of sea ice to MSA deposition at most locations on the continent (Figure 2.10b and 2.10d) and the relatively small interannual variability in sea ice extent compared to the mean ice extent, it is not surprising that we are unable to associate MSA deposition variability with DMS emissions variability due to changes in sea ice at most locations on the Antarctic continent.

2.4.4 Estimation of DMS emissions south of 60° S necessary to dominate Antarctic MSA deposition

A solid quantitative understanding of the DMS emissions, not just surface DMS concentrations, from within the sea ice zone is imperative. The magnitude of DMS emissions in the sea ice zone (i.e., south of 60°S) determines whether deposition of MSA and other sulfur species to the Antarctic continent is dominated by DMS emissions influenced by sea ice. Since the duration and timing of elevated sea surface DMS concentrations in the wake of the seasonal retreat of sea ice are not established and we do not attempt to model them in our scenarios here, we use the region south of 60°S as an estimate of the maximum areal extent of DMS emissions influenced by the seasonal cycle of sea ice. We then determine the contribution of DMS emissions from this area to Antarctic MSA deposition. The fractional contribution of DMS emissions from south of 60°S to MSA deposition in Antarctica is larger than that shown in Figure 2.10b and 2.10d because the area south of 60°S is larger than the area covered by sea ice.

In the Simó and Dachs uncapped run, the October-March average of DMS emissions in the region south of 60°S is 100 μg S m^{-2} d^{-1} and represents 26-30% (36-42%) of the

total MSA deposition at the coast (inland). Coastal areas are defined as coastal grid boxes for Antarctica plus one grid box to the north and south (±2° latitude) to estimate marine influence, and inland areas are defined as grid boxes poleward of coastal areas. To be the dominant source (i.e., >50%) of MSA deposition at the coast (inland), DMS emissions south of 60°S would need to increase by a factor of 1.6 (1.2). For the region south of 60°S to supply 80% of MSA at the coast (inland), DMS emissions would need to increase by a factor of 9-10 (6). *Curran and Jones* [2000] calculated a mean spring through summer surface DMS emissions flux of 300 μg S m^{-2} d^{-1} based on observed surface DMS concentrations in the Australian sector of the Southern Ocean (65°E to 162°E) and the *Liss and Merlivat* [1986] ocean-air gas transfer parameterization. The reported fluxes range from 54 μg S m^{-2} d^{-1} in the spring to the north of the sea ice to 1570 μg S m^{-2} d^{-1} in the summer in the seasonal sea ice zone. Thus, DMS emissions ∼1000 μg S m^{-2} d^{-1} are clearly possible but may be episodic. MSA deposition in the Kettle1999 simulations is already dominated by DMS emissions from south of 60°S, representing 54-62% (84-95%) of coastal (inland) MSA. Mean October-March DMS emissions south of 60°S in the Kettle1999 uncapped run are 320 μg S m^{-2} d^{-1}.

The new DMS dataset constructed by *Lana et al.* [2011] from updated measurements in the Global Surface Seawater Database reduces the magnitude and extent of seasonal hot-spots in DMS concentrations around Antarctica in the austral summer (Figure 2.1e) compared to the Kettle1999 dataset (Figure2.1c), which implies DMS concentrations and hence emissions in our Kettle1999 simulations are overestimated. The emissions estimates based on *Lana et al.* [2011] are bracketed by the DMS emissions estimates from Simó and Dachs and Kettle1999 datasets both globally (Section 3.1) and regionally south of 60°S (Table 2.3). *Lana et al.* [2011] do not address the question of DMS emissions estimates from within sea ice in their paper, and so the seasonal cycle and magnitude of DMS emissions from sea ice itself remains an open question.

2.4.5 Controls on DMS emissions variability: relative influence of sea ice extent and wind speeds

Here we seek to understand the model controls on DMS emissions in the Southern Ocean and just how strongly the DMS emissions are modulated by the variability in sea ice and the variability in wind. We first examine the relationship between DMS emissions south of 60°S and the latitude of mean October-March sea ice extent in the Simó and Dachs and Kettle1999 capped runs (Figure 2.11) and for the difference in emissions between the respective uncapped and capped runs (Figure 2.12). The Southern Ocean between 60°S and the Antarctic coast is divided into 15° longitudinal sectors and a time series of sea ice extent and DMS emissions is computed from the October-March mean in each sector. While recognizing that sea ice extent and DMS emissions in some sectors may have stronger correlations than in other sectors, we combine the time series from all sectors into a single scatter plot and compute a single correlation coefficient to represent general circumpolar relationships. We do the same to examine the relationship between DMS emissions and mean wind speed in each sector.

We expect the strongest relationship between sea ice extent and DMS emissions in our runs that have the largest gradient in DMS surface concentration across the ice edge. The strongest gradient exists in the Kettle1999 capped simulation (Figure 2.1c), and thus we see the strongest correlation ($r^2 = 0.30$) between DMS emissions and sea ice extent in the Kettle1999 capped run (Figure 2.11c). The much weaker gradient in the Simó and Dachs dataset results in a much smaller correlation ($r^2 = 0.11$) between sea ice extent and DMS emissions in the Simó and Dachs capped run (Figure 2.11a). The sea ice extent-DMS emissions relationship is weak in the Simó and Dachs capped run, and so the winds become a more important factor ($r^2 = 0.46$, Figure 2.11b).

The relationship between sea ice extent and DMS emissions for the difference between the Simó and Dachs uncapped and capped runs, which isolates DMS emissions from sea ice only, is shown in Figure 2.12a. As expected for DMS emissions restricted to the sea ice, there is a positive relationship between sea ice extent and DMS emissions. Surprisingly, at most only 60% of the variability in DMS emissions can be explained by variations in sea ice

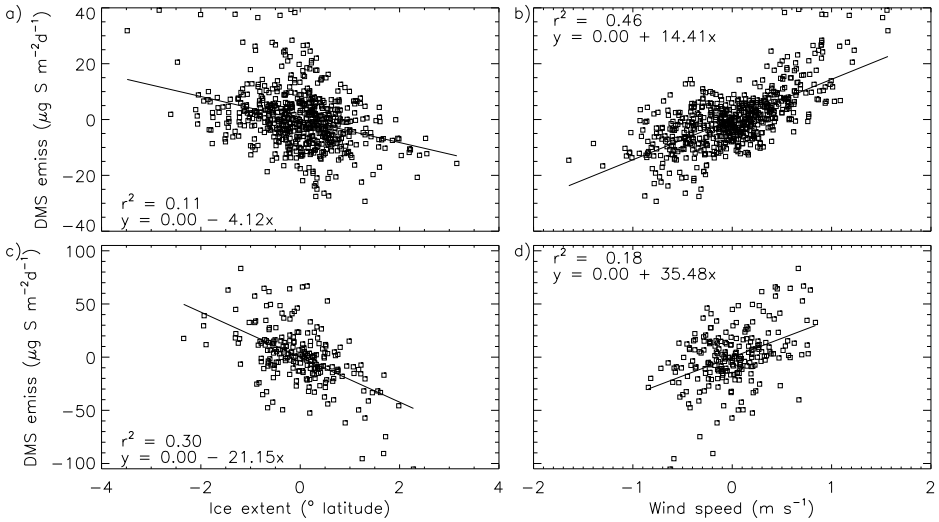

Figure 2.11: Correlation of (a) DMS emissions anomalies (μg S m^{-2} d^{-1}) versus sea ice extent anomalies (° latitude) ($r^2 = 0.11$), and (b) DMS emissions anomalies versus wind speed anomalies (m s^{-1}) ($r^2 = 0.46$) for Simó and Dachs capped run and (c) ($r^2 = 0.30$) and (d) ($r^2 = 0.18$) for the Kettle1999 capped run. Time series of seasonal October-March means are computed over 15° sectors south of 60°S for each field, and all sectors are combined to compute the correlation.

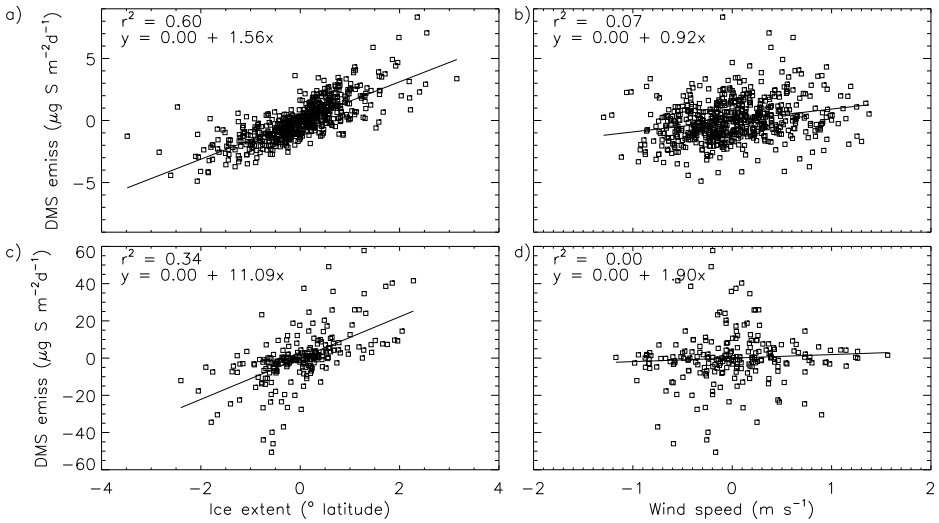

Figure 2.12: Same as Figure 2.11 for difference between Simó and Dachs uncapped and capped runs (a) ($r^2 = 0.60$) and (b) ($r^2 = 0.07$), and difference between Kettle1999 uncapped and capped runs (c) ($r^2 = 0.34$) and (d) (r^2<0.01).

extent itself. Emissions isolated from the sea ice in the Kettle1999 dataset yield a weaker positive relationship between sea ice extent and DMS emissions ($r^2 = 0.34$, Figure 2.12c) than the emissions isolated from the sea ice for the Simó and Dachs dataset. In neither case does wind speed explain much of the variability of DMS emissions ($r^2<0.07$) for emissions isolated from the sea ice (Figure 2.12b and d).

We expected a fairly strong relationship between sea ice extent and DMS emissions in our capped scenarios (both Simó and Dachs and Kettle1999) given the prescribed gradient in DMS concentrations across the sea ice edge. Seasonal attribution of DMS emissions variability, however, is strongly dependent on the characteristics of the underlying surface seawater DMS concentration dataset. The weak correlation between DMS emissions and sea ice extent in the Simó and Dachs capped run is a consequence of the interplay between the characteristics of DMS concentrations (magnitude, seasonal cycle, and meridional gradients), the seasonal cycle of ice extent, and the relative contribution of wind speed. Wind speed plays a dominant role in the Simó and Dachs capped simulation because of the combination of increasing wind speeds and increasing DMS concentrations equatorward. The stronger role of sea ice variability and reduced role of wind in the Kettle1999 sensitivity simulations can be ascribed to a combination of a stronger gradient of DMS concentrations across the ice edge in the Kettle1999 capped simulation, the increasing DMS concentrations poleward, and the influence of a stronger seasonal cycle of DMS surface concentrations in the Kettle1999 dataset.

When DMS emissions exclusively from the sea ice area are considered, (i.e., the difference between the uncapped and capped scenarios), we find that the sea ice variability explains only a fraction of the variability in DMS emissions (34-60%), for both the Simó and Dachs and Kettle1999 simulations. This is in spite of the fact that ice expands northward into regions associated with generally higher mean wind speeds. For sea ice to dominate the variability in DMS emissions in the sea ice zone, the effect of stronger winds north of the sea ice must be compensated by strong DMS emissions associated with the sea ice itself. A better understanding of the peculiarities of DMS emissions from within the sea ice is important for understanding whether DMS emissions in the Southern Ocean are dominated by variability in sea ice extent.

2.4.6 Sensitivity to BrO oxidation mechanism

The BrO sensitivity simulation results in a 55% increase in the global annual MSA production rate. The increase in MSA production leads to a commensurate increase in October-March MSA deposition in Antarctica of 49%. However, the addition of BrO chemistry does not change the fraction of sulfur deposition to Antarctica that originates from sea ice (∼7%).

The addition of the BrO oxidation pathway induces more rapid DMS oxidation in the high latitude boundary layer which leads to shorter DMS lifetimes. The lifetime of DMS in the high latitudes decreases to 0.9-1.1 days for October-March, and unlike the Simó and Dachs simulations, has no meridional gradient approaching the poles. Increased production of MSA in the boundary layer results in more efficient deposition and leads to shorter MSA lifetimes south of 60°S. The lifetime of MSA south of 60°S decreases to 5.6 days for October-March, compared to 8.9 days in the Simó and Dachs capped simulation. The yield of MSA from DMS oxidation increases to 34% in the BrO simulation from 17% in the Simó and Dachs simulations for the high latitudes south of 60°S.

The net transport of sulfur species originating from DMS emissions from the sea ice remains northward though the distribution is narrower than the Simó and Dachs simulations (See Figure 2.9); 50% is deposited to the north of 62°S. The sensitivity of MSA deposition to DMS emissions from the sea ice is nearly doubled in coastal regions compared to the Simó and Dachs simulations (See Figure 2.10b), and accounts for up to 20% of MSA deposition in the Ross, Amundsen-Bellingshausen, and Weddell seas regions along the coast (not shown). The sensitivity in the interior of the East Antarctic Plateau is approximately the same. The local (i.e., south of 60°S) source of MSA to the coastal (inland) areas of Antarctica increases to 46-48% (52-57%) compared to 26-30% (36-42%) in the Simó and Dachs simulations (See Sec. 4.4).

The shortening of the modeled DMS and MSA lifetimes under the BrO sensitivity simulation improves the probability of retaining an ice core signal of local DMS emissions from sea ice. The three year sensitivity simulation however is too short to estimate correlations between MSA and sea ice extent / DMS emissions. Since DMS from south of 60°S in the

BrO sensitivity simulations still does not dominate MSA deposition in Antarctica and there is still relatively small interannual variability in sea ice extent during this time period, we would not expect correlations between MSA and sea ice extent to be significantly improved. It does, however, warrant further study, with a more careful implementation of the BrO oxidation scheme.

2.4.7 Sensitivity to GEOS-5 meteorology

Here we investigate the sensitivity of our results to the underlying meteorological fields driving the model. The boundary layer is not well resolved in GEOS-4 meteorological reanalysis which might lead to an overestimation of the exchange between the boundary layer and the free troposphere and hence an overestimation of both DMS and MSA lifetimes. A GEOS-5 sensitivity study (Table 2.1) has been performed with the GEOS-5 meteorological fields, which have a higher boundary layer resolution of 13 layers in the lowest 2 km of the atmosphere, compared to 4.5 layers in GEOS-4.

These sensitivity simulations result in a shorter global October-March lifetime of DMS and MSA by 8% and 27% respectively compared to the capped simulation, which is significant with respect to the range of variability within the capped run (1.5% and 5% respectively). Since oxidant fields are unchanged and DMS is unaffected by changes in precipitation in GEOS-5, the main difference in the DMS lifetime between using the GEOS-4 and GEOS-5 reanalysis is related to the increased boundary layer resolution. Though the global DMS lifetime is shorter (by 8%) because of globally reduced vertical transport to the free troposphere in the GEOS-5 simulations, the DMS lifetimes calculated for the region south of 60°S and the Antarctic continent in the GEOS-5 capped sensitivity run fall consistently within the range of lifetimes found in the capped run.

Changes in precipitation play a role in the changes in regional MSA lifetimes in the GEOS-5 sensitivity runs. MSA lifetimes are substantially shorter in the global mean (27%), shorter for south of 60°S (11%), and much longer (by more than a factor of 2) over Antarctica, all outside the range of lifetimes found for the capped run. The precipitation between 30°S and 60°S increases by 25-100% in the GEOS-5 reanalysis relative to GEOS-4, a cor-

rection of the low bias noted by *Bloom et al.* [2005]. This leads to shorter lifetimes and lower burdens in air masses entering the high latitudes and therefore less transport of sulfur species toward the pole. Indeed, as discussed above, in the GEOS-5 sensitivity simulations only 4.1% of sulfur emitted from the sea ice is deposited in Antarctica, compared to 7.7% for the GEOS-4 Simó and Dachs simulations. The substantial increase in MSA lifetime over Antarctica is caused by the decrease in precipitation over the Antarctic continent which causes an increase in the fraction of MSA loss via dry deposition (31%, compared to 18% using GEOS-4). The area dominated by dry deposition in GEOS-4 is confined to the East Antarctic Plateau, with a gentle gradient toward more wet deposition at the coasts. In the GEOS-5 simulation, the area dominated by dry deposition expands greatly, leaving only coastal areas and the Ronne, Filchner and Ross ice shelves dominated by wet deposition. The transition between regions dominated by dry and wet deposition occurs over a much shorter spatial scale in the GEOS-5 simulation. Despite the impact of the meteorological fields on the spatial distribution of MSA wet and dry deposition, the GEOS-5 sensitivity simulations show that DMS emissions from south of 60°S account for 35-40% (50-61%) of coastal (inland) MSA deposition to Antarctica, which is similar to the results for the Simó and Dachs runs with GEOS-4.

2.5 Conclusions

We have run a series of global chemical transport model (GEOS-Chem) simulations in an effort to better understand the spatial patterns of MSA deposition and snow concentrations in Antarctica and its relationship to sea ice. Simulations span the period 1985 through 2004, forced with assimilated GEOS meteorological data and observed sea ice extent. We varied the sea surface DMS concentrations associated with sea ice over the austral summer from October through March to understand the influence of DMS emissions from the sea ice zone on the oxidation of DMS to MSA and the transport and deposition of MSA to the Antarctic continent. Our model scenarios by construction implement a relationship between sea ice extent and DMS sea surface concentrations. We estimated correlation coefficients of MSA concentrations in snow with sea ice extent within the model. The model can reproduce the magnitude of correlation coefficients but not the spatial relationship of

correlation coefficients reported in ice core studies.

We find that the net transport of DMS emissions from the sea ice zone is northward and only a small fraction (4–9.6%) of sulfur emissions from the sea ice zone is deposited in Antarctica. The fraction of MSA deposition that originates from DMS in the sea ice zone (i.e., from south of 60°S) ranges from 26–95%, depending on the simulation and region of Antarctica. This result is strongly dependent on the absolute magnitude of emissions in the sea ice zone. In order for Antarctic MSA deposition to be dominated (i.e., >50%) by DMS emissions within the sea ice zone, sustained DMS emissions throughout austral spring and summer would need to be on the order of 120-160 μg S m^{-2} d^{-1}, which falls within the wide range of observations [e.g., *Curran and Jones*, 2000]. More complete information about the magnitude of high-latitude seawater DMS concentrations and the influence of sea ice on DMS emissions is crucial.

Lifetimes of both DMS and MSA are highly sensitive to the presence of halogen oxidants. Without oxidation of DMS by BrO, high latitude lifetimes of DMS and MSA are longer than in the global means and local and regional signals of DMS emissions would be expected to be diluted by transport and mixing. Inclusion of a BrO oxidation mechanism demonstrates a strong relative importance of this pathway at high latitudes and improves the potential for retaining a local signal of DMS emissions in MSA deposition in Antarctica.

In order for MSA recorded in ice cores to be related to sea ice extent, not only must DMS emissions from the sea ice zone be the dominant source region of MSA to Antarctica but sufficient variability of DMS emissions must be attributed to sea ice variability (as opposed to variability related to other factors such as wind speeds). We find that the variability in sea ice extent explains only 11–30% of the variability of DMS emissions south of 60°S, and only 34-60% of the variability of DMS emissions when considering only DMS emissions from the sea ice itself. This is consistent with the findings of *Preunkert et al.* [2007], who reported a poor correlation of DMS seawater concentrations with sea ice extent, and might be expected given the small interannual variability in sea ice extent compared to the area over which DMS emissions in the Southern Ocean are derived. Wind speeds also play a role in DMS emissions variability, but the relative influence of sea ice extent compared to wind speed on DMS emissions is dependent on the seasonal cycle, magnitude, and meridional gradients of

the seawater DMS concentrations. In addition to a need for improved information about seawater DMS concentrations in the sea ice zone, information on the sea-to-air transfer of DMS from sea ice and its dependence on physical factors such as as wind speed and SST are crucial for evaluation of the importance of sea ice on Southern Ocean DMS emissions and the resulting MSA deposition to Antarctica. Our analysis has focused on present-day conditions and sea ice extents on interannual timescales. Interpretation of MSA deposition in ice core records on glacial-interglacial timescales, for which variability in sea ice extent is much larger, remains an open question.

Acknowledgements

This project was supported through NSF grant ANT-0739127. The authors would like to thank A. Lana and R. Simó for providing the gridded Simó and Dachs DMS dataset, and N. Bertler for providing the dataset of Antarctic snow and ice core MSA measurements. Measurements performed at Amsterdam Island were supported by the French Polar Institute (IPEV) within the AEROTRACE program. The authors would also like to thank S. Elliott and two anonymous reviewers for comments and suggestions that strengthened and improved the manuscript.

Chapter 3

MODELED MODERN VERSUS LGM NON-SEA-SALT SULFATE AND METHANESULFONIC ACID (MSA) DEPOSITION IN ANTARCTICA

This chapter discusses the glacial-interglacial variations in MSA and nssSO_4^{2-}. It is to be submitted to the journal *Geophysical Research Letters*. Co-authors will include Becky Alexander, Cecilia M. Bitz, Eric J. Steig and others.

Abstract

Ice core observations on the East Antarctic Plateau (EAP) show that MSA concentrations are much larger than non-sea-salt sulfate (nssSO_4^{2-}) concentrations during the last glacial maximum (LGM) relative to the modern period, though both are primarily from the same source, dimethylsulfide (DMS). It has been suggested that very high MSA concentrations during the LGM were indicative of higher oceanic primary productivity and DMS emissions from the ocean in the LGM compared to the modern day. Studies have also shown that MSA is subject to post-depositional volatilization, especially during the modern period in low snow accumulation and high acidity environments. Using a chemical transport model driven by meteorology from a global climate model, we examine the sensitivity of both MSA and nssSO_4^{2-} deposition to the differences between the modern and LGM climates, including sea ice extent, atmospheric and sea surface temperatures, atmospheric oxidant concentrations, and meteorological conditions. We are unable to find a mechanism whereby MSA deposition fluxes are much larger than nssSO_4^{2-} deposition fluxes in the LGM relative to the modern period on the East Antarctic Plateau. We conclude that the observed differences between MSA and nssSO_4^{2-} on glacial-interglacial time scales are primarily due to post-depositional processes that affect the ice core MSA concentrations, and MSA on the EAP therefore is indicative of neither ice extent nor biological productivity on these time scales. Based on modeled nssSO_4^{2-}deposition, we can not rule out the possibility of higher DMS emissions in the LGM. If oceanic DMS production and ocean-to-air fluxes in the sea ice zone are significantly enhanced by the presence of sea ice as indicated by modern day observations, we suggest that the potentially larger amplitude of the seasonal cycle in sea ice extent in the LGM implies a more important role for sea ice in modulating the sulfur cycle during the LGM compared to the modern period.

3.1 Introduction

Dimethylsulfide (DMS) is biogenically produced in the surface ocean and oxidizes in the atmosphere to become the major source of both methanesulfonic acid (MSA) and non-sea-salt sulfate ($nssSO_4^{2-}$) aerosol in the remote marine troposphere. MSA and $nssSO_4^{2-}$ are removed from the atmosphere via wet and dry deposition to the surface, and they accumulate in ice cores. Ice core concentrations of these compounds on the East Antarctic Plateau (EAP, at Dome C and Vostok) from the last glacial maximum (LGM) compared to the modern period are a factor of 5 to 9 times higher in the LGM for MSA but only a factor of 2 higher in the LGM for $nssSO_4^{2-}$ [*Legrand et al.*, 1991; *Udisti et al.*, 2004]. An increase by factor of two in the LGM for either species can be explained by the lower accumulation rate of the LGM compared to the modern day, but the much larger factor for MSA requires an additional explanation.

In contrast, glacial-interglacial variation in MSA concentrations in the Siple Dome ice core are of opposite sign and are lower in magnitude. For the LGM, the Siple Dome ice core MSA concentrations are lower than the modern period by 30-40% [*Saltzman et al.*, 2006], while $nssSO_4^{2-}$ concentrations are lower than modern day by 20% [*Kurbatov et al.*, 2006; *Dunbar and Kurbatov*, 2011].

Surface seawater DMS concentrations in the modern period are known to be high in the sea ice zone near Antarctica compared to the global average [e.g., *Trevena and Jones*, 2006], though the mechanisms and magnitude of DMS emissions and gas exchange from within the sea ice zone is still the subject of active research [e.g., *Loose et al.*, 2011; *Stefels et al.*, 2012]. It has been suggested that the high LGM MSA concentrations on the East Antarctic Plateau are indicative of increased oceanic DMS production and emissions as a result of increased biological activity during the LGM [*Legrand et al.*, 1991]. However, it has since been demonstrated that MSA is volatilized in firn layers under conditions of low snow accumulation rates and high acidity, as is found on the EAP during interglacial periods. In glacial periods, higher alkalinity due to increased dust concentrations is thought to reduce this post-depositional loss of MSA [*Wagnon et al.*, 1999; *Weller et al.*, 2004]. $NssSO_4^{2-}$, by contrast, is stable at deposition and is not influenced by post-depositional processes

[*Silvente and Legrand*, 1993]. The snow accumulation rate also affects MSA volatility, and the higher accumulation rate at Siple Dome may inhibit the post-depositional loss of MSA in the modern period there.

Here, we investigate the influence of climatic factors such as sea ice, sea surface and atmospheric temperatures, precipitation, circulation, and ocean-to-atmosphere DMS emissions on the variability in MSA and nssSO_4^{2-} snow concentrations and deposition fluxes on the EAP. Using a global chemical transport model we show that these climatic factors generally have the same effect on both MSA and nssSO_4^{2-} deposition with small ($< \pm 12\%$) variations, and explain only only a small amount of the differences in the comparison of modern and LGM MSA and nssSO_4^{2-} concentrations. The observed large differences in MSA between the modern and LGM periods on the EAP are likely due primarily to enhanced post-depositional loss during interglacial periods relative to the last glacial period. The nssSO_4^{2-} deposition fluxes also suggest that DMS emissions in the LGM were likely at least as high as the modern period.

3.2 Model description and methods

The ICECAP (ICE age Chemistry And Proxies) model used in this study combines (1) a global climate model (GCM, the GISS Model-E) [*Schmidt et al.*, 2006], (2) an equilibrium global terrestrial vegetation model (BIOME4) [*Kaplan et al.*, 2003], (3) a stratospheric chemistry model (Linoz) [*McLinden et al.*, 2000], and (4) a global chemical transport model (GEOS-Chem v8-01-04) [*Bey et al.*, 2001]. The GISS Model-E produces meteorology consistent with present-day, preindustrial, or LGM climate boundary conditions. The meteorological fields are then used to drive GEOS-Chem and BIOME4. GEOS-Chem uses the vegetation type and leaf area index calculated by BIOME4 to determine biogenic volatile organic compound emissions as a function of temperature, solar radiation, leaf area index, and plant functional type [*Guenther et al.*, 2006]. In addition, GEOS-Chem is coupled to Linoz to capture the effect of a changing stratospheric ozone column on tropospheric photolysis rates and cross-tropopause fluxes. GEOS-Chem is then run to generate a set of climatological oxidant fields for each climate scenario generated by GISS Model-E. Finally, these oxidant concentrations are used to run the offline-aerosol simulations with GEOS-

Chem described herein. In forthcoming studies, the ICECAP model will be used to study the effect of atmospheric oxidant conditions on chemistry and isotopes on glacial-interglacial time scales.

Boundary conditions for GISS Model-E include sea ice extent, sea surface temperatures (SSTs), topography, greenhouse gas concentrations, and orbital forcing, as summarized in Table 3.1. Four climate scenarios were produced from GISS Model-E: Present-day (PRES), pre-industrial holocene (PIH), and LGM scenarios based on *CLIMAP* [1976] (CLIMAP) and *Webb et al.* [1997] (WEBB) sea ice and SSTs. The GISS Model-E and GEOS-Chem models were run at $4^\circ \times 5^\circ$ resolution. Surface seawater DMS concentrations are specified from the climatology of *Lana et al.* [2011] for all climate scenarios (for lack of better information in the LGM), and DMS emissions are parameterized from wind speed and SSTs following *Liss and Merlivat* [1986] for wind speeds <2.25 m s^{-1} and *Huebert et al.* [2010] for wind speeds >2.25 m s^{-1}. We run the ICECAP model for three years for each of the four climate scenarios, after a 1.5 year spinup.

Table 3.1: Climate scenarios and boundary conditions used in this study.

Period	Modern		LGM	
Climate scenario	Present-day (PRES)	Pre-Industrial Holocene (PIH)	CLIMAP	WEBB
Sea Ice/SSTs	HadISST 1990s[a]	HadISST 1880s[a]	*CLIMAP* [1976]	*Webb et al.* [1997]
Topography	modern	modern	ICE-5G[b]	ICE-5G[b]
Greenhouse gases				
CO_2 (ppm)	354.3	280.4	188	188
CH_4 (ppm)	1.69	0.73	0.39	0.39
Strat. O_3[c]	1990s	1880s	1880s	1880s

[a] *Rayner et al.* [2003]
[b] *Peltier* [2004]
[c] *Hansen et al.* [2007]

DMS chemistry in the model is simplified as in *Chin et al.* [1996, 2000] as follows:

$$\mathrm{DMS} + \mathrm{OH} \rightarrow \mathrm{SO_2} + ... \tag{3.1}$$

$$\mathrm{DMS} + \mathrm{OH} \rightarrow 0.75 \cdot \mathrm{SO_2} + 0.25 \cdot \mathrm{MSA} + ... \tag{3.2}$$

$$\mathrm{DMS} + \mathrm{NO_3} \rightarrow \mathrm{SO_2} + ... \tag{3.3}$$

An additional reaction for BrO oxidation was added as in *Hezel et al.* [2011], and used in a set of sensitivity studies:

$$\mathrm{DMS} + \mathrm{BrO} \rightarrow 0.6 \cdot \mathrm{SO_2} + 0.4 \cdot \mathrm{MSA} \tag{3.4}$$

The same climatological BrO concentrations were used in both the modern and LGM climate simulations.

For each climate scenario, we examine the effect of sea ice on DMS emissions in two methods. In the first, sea ice impedes DMS emissions, i.e., DMS emissions are 'capped' where there is sea ice concentrations are greater than zero. In the second, sea ice has no effect on DMS emissions during the austral summer (October through March), i.e., DMS emissions are 'uncapped.'

In our analysis, we show snow concentrations and deposition fluxes of MSA and nss$\mathrm{SO_4^{2-}}$ normalized to the modern period (in both observations and model results) to focus on the relative change between the modern and LGM periods. By normalizing LGM observations and model results to the modern period, we minimize the impacts of biases in the model compared to the observations, given the assumption that biases in the model do not change substantially under different climate scenarios (e.g., uncertainties in modeled deposition fluxes are similar in all climates). We compare modeled snow concentrations to observations, and we also analyze deposition fluxes which are expected to better reflect the atmospheric concentrations at low accumulation sites [*Wolff et al.*, 2006].

3.3 Results and Discussion

3.3.1 Comparison of LGM to modern day snow concentrations and deposition fluxes

In Fig. 3.1, we show observed and modeled MSA and nssSO_4^{2-} snow concentrations for the LGM on the EAP, normalized to the modern period. The simulated snow concentrations are higher in the LGM than the modern period only when we allow DMS emissions to be uninfluenced by the presence of sea ice as in the uncapped simulations. Since the DMS emissions are highest at the minimum sea ice extent in the modern climate, there are relatively small differences between the capped and uncapped runs in the modern period as discussed in *Hezel et al.* [2011]. In contrast, the summer sea ice cover is quite large in the LGM (according to the *CLIMAP* [1976] and *Webb et al.* [1997] datasets), so capping DMS emissions has a considerable effect on MSA and nssSO_4^{2-} deposition. We return to the issue of sea ice extent and DMS emissions in the next section.

In Fig. 3.2, we show observed and modeled MSA and nssSO_4^{2-} surface deposition fluxes for the LGM on the EAP, again normalized to the modern period. Observed deposition fluxes are calculated using the measured ice core concentrations [*Udisti et al.*, 2004] multiplied by the accumulation rate [*Parrenin et al.*, 2007]. In contrast to the observations, which show similar (nssSO_4^{2-}) or enhanced (MSA) deposition fluxes in the LGM relative to the modern period, the model calculates lower MSA and nssSO_4^{2-} deposition fluxes in the LGM than modern by nearly 50% for all simulations.

The modeled LGM precipitation on the EAP is roughly half of that inferred from ice cores (Fig. 3.3, both in absolute values and relative to the modern period) [*Parrenin et al.*, 2007]. The underestimate of modeled LGM precipitation rate compared to observations explains why the model agrees with observations of nssSO_4^{2-} snow concentrations, but not with deposition fluxes. Atmospheric circulation affects modeled temperature and moisture availability and hence the precipitation flux and the MSA and nssSO_4^{2-} deposition fluxes. It is impossible to determine whether it is the uncertainties in ice core accumulation rate or the uncertainties in GCM precipitation estimates that dominate the mismatch in the model precipitation compared to the observed ice core accumulation rate in the LGM. We note, however, that the observed deposition fluxes are very sensitive to uncertainties in the

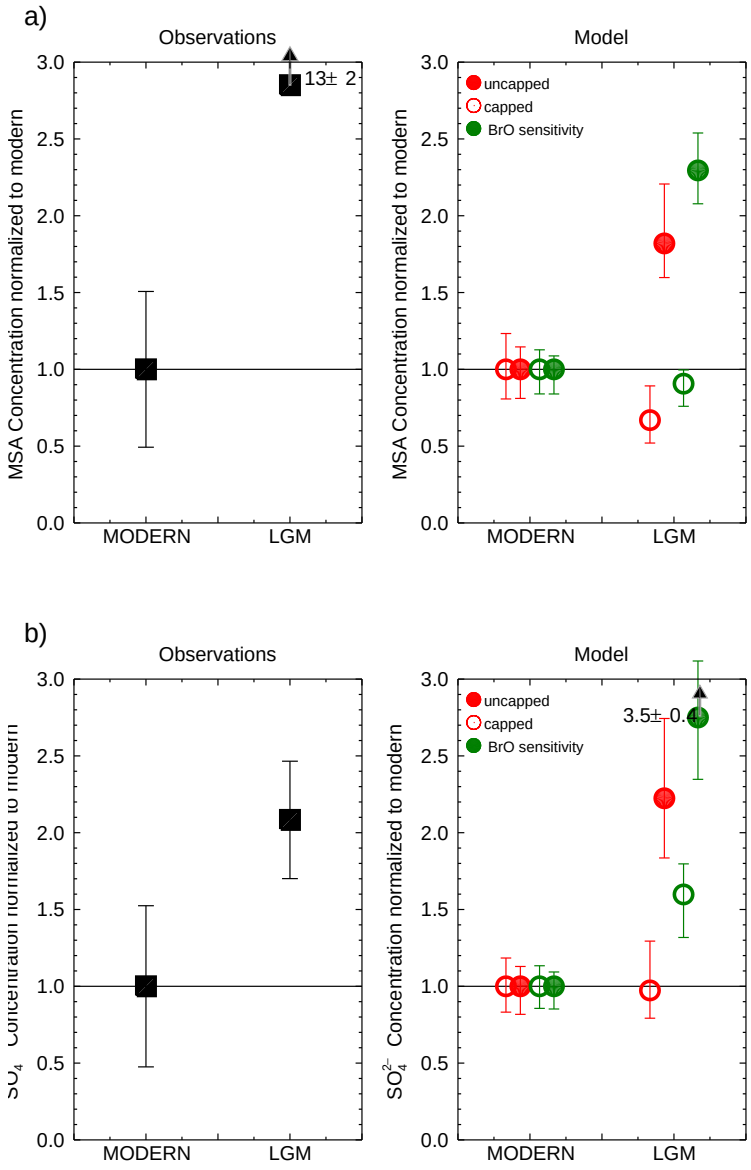

Figure 3.1: MSA (a) and nssSO_4^{2-} (b) snow concentrations (unitless, normalized to modern) on the East Antarctic Plateau for observations at EPICA Dome C (black) [*Udisti et al.*, 2004; *Wolff*, 2006], modern (PRES and PIH) and LGM (CLIMAP and WEBB) climate scenarios. DMS emissions scenarios are uncapped (open circles) and capped (closed circles). Standard chemistry is red, and BrO sensitivity simulations are green. For observations, error bars indicate one standard deviation of all measurements from present to 500 yr BP and 20-22 ky BP. For the model, the error bars represent the range of annual-mean values from the 3-year simulations.

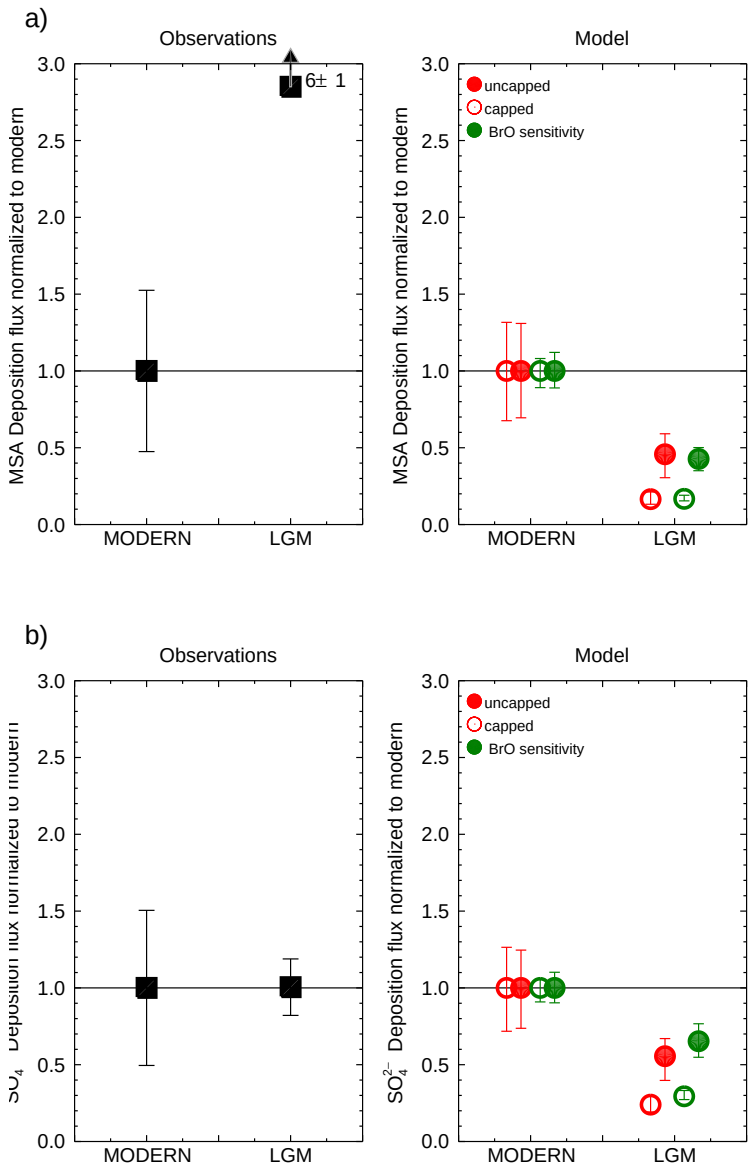

Figure 3.2: MSA (a) and nssSO_4^{2-} (b) deposition fluxes (unitless, normalized to the modern period), averaged on the East Antarctic Plateau, as in Fig. 3.1. Observations from *Udisti et al.* [2004]; *Wolff* [2006]

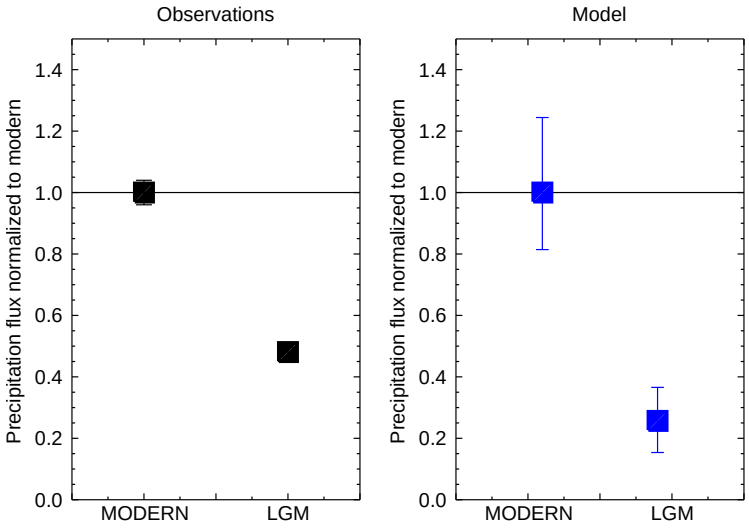

Figure 3.3: Precipitation on the East Antarctic Plateau normalized to modern period in the observations (left, EPICA Dome C [*Parrenin et al.*, 2007])and on the right in the model. Error bars as in Fig. 3.1

accumulation rate estimate, especially in areas such as the EAP where accumulation is low.

3.3.2 LGM sea ice and DMS emissions

GCM estimates of sea ice extent during the LGM austral summer vary widely [*Braconnot et al.*, 2007b; *Otto-Bliesner et al.*, 2007]. Summer sea ice extent in the SST reconstructions from *CLIMAP* [1976] and *Webb et al.* [1997] are quite extensive (up to 48°S and 44°S, respectively). The underestimate in both the LGM concentrations and deposition fluxes of MSA and nssSO_4^{2-} on the EAP in the capped scenarios compared to observations suggest that the DMS emissions are severely underestimated when sea ice prevents gas exchange at the ocean-atmosphere interface. The better agreement of concentrations and deposition fluxes in the uncapped scenarios suggests that DMS emissions in the LGM are at least as high as modern day emissions in spite of presumably more extensive LGM sea ice. There is still a modeled underestimate in deposition flux for both MSA and nssSO_4^{2-} for the uncapped simulations. We discuss the sensitivity of deposition flux to DMS emissions in

the model in section 3.3.6 below.

There are two possible mechanisms for achieving DMS emissions in the LGM that are similar to the modern period. (a) Summer sea ice extent is closer to modern day summer ice extent than suggested by the *CLIMAP* [1976] and *Webb et al.* [1997] SSTs. This possibility is corroborated by more recent ocean sediment core interpretations that suggest a low LGM summer sea ice extent [*Gersonde et al.*, 2005]. This is also consistent with the findings of *Castebrunet et al.* [2006] who showed that relaxing the cap on DMS emissions in the LGM led to better agreement in nssSO_4^{2-} deposition fluxes with observations. (b) Relatively large sea ice extent with low fractional coverage could persist in the LGM summer which could enable and/or enhance DMS emissions from open water leads [*Zemmelink et al.*, 2005].

We assume in this study that the *Lana et al.* [2011] seawater DMS concentration dataset captures broad seasonal variations in DMS in the Southern Ocean in the wake of retreating sea ice for the modern period. Since LGM winter sea ice extent is much larger than modern winter ice extent, the spatial pattern of the *Lana et al.* [2011] dataset may not reflect the spatial distribution of DMS concentrations appropriately for seasonal ice retreat in the LGM. Because of the much larger seasonal maximum of sea ice in the LGM, enhanced DMS emissions in the sea ice zone could have a greater effect on the sulfur cycle in the glacial periods than in the interglacials. DMS emissions from within the sea ice area is the subject of active research, and the implications of sea ice emissions in the LGM would be more appropriately studied with a coupled sea ice-biogeochemical model, such as that described in *Cameron-Smith et al.* [2011]. We focus instead on examining whether there is a mechanism by which the surface deposition fluxes of MSA increase more than nssSO_4^{2-} in the LGM climate compared to modern day, as in the observations from the EAP.

3.3.3 Effect of wind speed and SSTs on DMS emissions in different climates

Since the uncapped simulations all make use of the same seawater DMS concentrations, we can evaluate the influence of differences in wind speed and SSTs on DMS emissions among the four different climate scenarios. Differences in modeled DMS emissions in the modern and LGM simulations are <12% (globally and south of 60°S), and therefore the net effect

of variability in wind speed and SSTs on DMS emissions is small. For the remainder of this paper, we consider the DMS emissions in the uncapped scenarios to be relatively constant among all four climate scenarios. We acknowledge that the surface wind stress in the GISS Model-E is low over the Southern Ocean compared to reanalysis [*Schmidt et al.*, 2006], and this may contribute to smaller than expected differences in glacial-interglacial wind speed, and hence DMS emissions, at the surface.

3.3.4 Role of temperature and oxidants in MSA yield relative to SO_2 *during DMS oxidation*

Kinetics and observations show that the MSA yield from DMS oxidation increases with decreasing temperature due to an increase in the rate constant of DMS oxidation via the OH adduction pathway [*Barnes et al.*, 2006]. This is often invoked as an explanation for the increasing gradient in the ratio of MSA to nssSO_4^{2-} aerosol from the equator to the poles [See *Castebrunet et al.*, 2009, for a discussion]. It might be expected that lower temperatures in the LGM simulations compared to modern day would also result in an increase in the relative yield of MSA. Our simulations show that the global relative yield of MSA from DMS in the LGM increases by 4-15% over the modern day due to temperature differences using the simplified DMS chemistry of *Chin et al.* [1996, 2000], with an additional increase of up to 17% due to differences in oxidant (mainly OH) concentrations among the climate scenarios. In the high latitudes south of 60°S, however, the relative yield of MSA increases in the LGM by less than 3% compared to the modern day due to both temperature and oxidants. The differences in high latitude glacial-interglacial temperatures force only a small change in MSA yield because the oxidants and temperatures (and therefore reaction rate constants) already favor MSA production during both periods.

3.3.5 Sensitivity of MSA and nssSO_4^{2-} *deposition flux to DMS + BrO oxidation*

Halogen chemistry has been shown to be important in the oxidation of DMS [*Boucher et al.*, 2003; *Read et al.*, 2008]. To understand the potential impact of this chemistry on MSA and nssSO_4^{2-} deposition fluxes, we discuss here the sensitivity simulations that include the DMS + BrO oxidation pathway added to the PRES and WEBB simulations, here referred to as

PRES-BrO and WEBB-BrO. The BrO oxidation mechanism shortens the austral summer lifetime of DMS from the range of 1.2-3 days to < 1 day at all latitudes and results in a much greater relative yield of MSA compared to simulations without BrO oxidation. This increase is due to the MSA branching ratio (0.4) imposed in the DMS + BrO oxidation that is higher than that for DMS + OH (0.25, addition channel). In the southern high latitudes in the austral summer, DMS oxidiation by BrO dominates DMS oxidation in both climate scenarios, with the model having up to 75% of summer DMS oxidation via BrO in the PRES-BrO scenario. . MSA deposition fluxes increase and nssSO_4^{2-} deposition fluxes decrease in these PRES-BrO and WEBB-BrO simulations compared to PRES and WEBB simulations respectively.

The BrO simulations (Figs. 3.1 and 3.2 in green) still result in similar behavior in MSA and nssSO_4^{2-} in the LGM compared to the modern period on the EAP, even though BrO dominates DMS oxidation in the high latitudes due to the strong latitudinal gradient in BrO [*Theys et al.*, 2011]. If the dominant chemistry differs between the LGM and the modern periods, then there could be a mechanism for a larger increase in MSA than nssSO_4^{2-} in the LGM relative to the modern period. However, we know of no evidence currently that lends support to this possibility.

3.3.6 Sensitivity of MSA and nssSO_4^{2-} deposition to increased DMS emissions

A increase in DMS emissions was simulated to gauge the sensitivity of MSA and nssSO_4^{2-} deposition to DMS emissions. The first sensitivity test doubled the DMS emissions in the PRES and CLIMAP uncapped scenarios globally. The model response is nearly linear in the MSA deposition response, i.e., a doubling of DMS emissions at every grid cell results in a doubling of MSA deposition at every point. NssSO_4^{2-} deposition also doubled, but exhibited some slight non-linearities in the response due to the greater number of steps involved in the modeled oxidation pathway. The second test looked at the relative influence of emissions from the regions 60°S to the Antarctic continent and 30°to 60°S. On the EAP, about 55-70% of MSA and nssSO_4^{2-} deposition is from the region south of 60°S, and most of the remainder originates from within 30° to 60°S. These ratios were similar among the

three climate scenarios tested (PRES, PIH, and CLIMAP).

We can estimate the increase in modeled DMS emissions in the LGM that would cause modeled LGM deposition fluxes to match the modeled modern MSA and nssSO_4^{2-} deposition fluxes on the EAP. This indicates the sensitivity of deposition to the DMS emissions given the assumptions of the modeling scenarios. We make these estimates for the two regions described above, 60°S to Antarctica, and 30-60°S. If all additional LGM DMS emissions originated from south of 60°S, additional DMS emissions of 0.9 to 1.8 (1.2 to 2.5) times greater than simulated are necessary to match nssSO_4^{2-} (MSA) deposition fluxes in the modern period. If all additional DMS emissions originate from between 30°S and 60°S, additional DMS emissions of 1.4 to 3.1 (2.4 to 5.1) times greater than simulated are necessary to match nssSO_4^{2-} (MSA) deposition fluxes in the modern period. Whether physical and/or biological enhancements to seawater DMS production and emissions under LGM climatic conditions could be responsible for an increase in DMS emissions of this magnitude is an open question.

3.3.7 Post-depositional processes on the EAP

We have attempted to reproduce the relative differences in observed MSA and nssSO_4^{2-} snow concentrations and deposition fluxes in the LGM period compared to the modern period, as shown in Figs. 3.1 and 3.2. In all of our simulations we have found that MSA and nssSO_4^{2-} vary together in the LGM compared to the modern period. We are left to conclude that the observed glacial–interglacial variation in MSA on the EAP is the result of enhanced post-depositional loss in the modern period relative to the glacial period. This is consistent with the interpretation of these processes investigated in *Wagnon et al.* [1999]; *Weller et al.* [2004], which show that increased dust concentrations in the LGM result in reduced volatility of MSA.

Siple Dome observations of MSA and nssSO_4^{2-} also support this conclusion. Since snow accumulation rates are higher at Siple Dome than the EAP (by a factor of 4), there is reduced modern-day post-depositional losses of MSA, and snow concentrations should be roughly proportional to atmospheric concentrations of each species. Both the model and

observations agree that MSA and nssSO_4^{2-} vary synchronously in the glacial period compared to the interglacial. The spatial variability in the West Antarctic region of Siple Dome is large in the model, and so the quality of comparisons to the observations are a function of the precipitation rate in the model at the selected location.

3.4 Conclusions

We have investigated the glacial–interglacial differences in MSA and nssSO_4^{2-} snow concentrations and deposition fluxes in Antarctica using a chemical transport model forced with meteorology from global climate model simulations for the modern period and the LGM. Observations on the East Antarctic Plateau suggest the MSA deposition flux is much higher in the LGM than the modern day, while nssSO_4^{2-} is similar in both periods, indicating a divergence of the two species in the LGM. We have investigated the sensitivity of MSA and nssSO_4^{2-} deposition in the LGM as it relates to climatic influences (SSTs, atmospheric temperatures, atmospheric circulation, precipitation, and oxidant concentrations), and we are unable to reproduce the divergence in these species between the modern and the LGM simulations. We are left to conclude that the observed glacial–interglacial variation in MSA is the result of enhanced post-depositional loss in the modern period relative to the glacial period. This difference in the preservation of the MSA record in these two periods makes it difficult, if not impossible, to interpret MSA records on these time scales in low accumulation areas such as the East Antarctic Plateau, as has been suggested elsewhere [*Wolff et al.*, 2010].

A comparison of observed and simulated nssSO_4^{2-} deposition fluxes (Fig. 3.2) on the East Antarctic Plateau suggests that DMS emissions in the LGM are at least as high as modern day DMS emissions. Given the larger winter ice extent in the LGM (and therefore potentially larger area of retreating ice extent in the austral summer), the contribution of DMS associated with sea ice in the LGM may be more important to the sulfur cycle in the LGM than in the modern day. The model underestimates the relative deposition fluxes of nssSO_4^{2-}on the EAP in the LGM compared to the modern day, and so the possibility of increased DMS emissions during the LGM relative to the modern period can not be ruled out.

Acknowledgements

We would like to thank Loretta Mickley, Lee Murray, Gavin Schmidt, Jed Kaplan, Dylan Jones and Eric Sofen for their work in combining the components of the ICECAP model, on which this project is based. We would also like to thank the EPICA Chemistry Consortium for supplying the Dome C data and Eric Wolff for assistance, as well as Andrei Kurbatov, Eric Saltzman, Ed Brook, and Paul Mayewski for assistance with data from Siple Dome. This project has been supported through NSF grant ANT-0739127.

Chapter 4

PROJECTED DECLINE IN SPRING SNOW DEPTH ON ARCTIC SEA ICE CAUSED BY PROGRESSIVELY LATER AUTUMN OPEN OCEAN FREEZE-UP THIS CENTURY

This chapter is published as an article in *Geophysical Research Letters*, and is reproduced here by permission of the American Geophysical Union.

Hezel, P. J., X. Zhang, C. M. Bitz, B. P. Kelly, and F. Massonnet (2012), Projected decline in spring snow depth on Arctic sea ice caused by progressively later autumn open ocean freeze-up this century, *Geophys. Res. Lett.*, doi:10.1029/2012GL052794, in press.

Abstract

We present the first analysis of snow depths on Arctic sea ice in the Coupled Model Intercomparison Project 5 (CMIP5) because of its importance for sea ice thermodynamics and ringed seal (*Phoca hispida*) habitat. Snow depths in April on Arctic sea ice decrease over the 21st century in RCP2.6, RCP4.5, and RCP8.5 scenarios. The chief cause is loss of sea ice area in autumn and, to a lesser extent, winter. By the end of the 21st century in the RCP8.5 scenario, snowfall accumulation is delayed by about three months compared to the late 20th century in the multi-model mean. Mean April snow depth north of 70°N declines from about 28 cm to 16 cm. Precipitation increases as expected in a warmer climate, but much of this increase in the Arctic occurs as rainfall. The seasonality of snowfall rate grows, with increasing rates in winter and decreasing rates in summer and autumn, but the cumulative snowfall from September to April does not change. Ringed seals depend on spring snow cover on Arctic sea ice to create subnivean birth lairs. The area with snow depths above 20 cm — a threshold needed for ringed seals to build snow caves — declines by 70%.

4.1 Introduction

Despite its importance for physical and biological systems, little is known about current trends in snow depths on sea ice and how snow depths will respond to climate change in the future. It is expected that spring snow depths on sea ice are sensitive to changes in both the sea ice extent and hydrologic cycle, but little is known about current or future expected trends. Competing effects in a warmer climate could drive snow depths in either direction compared to today. It is unclear *a priori* which effect will dominate.

In contrast, the retreat of Arctic sea ice is a well-studied problem. There is clear evidence of a decline in sea ice extent and thickness in the past few decades [e.g., *Kwok and Rothrock*, 2009; *Comiso et al.*, 2008], and climate models predict declines will continue at an equally rapid or, in some cases, an even faster pace through this century [e.g., *Arzel et al.*, 2006; *Zhang and Walsh*, 2006]. A change in snow depth is thought to be a factor in sea ice loss but also with competing effects. Snow accumulation on top of sea ice insulates the sea ice and reduces ocean heat loss to the atmosphere, leading to reduced sea ice growth rates. Reduced snow depth should therefore enhance sea ice growth rates. If this were the only consideration, a decrease in snow depth resulting from the loss of autumn and winter sea ice area would in turn slow the reduction of sea ice area into the future, a negative feedback described in more detail by [*Notz*, 2009]. At the same time, reduced snow depth would melt earlier in spring and more rapidly reveal bare sea ice with its lower surface albedo, a positive feedback which would tend to melt more sea ice.

In a warmer climate the atmospheric moisture flux convergence into the Arctic is expected to increase from rising evaporation rates in lower latitudes. A higher moisture flux combined with greater moisture recycling should increase the precipitation rate, as found in recent observations and in climate models [*Kattsov et al.*, 2007; *Rawlins et al.*, 2010]. If this increase occurs when air temperatures are below freezing, snowfall rates should rise. The question remains whether the rise occurs seasonally when sea ice is present to capture it.

Snow cover on sea ice in spring also provides critical habitat for ringed seals (*Phoca hispida*) to create subnivean birth lairs [e.g., *Smith and Stirling*, 1975; *Smith and Lydersen*,

1991]. To successfully rear young, ringed seals in the central Arctic need on-ice snow depths in April of at least 50 cm in which to form subnivean lairs. Such depths are found in snow drifts next to ridges at times when depths on level ice are at least 20 cm. Thus, the period over which snow accumulates on ice is considered to be "the primary factor influencing the quality of ringed seal breeding habitat" [*Smith and Lydersen*, 1991]. Inadequate snow depths increase pup mortality through exposure and predation [e.g., *Kelly*, 2001; *Ferguson et al.*, 2005; *Lukin et al.*, 2006].

For the first time the CMIP5 has archived snow depth on sea ice. Here we show the evolution of snow depth on Arctic sea ice in 20th and 21st century integrations. We consider these snow depth changes in the context of the changing Arctic sea ice area and snowfall rates. We focus attention on the time evolution of snow depth in April as a measure of integrated snow accumulation at the end of the ice-growth season. April also coincides with the time when ringed seals most depend on snow to raise their young.

4.2 Methods and Validation

We use model output from historical and 21st century integrations from the CMIP5 archive [*Taylor et al.*, 2012b]. We show results for Representative Concentration Pathway (RCP) 8.5 for the 21st century scenario. We choose this scenario because it has the highest radiative forcing and hence is an upper bound of available scenarios. Declines in snow depth in the RCP2.6 and RCP4.5 scenarios (shown in the Auxiliary materials Figure 4.5) occur on a slower timescale. We use all models that archive snow data on sea ice and every available ensemble member (Table 4.1) except where the CMIP5 archived data appeared incorrect. Ensemble means are computed for each model, and then each model mean is weighted uniformly in the multi-model means.

In the CMIP5 archive, the variable for snow depth on sea ice is the average over the ocean covered portion of a grid cell (i.e., snow volume normalized by ocean area), with zero depth over open water. We are interested in the snow depth on sea ice (i.e., snow volume normalized by the sea ice area in each grid cell), so we divide the snow depth per unit ocean area by the sea ice fraction per unit ocean area. We then compute monthly averages of snow depth (normalized by sea ice area) weighted by area for sea ice-covered portion of the

Table 4.1: Models used in snow depth on sea ice study.

Model	Institution	Ensembles	
		Hist.	RCP8.5
BCC-CSM1.1	Beijing Climate Center, China Meteorological Administration (BCC)	3	1
CanESM2	Canadian Centre for Climate Modelling and Analysis (CCCMA)	5	5
CCSM4	National Center for Atmospheric Research (NCAR)	4	5
CNRM-CM5	Centre National de Recherches Meteorologiques / Centre Europeen de Recherche et Formation Avancees en Calcul Scientifique (CNRM-CERFACS)	10	5
GFDL-CM3	NOAA Geophysical Fluid Dynamics Laboratory (NOAA GFDL)	5	1
HadGEM2-ES	Met Office Hadley Centre (MOHC)	1	1
MIROC5	Atmosphere and Ocean Research Institute (The University of Tokyo), National Institute for Environmental Studies, and Japan Agency for Marine-Earth Science and Technology (MIROC)	1	1
MPI-ESM-LR	Max Planck Institute for Meteorology (MPI-M)	3	3
MRI-CGCM3	Meteorological Research Institute (MRI)	5	1
NorESM1-M	Norwegian Climate Centre (NCC)	3	1

ocean north of 70°N using the minimum threshold of 15% ice concentration on the ocean grid. Henceforth in this paper we refer to this quantity as the snow depth north of 70°N.

In spring to first order, the depth of accumulated snow on sea ice depends on the timing of autumn freeze-up and the winter snowfall rates. Second order impacts are discussed at the end of this section. We assess the influence of both of these factors on April snow depths. April is minimally affected by intermodel differences in melt-onset, and therefore, analysis of April focuses our analysis on the cumulative effect of winter processes only. Snow depths on flat ice of 20 – 32 cm are necessary to adequately protect young ringed seals from predation and hypothermia [*Lydersen et al.*, 1990; *Hammill and Smith*, 1991; *Smith and Lydersen*, 1991; *Ferguson et al.*, 2005]. For this analysis, we choose a conservative threshold of 20 cm of snow in April to compare changes in area of sufficient snow depth for ringed seal habitat.

Mean precipitation (both snow and rain) in the Arctic is computed for the Arctic ocean area north of 70°N as area-weighted averages on the atmospheric grid. We compute mean monthly precipitation from November to March as a conservative estimate of winter precipitation occurring after freeze-up and before melt-onset. In a given model over a given time

period, the fraction of precipitation that falls as snow is roughly uniform from November to March, though this fraction differs among models (See Aux. Fig. 4.5).

The multi-model mean April snow depth in the central Arctic (Fig. 4.1) compares well with observational estimates from two sources. *Warren et al.* [1999] produced a climatological mean from measurements made by the Soviet North Pole drifting stations from 1954-1991 over a domain occupied by the stations in the central Arctic. In the same years over the same domain, the multi-model mean April snow depth is 30.1 cm, about 10% below the estimate from the drifting stations, and the root mean square error (RMSE) after removing the area mean bias is 2.4 cm. *Warren et al.* [1999] note that the drifting station depths are measured only for multiyear ice and leads refrozen in early autumn, and they argue that new ice forming after the first snow in September occupies only about 1% of the area of the central Arctic in April. *Kwok et al.* [2011] provide a more recent snow depth estimate using microwave radar measurements along three ∼2000 km transects in April 2009 primarily over the western central Arctic from Operation IceBridge. The multi-model mean along the same transects for 2009 is 31.6 cm, about 11% below the IceBridge depths. The individual models have spatial means in the range ±30% of the multi-model mean, and more than 1/3 of the models have spatial means that are greater than observed. The spatial pattern in the multi-model mean (Fig. 4.1) agrees well with the drifting station climatology (See Fig. 9 in *Warren et al.* [1999]). Given this satisfactory agreement between model and observations, we proceed with an analysis of the future change in snow depths.

The physical processes associated with snow cover in the sea ice component of climate models are often simplified compared to those in the land component because of the computational expense involved with advection of every variable that describes sea ice conditions. We are unaware of any fully-coupled climate models in which the sea ice component has a time-varying snow density, takes into account degradation of snow from rain and refreezing, or explicitly allows wind-blown snow redistribution (though some redistribute snow during ice deformation events). The models also do not distinguish between level and ridged ice or between multiyear and first-year ice, and so we are unable to characterize responses among these different ice conditions. We discuss the consequences of these model simplifications later.

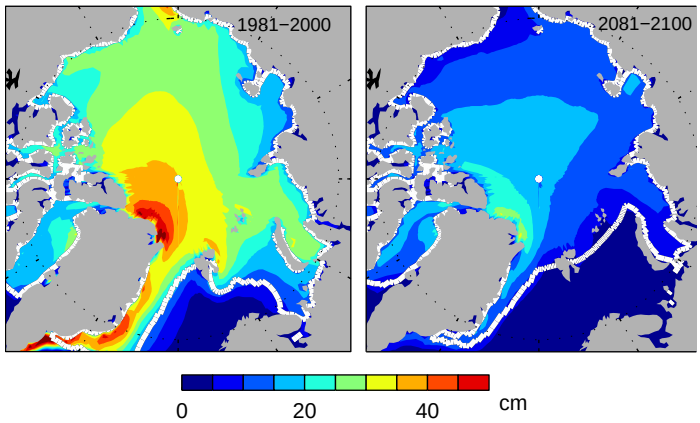

Figure 4.1: Multi-model mean April snow depth (cm) on sea ice for the periods 1981-2000 (left) and 2081-2100 (right) for RCP8.5. The multi-model mean is calculated from the time-mean snow depths on sea ice for each model (or from each model ensemble), including zeros from models when sea ice is absent. The white line is the multi-model mean 15% ice concentration line for each period.

4.3 Results

Arctic snow depths averaged north of 70°N in April from 1850-2100 have little trend prior to the 21st century in the multi-model mean and among individual models (Fig. 4.2a), but snow depths in every model decrease substantially by the end of the period. In the RCP8.5 scenario, the multi-model mean snow depth in April is 28±7 cm for 1981-2000 and 16±5 cm for 2081-2100. The uncertainty represents the intermodel spread and is calculated as one standard deviation of the monthly means for all models over each period. In the RCP4.5 (RCP2.6) scenario, multi-model mean snow depth in April is 22±6 cm (25±6 cm) for 2081-2100, which corresponds to the mean snow depth for a 20-year period centered at 2053 (2034) under the RCP8.5 scenario. The multi-model mean of the relative decline in snow depth in each model (i.e., relative decline of mean at 2081-2100 compared to 1981-2000) for the RCP8.5 (RCP4.5, RCP2.6) scenario is 45±12% (23±7%, 13±6%) (See Aux. Fig. 4.5). We also note that the relationship between snow depth in April versus global mean annual temperature (a proxy for radiative forcing) is approximately linear across models. The same can be said for the relationship between April snow depth and the minimum sea ice

area in September until perennial sea ice disappears. That the slopes of these relationships are similar under each RCP scenario indicates that modeled snow depth responds in the same way in each model to both the forcing and the ice area, with only slightly different sensitivities among models (See Aux. Fig. 4.6).

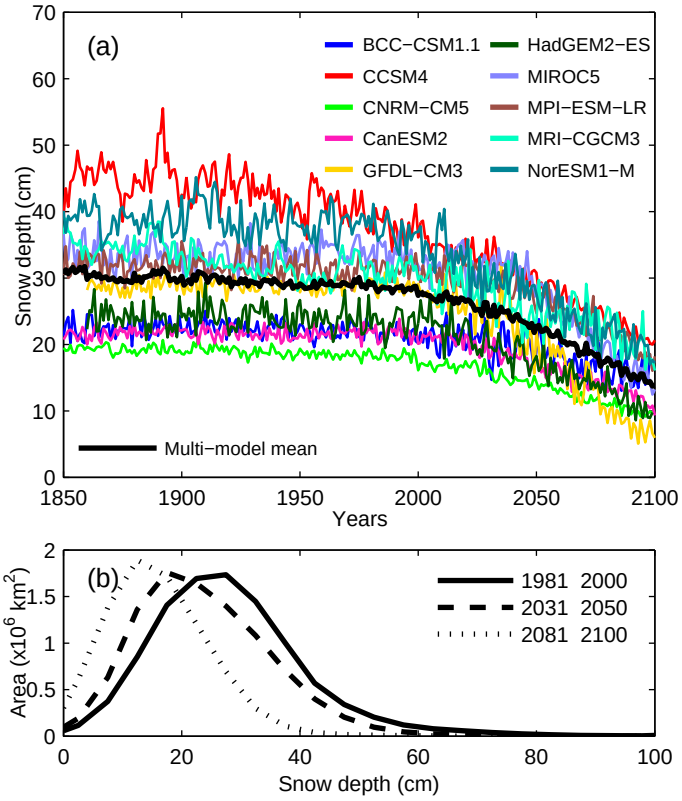

Figure 4.2: (a) 1850-2100 April snow depth averaged north of 70°N on sea ice, RCP8.5, for ensemble means of individual CMIP5 models and the multi-model ensemble mean (black). (b) Multi-model mean snow depth distribution in area for April, in 5 cm bins for the periods 1981-2000, 2031-2050, and 2081-2100. The distributions are calculated as the mean of the snow depth distribution obtained for each model over each time period for north of 70◦N where the sea ice concentration is >15%. This is different from the distribution for the multi-model mean snow depth shown in Fig. 4.1, for which the variance has been much reduced as a result of the averaging.

The decline in model spread over time (Fig. 4.2a) indicates that the models with larger initial snow depths have greater rates of decline. Similar behavior is seen for the intermodel

spread in sea ice thickness averaged north of 70°N but not for Arctic sea ice area [*Bitz*, 2008]. This similarity between transient rates of change in snow depth and sea ice thickness across models is perhaps unsurprising considering that greater snow depths tend to accumulate on thicker sea ice found along the Canadian archipelago — a behavior also seen in spatial maps of snow depth from the drifting stations [*Warren et al.*, 1999] and in an across-model correlation of 1981-2000 April means of snow depth and sea ice thickness for averages north of 70°N (R=0.56, no implied causality).

To demonstrate the impact on potential seal habitat, we show the multi-model mean snow depth distribution in area for April in RCP8.5 (Fig. 4.2b). This indicates a substantial loss of coverage for snow depths >20 cm over the 21st century. The total area of snow depth >20 cm declines in RCP8.5 (RCP4.5) from a multi-model mean of 7.4±1.8 $\times$ 10^6 km^2 in 1981-2000 to 2.4±1.9 $\times$ 10^6 km^2 (4.7±2.4 $\times$ 10^6 km^2) in 2081-2100. The multi-model mean relative decline in the area of snow depth >20 cm across all models in RCP8.5 (RCP4.5) is 69±21% (39±22%). The distributions are constructed as the average of the distribution for each model for each time period, and thus retain information about the variance that is lost in the spatial plot of multi-model mean snow depth as shown in Fig. 4.1. The spatial maps of multi-model mean snow depth (Fig. 4.1) show the spatial pattern of decline by the end of the 21st century. The relative decline in snow depth between the two periods is similar across models and is in the range of 30 to 50% over most of the Arctic basin from the 20th to the 21st century (not shown), which is consistent with the decline in the mean snow depth. (See Aux. Figs. 4.7 and 4.8 for spatial maps of snow depth in individual models.)

The decrease in April snow cover occurs in spite of an increase in snowfall in winter months over the Arctic ocean (Fig. 4.3). The total precipitation (rain plus snow) in winter months increases through the 21st century because moisture convergence into the Arctic increases roughly according to the temperature dependence of the Clausius-Clapeyron equation. This effect is seen in Fig. 4.3 and has been demonstrated in other studies of future climate projections [*Bengtsson et al.*, 2011]. For the months of November to March, the multi-model mean snowfall rate increases in all models from 1981-2000 to 2081-2100, with a mean increase of 27±16%, and a range from 5% to 51%. In the same months the multi-model mean increase in total precipitation is 69±21%, and so a substantial fraction of the

increase in precipitation occurs as rain.

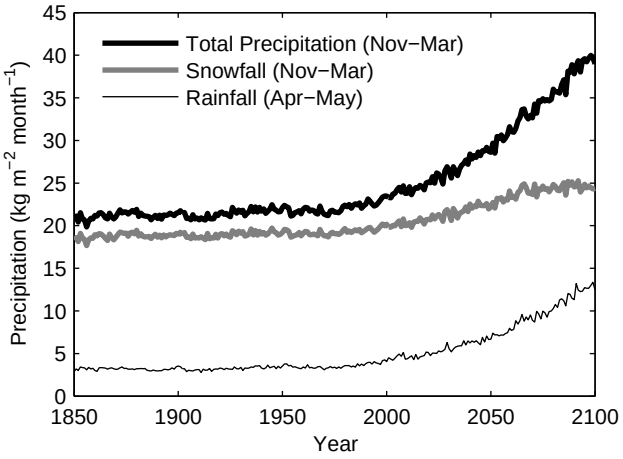

Figure 4.3: Time series of multi-model mean November-March total precipitation (thick black) and snowfall (thick grey) (kg m^{-2} month^{-1}) from 1850-2100 in RCP8.5. Note the increase in rainfall (the difference between these two curves) toward the end of the 21st century. April-May mean rainfall (thin black) (kg m^{-2} month^{-1}) also shows a strong increase over the same period and would contribute to faster spring melting of snow.

The time series of muti-model mean monthly rainfall averaged over April and May shows an increase through the end of the 21st century in RCP8.5 (The lowest curve in Fig. 4.3). The fraction of precipitation that falls as rain in April and May increases from 19±7% to 44±7% in the multi-model mean over these two periods. Snowfall is roughly constant in the multi-model mean for April and May, and therefore almost all of the increase in precipitation in these months is in the form of rain.

We find that most of the change in snow depth in April during the 21st century is caused by the delay in open water freeze-up, as illustrated by the multi-model mean climatology of snowfall rate, snow depth on sea ice, and sea ice area for the two periods 1981-2000 and 2081-2100 (Fig. 4.4). The end of the 20th century has a roughly uniform snowfall rate in autumn and winter months with a slight peak in October. The nearly linear increase in snow depth on sea ice follows the linear increase in cumulative snowfall from September through the beginning of the melt season in April. The sea ice area is lowest in September, but grows rapidly to reach a plateau of maximum area in the region north of 70°N from

December until the start of the melt season.

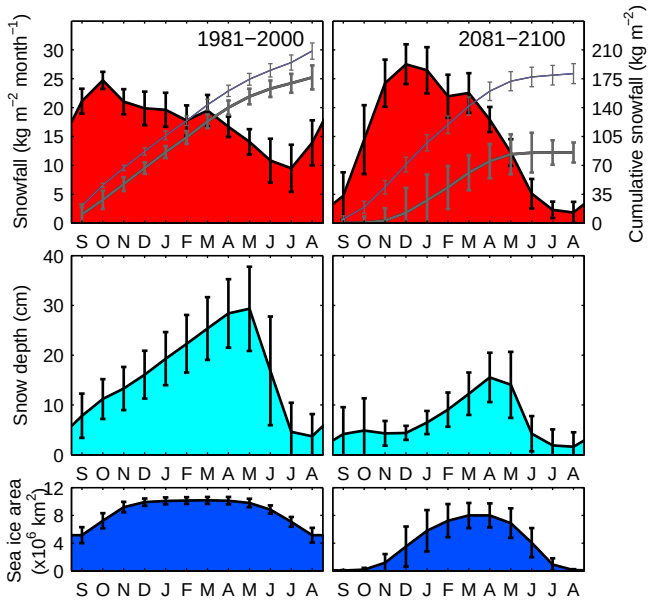

Figure 4.4: Multi-model mean climatology of snowfall (top, kg m^{-2} month^{-1}), snow depth (middle, cm), and sea ice area (bottom, $\times 10^6$ km^2) for the periods 1981-2000 (left) and 2081-2100 (right). The area-weighted monthly means are computed for north of 70°N over ocean (top) and for sea ice concentrations >15%, and the error bars represent one standard deviation in monthly means across CMIP5 models used in this study. The top plots also show the cumulative snowfall beginning in September (thin grey line, right axis, kg m^{-2} month^{-1}) and the cumulative snowfall weighted by sea ice area (i.e., the lower panel) and normalized by the maximum climatological sea ice area from 1981-2000 (thick grey line, right axis, kg m^{-2} month^{-1}). Months are from September through August.

By the end of the 21st century, the multi-model mean snowfall rates averaged north of 70°N have a larger seasonal variation, with a higher peak in winter and lower trough in summer compared to the end of the 20th century (top panels, Fig. 4.4). In addition, the timing of the snowfall peak shifts from October to December, as more of the precipitation falls as rain in autumn months. The cumulative snowfall averaged north of 70°N increases slowly at first and then roughly linearly after December before plateauing by May. The cumulative snowfall by April changes little over the 21st century (thin grey lines in top panels of Fig. 4.4). Over the period 2081-2100, mean snow depths do not follow the seasonal timing of cumulative snowfall, however. Instead, snow depths begin their seasonal

increase only in December and then increase linearly through April. Snow on sea ice does not deepen in autumn for lack of sea ice on which to accumulate. By the end of the 21st century, the multi-model mean April snow depth north of 70°N is 55% as deep as at the end of the 20th century. The cumulative sum of snowfall weighted by the sea ice area (thick grey lines in upper panels of Fig. 4.4) in April in 2081-2100 is 54% as large as in 1981-2000, indicating that the reduction in sea ice area in autumn and early winter is the primary cause of the decline in April snow depth. (See Auxiliary materials Figure 4.5 for climatology of snowfall, rainfall, snow depth, and sea ice area for individual models.)

4.4 Discussion and Conclusions

In CMIP5 models April snow depths in the central Arctic hold fairly steady throughout the 20th century and then decline sharply during the 21st. Mean April snow depths north of 70°N decrease by 45% in the RCP8.5 scenario at the end of the 21st century compared to the 20th century. Regions with deeper snow decrease fastest, as do models with unusually deep snow.

The decrease in snow depths is caused by the decrease in sea ice area in the autumn and early winter in the 21st century, corresponding to a reduction in the area of ice that survives the melt season (hence a loss of multiyear sea ice). Though the winter snowfall rate increases, there is a compensating decrease in snowfall rate during autumn, so the cumulative snowfall from September to April is nearly unchanged at the end of the 21st century. When accounting for the loss of sea ice as a platform to collect snow in autumn and early winter, the amount of snowfall that can accumulate is greatly reduced over the 21st century.

The observed distribution of snow depths across the Arctic today and recent sharp decline in multiyear sea ice lend support to our findings. April snow depths are greatest where sea ice is thick and concentrations are highest in early autumn (in observations, *Warren et al.* [1999], and models, Fig. 4.1). In contrast snow depths are usually below average where much of the area is covered by firstyear sea ice. Even in regions that have a mixed population of firstyear and multiyear sea ice, April snow depths on multiyear sea ice are about double those on firstyear ice [*Kurtz and Farrell*, 2011]. A characteristic of Arctic

sea ice trends is the faster pace of decline of thicker, multiyear sea ice compared to firstyear sea ice [*Comiso*, 2012], so it stands to reason that there would be a corresponding reduction in the mean snow depth in April.

Our conclusions about the controls on 21st century snow depths hinge on only a modest increase in winter snowfall rates as demonstrated by the models. However, from the cumulative snowfall rates in (Fig. 4.4, thick gray lines), we estimate that by end of the 21st century in RCP8.5 snowfall rates would need to double from September through April to compensate for the effect of the later freeze-up of autumn sea ice.

Modeling studies show that artificially enhancing the snow depth causes sea ice to become thinner via reduced growth rates at either pole [*Maykut and Untersteiner*, 1971; *Huwald et al.*, 2005; *Powell et al.*, 2005], provided the snow mass is insufficient to drive the sea ice-snow interface below sea level and cause snow-to-ice conversion. The CCSM4, which has among the deepest snow covers among the models we analyzed, has a negligible amount of snow-to-ice conversion in the Arctic and it remains negligible throughout the 21st century even for RCP8.5. Since decreases in snow depth induce enhanced growth rates, we infer that reduced snow depths as the Arctic warms in the 21st century will lessen the thinning of sea ice.

Based solely on a 20 cm April snow depth threshold, we estimate that the mean area of potential habitat for ringed seal reproduction north of 70°N decreases by nearly 70% over the 21st century in RCP8.5 in the CMIP5 models. Ringed seals build subnivean lairs in snow drifts that form near hummocks of deformed sea ice, and survival of seal pups diminishes in locations without at least 20 cm of snow on level sea ice in April [e.g., *Hammill and Smith*, 1991; *Ferguson et al.*, 2005; *Lukin et al.*, 2006]. We have used the lower estimate (20 cm) for the minimum snow depth on level ice necessary for seal subnivean lair success, though *Ferguson et al.* [2005] found that the snow depth needs to be greater than 32 cm. These studies also show that sea ice deformation is a necessary but not a sufficient condition for lair success. We have not excluded deformation-free regions in our analysis of the snow depth distribution in the models because deformation data are absent in the CMIP5 archive. Rain events in the Arctic spring are also known to cause the collapse of snow caves [*Stirling and Smith*, 2004]. We note therefore that an increase in April and May rainfall as simulated

in the CMIP5 models would further impact seal habitat, an impact not quantified here. Though the calculated change in area of suitable ringed seal habitat depends in part on knowledge of the relevant snow depth threshold, the effect of a different choice of threshold can be ascertained from Fig. 4.2b.

To the best of our knowledge, the sea ice in CMIP5 models is generally unaffected by rainfall since rainfall is deposited directly into the ocean in the models, with no interaction with snow or sea ice. In reality rain falling during the ice growth season would likely affect snow aging, density, and thermodynamic processes associated with ice growth. Rain falling on sea ice during the melt season would affect snow morphology and albedo, accelerate snow loss during the beginning of the melt season and potentially accelerate ice loss. These and other thermodynamic effects associated with snow on sea ice are only now being investigated in the context of a global model [O. Lecomte, pers. comm.].

For a given forcing scenario, CMIP5 models may underestimate the decrease in wintertime accumulated snow depth for at least two reasons. First, rainfall rates in CMIP5 models increase during both the winter and spring, though the effect on net snow accumulation and morphology is not fully considered in the sea ice components of global climate models. Second, decreases in sea ice concentration in the autumn and early winter could also cause loss of drifting snow into leads. Changes to the sea ice surface topography (hummock height and distribution) are expected due to changes in the deformation rate as well as the proportion of firstyear and multiyear ice. The nature and seasonality of these changes and their effect on drifting snow, and by extension seal habitat, is unknown. The considerable decline in 21st century snow depths in the CMIP5 models and the relevance for seal habitat motivate further investigation into the impact of these additional factors.

Acknowledgements

We thank O. Lecomte for useful conversations about modeling snow on sea ice, S.G. Warren and R. Kwok for assistance with observations of snow depth on sea ice, D. Notz and M. Winton for assistance acquiring data from their models, and S. Amstrup and S. Dahle for comments on the manuscript. This research was supported by the Office of Naval Research through grant N00014-11-1-0550. We acknowledge the World Climate Research Programme's Working Group on Coupled Modelling, which is responsible for CMIP, and we

thank the climate modeling groups (listed in Table 4.1) for producing and making available their model output. The U.S. Department of Energy's Program for Climate Model Diagnosis and Intercomparison provides coordinating support and led development of CMIP software and infrastructure in partnership with the Global Organization for Earth System Science Portals.

4.5 Auxiliary Figures

The following figures (Fig. 4.5 through 4.5) are contained in the Auxiliary Materials of the manuscript for this chapter.

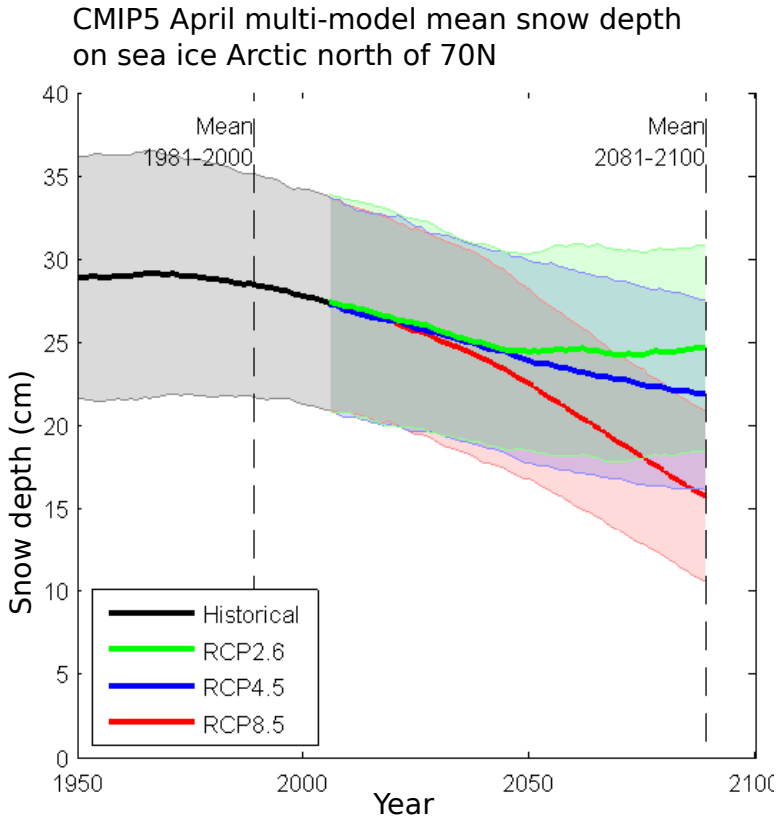

Figure 4.5: Time series of multi-model mean snow depth (cm) for all models in RCP8.5, RCP4.5, and RCP2.6 scenarios. Calculated as a 20 year centered running mean. Shaded regions represent one standard deviation in the multi-model mean across all models.

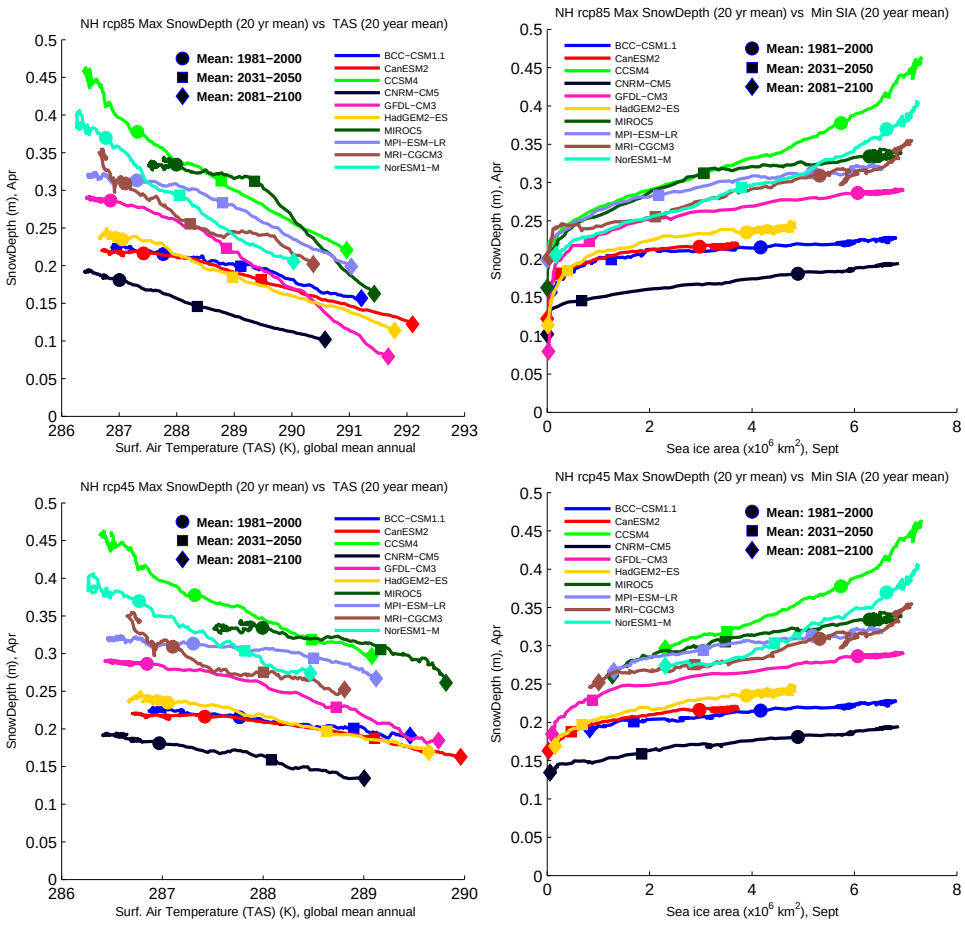

Figure 4.6: For each model, the mean April snow depth (m) versus global annual mean temperature (K) (left panels) and mean snow depth (m) versus sea ice area ($\times 10^6$ km^2) (right panels) for the RCP8.5 (top) and RCP4.5 (bottom) scenarios. The time series for each quantity is calculated as a 20 year running mean and means for 1981-2000 (circle), 2031-2050 (square) and 2081-2100 (diamond) are noted. The slopes in left panels indicate roughly similar sensitivity in each model to global annual mean temperature (an approximation to global mean forcing). The spread among the lines (in both snow depth as well as global mean temperature) is indicative of the climate bias in each model. The sensitivity of snow depth to increases in global mean temperature is -0.034 m/K (range: -0.019 to 0.051 m/K) for RCP8.5 and -0.032 m/K (range: -0.015 to -0.056 m/K) for RCP4.5 for the period 1981-2100. The right panels show that the sensitivity of snow depth to the rapid loss in minimum sea ice area is roughly uniform (i.e. similar slopes) until mid-century, when snow depths decline dramatically though minimum sea ice areas are already near zero. Declines in mean snow depth for both RCP4.5 and RCP8.5 are 0.013 m/10^6 km^2 (range: 0.005 to 0.027 m/10^6 km^2) for 1981-2050. Declines increase to 0.027 m/10^6 km^2 (range: 0.012 to 0.066 m/10^6 km^2) for RCP4.5 and 0.080 m/10^6 km^2 (range: 0.015 to 0.20 m/10^6 km^2) for RCP8.5 for 2031-2100.

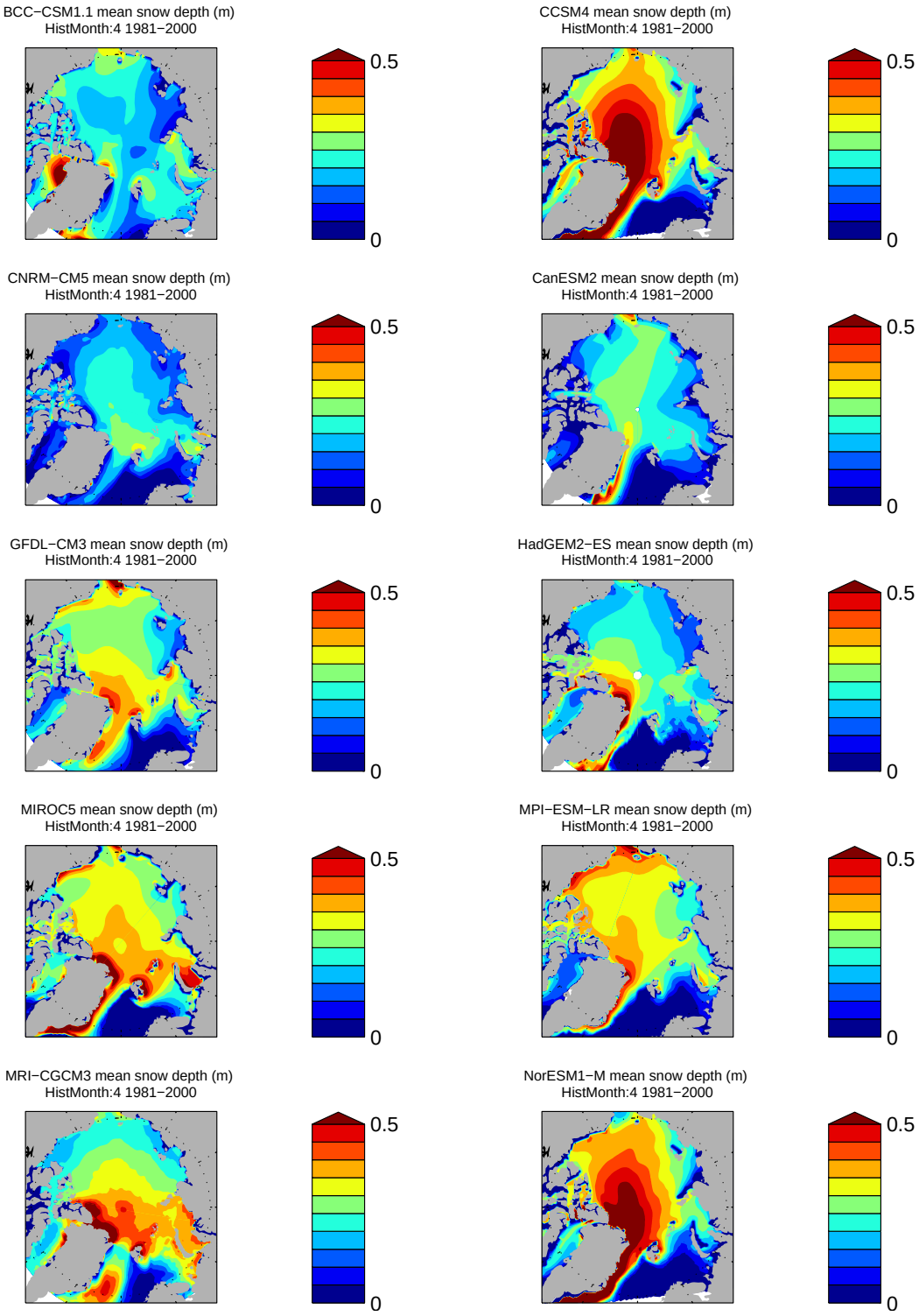

Figure 4.7: Mean snow depth (m) (1981-2000) on sea ice for each of the 10 models as in Figure 1 of the main manuscript.

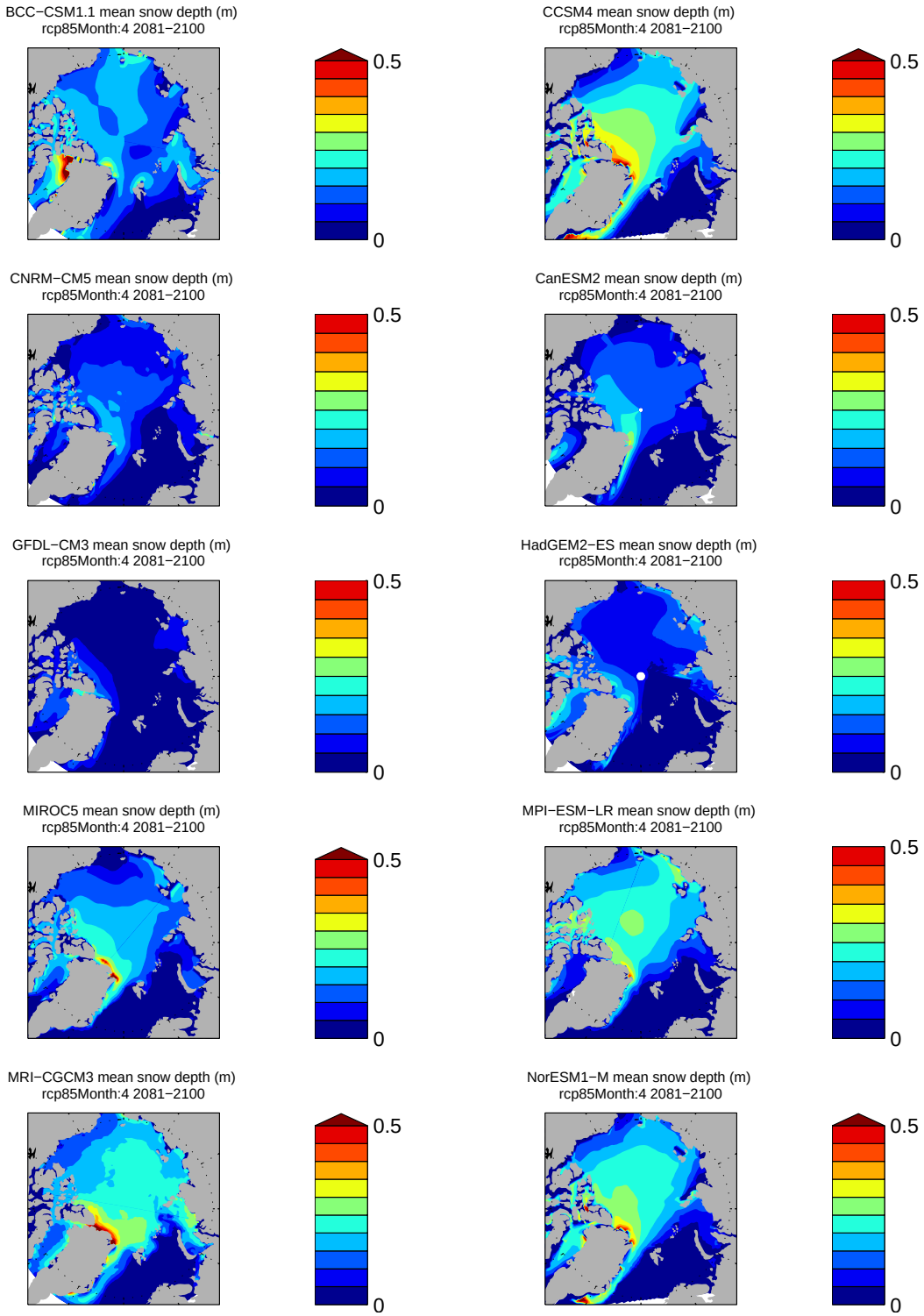

Figure 4.8: Mean snow depth (m) (2081-2100) on sea ice for each of the 10 models as in Figure 4.1 of the main manuscript.

Chapter 5

CONCLUSIONS

Past studies have claimed a relationship between ice core records of MSA and sea ice extent. This first part (Chapters 2 and 3) of this dissertation examines this relationship in detail within the context of a chemical transport model. In the model, we probe the relationships of component steps in the sulfur cycle, from DMS emissions from the ocean surface to MSA and nssSO_4^{2-} deposition in Antarctica, and show no robust relationship on interannual time scales between MSA and sea ice. On glacial-interglacial time scales, we use nssSO_4^{2-} to show that the MSA variability is likely related to post-depositional processes. In this chapter, we discuss the results in the broader context of primary productivity and DMS emissions from the sea ice zone, the sulfur cycle and halogen oxidation, and wet and dry deposition processes in Antarctica.

The second part (Chapter 4) of this dissertation examines the effect a warming climate on snow depth on Arctic sea ice, using the CMIP5 model data archive. We find that the decrease in sea ice extent during the autumn (ie., later sea ice freeze-up) dominates the decrease in snow depth at the end of the winter, in spite of an increase in snowfall rates during the winter in the 21st century. In a conservative estimate, the models predict a decrease by 70% in potential habitat of ringed seals in the spring. In Section 5.4 below, we discuss future work for a similar study for Antarctic sea ice.

5.1 DMS emissions from the sea ice

Chapter 3 leaves open the question of whether DMS emissions are higher in the LGM than in the modern period. Though we think that DMS emissions are at least as high in the LGM as the modern period based on modeled nssSO_4^{2-} compared to observations on the East Antarctic Plateau, it is possible that DMS emissions could be much higher in the sea ice zone during during the LGM. Given the larger winter extent of sea ice in the LGM and the

Figure 4.9: Climatology for each of the 10 models for snowfall and rainfall, snow depth, and ice area for north of 70 N, similar to Figure 4.4 in the main manuscript. For each model, the climatology is given for the periods 1981-2000 (Historical) (left) and 2081-2100 (RCP8.5) (right). Errorbars are 1 standard deviation of means from all available ensemble members in the given period. (Top) Stacked snowfall (red) and rainfall rates (yellow), where the total represents the the total precipitation rate (kg/m^2/month), as an area-weighted average over the ocean north of 70 N. The grey line is the cumulative snowfall (kg/m^2, right axis). (Middle) Snow depth (cm), area-weighted average over sea ice north of 70 N for sea ice concentration $> 15\%$. (Bottom) Ice area (x10^6 km^2) north of 70 N for sea ice concentration $> 15\%$. Months are from September through August.

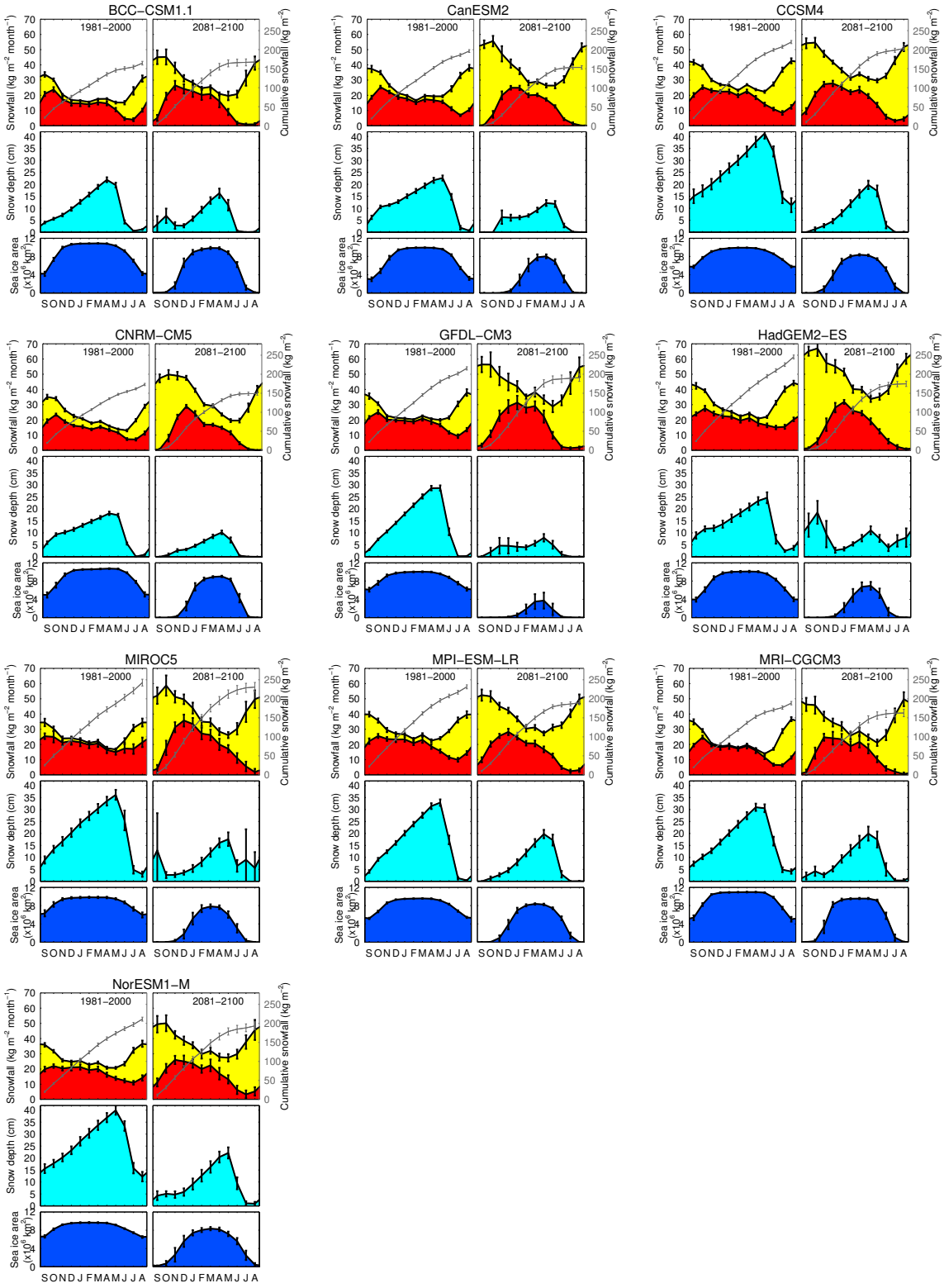
BCC–CSM1.1
CanESM2
CCSM4
CNRM–CM5
GFDL–CM3
HadGEM2–ES
MIROC5
MPI–ESM–LR
MRI–CGCM3
NorESM1–M
1981–2000
2081–2100
Snowfall (kg m^{-2} month^{-1})
Cumulative snowfall (kg m^{-2})
Snow depth (cm)
Sea ice area (x10^6 km^2)
SONDJFMAMJJA

potentially large seasonal ice zone, if summer sea ice extent is in fact close to the modern day extent, the sea ice may have a much larger impact on the sulfur cycle in the LGM than in the modern period. A biogeochemical model of sea ice and biological productivity coupled with a global climate model could yield interesting insights into the potential magnitude of DMS emissions in the LGM and information about aerosol formation and cloud condensation nucleii (CCN) over an ice covered Southern Ocean. A biogeochemical model would also help constrain the variation in DMS production between the open ocean and sea ice zones, and estimate the effect of sea ice on the seawater DMS concentrations as a result of some of the strong physical drivers in the retreating sea ice such as the stratification in the surface ocean. There may also be other influences of the sea ice zone on gas exchange with the atmosphere, some of which are outlined by *Loose et al.* [2011] and include sea ice motion as a mixing mechanism in the upper ocean layer.

5.2 DMS oxidation and influence of halogens

The oxidation chemistry of DMS in the atmosphere is very complex and still not well understood [*von Glasow and Crutzen*, 2004]. Global model simulations of the sulfur cycle using both very simple and complex chemistry mechanisms capture the broad features of SO_2 and SO_4^{2-} reasonably well. However, evidence of high halogen concentrations associated with sea ice combined with the sensitivity of DMS to oxidation by BrO as shown here demonstrates that an understanding of DMS chemistry with regard to halogens is especially important in the polar regions. Our results indicate that reaction of DMS with halogens may be an important control on the relative yields of MSA to nssSO_4^{2-}. Constraints on both the seasonal concentrations of the oxidants (e.g., BrO) and the chemical mechanisms are necessary to capture the specifics of the sulfur cycle in the high latitudes.

5.3 Wet and dry deposition in the polar regions

The Antarctic atmosphere is characterized by a persistent stable boundary layer, diurnal katabatic surface wind regime, steep topographical features originating at the coast, and a precipitation regime that varies by more than two orders of magntitude from the coast to the interior plateau. We have found in a sensitivity simulation that variation of the wet

deposition scavenging rate has the potential to set the coast-to-inland gradient in deposition fluxes. The parameterization also determines the total amount of MSA and nssSO_4^{2-} transport to Antarctica since it influences the lifetimes of both MSA and nssSO_4^{2-}. Since the wet deposition flux parameterization in GEOS-Chem has not been adapted to the specific conditions for Antarctica, the ability of the model to capture the absolute magnitudes of deposition fluxes in agreement with observations remains challenging.

The resolution of the model, here $2^\circ \times 2.5^\circ$ or $4^\circ \times 5^\circ$, also influences the deposition rates in Antarctica via the influence on precipitation. Since even the $2^\circ \times 2.5^\circ$ resolution does not resolve Antarctic topography very well, the influence of topographical features in the precipitation and thus the wet deposition may not be well captured. Furthermore, in Chapter 2 we investigated the impact of a higher resolution boundary layer on model results. In the $2^\circ \times 2.5^\circ$ simulations that use meteorological data from a better resolved boundary layer (GEOS-5) there was less sulfur transport to Antarctica, a larger fraction of dry deposition, and shorter DMS lifetimes due to less transport out of the boundary layer into the free troposphere. Though this difference still did not change the results presented in Chapter 2, it is conceivable that the combination horizontal and boundary layer resolution in the model affects the ability to correctly model the absolute deposition fluxes of MSA and nssSO_4^{2-} especially in the coastal regions.

5.4 Snow depths on sea ice

In Chapter 4, we showed that the decline in spring snow depth through the 21st century in the CMIP5 models is primarily related to the decrease in early autumn ice extent, which results in a decreased amount of time for snow to accumulate through the winter. This occurs in spite of an increase in winter snowfall in the models. Given the simplified treatment of modeled snow accumulation in the sea ice domain and expected increases in rainfall as a fraction of precipitation, the decline in snow depth shown by the models is likely conservative. Other thermodynamic and radiative effects resulting from the interactions between snow, rain-on-snow, and sea ice are not considered by the current generation of climate models. Snow redistribution and changes in sea ice deformation rates are also expected in the future, and their effect on snow depths and seal habitat is unknown.

A similar study of Southern Ocean snow depth on sea ice will follow. A preliminary analysis of the Antarctic snow depths on sea ice shows that the analysis of snow depth decline in the Arctic is not applicable to the Antarctic. The Antarctic sea ice area has been increasing slightly in past decades, in contrast to the strong decrease in the Arctic, though it is expected that a warmer climate will result in reduced sea ice extent in the Antarctic as well [*Arzel et al.*, 2006]. Furthermore, the large area of first year (i.e., relatively thin) sea ice and the formation of snow-ice may determine the maximum snow depth at the end of the austral winter, even in the face of an increasing snowfall rate.

BIBLIOGRAPHY

Abram, N. J., R. Mulvaney, E. W. Wolff, and M. Mudelsee (2007), Ice core records as sea ice proxies: An evaluation from the weddell sea region of antarctica, *Journal of Geophysical Research-Atmospheres*, *112*(D15).

Abram, N. J., E. R. Thomas, J. R. McConnell, R. Mulvaney, T. J. Bracegirdle, L. C. Sime, and A. J. Aristarain (2010), Ice core evidence for a 20th century decline of sea ice in the bellingshausen sea, antarctica, *Journal of Geophysical Research-Atmospheres*, *115*.

Alvarez-Aviles, L., W. R. Simpson, T. A. Douglas, M. Sturm, D. Perovich, and F. Domine (2008), Frost flower chemical composition during growth and its implications for aerosol production and bromine activation, *Journal of Geophysical Research-Atmospheres*, *113*(D21).

Arzel, O., T. Fichefet, and H. Goosse (2006), Sea ice evolution over the 20th and 21st centures as simulated by current AOGCMs, *Ocean Modell.*, *12*, 401–415.

Ayers, G. P., S. T. Bentley, J. P. Ivey, and B. W. Forgan (1995), Dimethylsulfide in marine air at cape-grim, 41-degrees-s, *Journal of Geophysical Research-Atmospheres*, *100*(D10), 21,013–21,021.

Barnes, I., J. Hjorth, and N. Mihalopoulos (2006), Dimethyl sulfide and dimethyl sulfoxide and their oxidation in the atmosphere, *Chemical Reviews*, *106*(3), 940–975.

Becagli, S., et al. (2009), Methanesulphonic acid (msa) stratigraphy from a talos dome ice core as a tool in depicting sea ice changes and southern atmospheric circulation over the previous 140 years, *Atmospheric Environment*, *43*(5), 1051–1058.

Bengtsson, L., K. I. Hodges, S. Koumoutsaris, M. Zahn, and N. Keenlyside (2011), The changing atmospheric water cycle in Polar Regions in a warmer climate, *Tellus Series A-Dynamic Meteorology and Oceanography*, *63*(5), 907–920.

Berglen, T. F., T. K. Berntsen, I. S. A. Isaksen, and J. K. Sundet (2004), A global model of the coupled sulfur/oxidant chemistry in the troposphere: The sulfur cycle, *Journal of Geophysical Research-Atmospheres*, *109*(D19), 27.

Bertler, N., et al. (2005), Snow chemistry across antarctica, *Annals of Glaciology, Vol 41, 2005*, *41*, 167–179.

Bey, I., et al. (2001), Global modeling of tropospheric chemistry with assimilated meteorology: Model description and evaluation, *Journal of Geophysical Research-Atmospheres*, *106*(D19), 23,073–23,095.

Bitz, C. M. (2008), Some aspects of uncertainty in predicting sea ice thinning, in *Sea Ice Decline*, edited by E. deWeaver, C. M. Bitz, and B. Tremblay, pp. 63–76, AGU.

Bloom, S., et al. (2005), Documentation and validation of the goddard earth observing system (geos) data assimilation system - version 4, *Tech. Rep. 104606*, NASA Goddard Space Flight Center, Greenbelt, MD.

Boucher, O., M. Pham, and C. Venkataraman (2002), Simulation of the atmospheric sulfur cycle in the laboratoire de meteorologie dynamique general circulation model. model description, model evaluation, and global and european budgets, *Tech. rep.*

Boucher, O., et al. (2003), Dms atmospheric concentrations and sulphate aerosol indirect radiative forcing: a sensitivity study to the dms source representation and oxidation, *Atmospheric Chemistry and Physics*, *3*, 49–65.

Braconnot, P., et al. (2007a), Results of pmip2 coupled simulations of the mid-holocene and last glacial maximum - part 2: feedbacks with emphasis on the location of the itcz and mid- and high latitudes heat budget, *Climate of the Past*, *3*(2), 279–296.

Braconnot, P., et al. (2007b), Results of pmip2 coupled simulations of the mid-holocene and last glacial maximum - part 1: experiments and large-scale features, *Climate of the Past*, *3*(2), 261–277.

Breider, T. J., M. P. Chipperfield, N. A. D. Richards, K. S. Carslaw, G. W. Mann, and D. V. Spracklen (2010), Impact of bro on dimethylsulfide in the remote marine boundary layer, *Geophysical Research Letters*, *37*, 6.

Cameron-Smith, P., S. Elliott, M. Maltrud, D. Erickson, and O. Wingenter (2011), Changes in dimethyl sulfide oceanic distribution due to climate change, *Geophysical Research Letters*, *38*.

Castebrunet, H., C. Genthon, and P. Martinerie (2006), Sulfur cycle at last glacial maximum: Model results versus antarctic ice core data, *Geophysical Research Letters*, *33*(22).

Castebrunet, H., P. Martinerie, C. Genthon, and E. Cosme (2009), A three-dimensional model study of methanesulphonic acid to non sea salt sulphate ratio at mid and high-southern latitudes, *Atmospheric Chemistry and Physics*, *9*(24), 9449–9469.

Chatfield, R. B., and P. J. Crutzen (1990), Are there interactions of iodine and sulfur species in marine air photochemistry, *Journal of Geophysical Research-Atmospheres*, *95*(D13), 22,319–22,341.

Chin, M., D. J. Jacob, G. M. Gardner, M. S. ForemanFowler, P. A. Spiro, and D. L. Savoie (1996), A global three-dimensional model of tropospheric sulfate, *Journal of Geophysical Research-Atmospheres*, *101*(D13), 18,667–18,690.

Chin, M., R. B. Rood, S. J. Lin, J. F. Muller, and A. M. Thompson (2000), Atmospheric sulfur cycle simulated in the global model gocart: Model description and global properties, *Journal of Geophysical Research-Atmospheres*, *105*(D20), 24,671–24,687.

CLIMAP (1976), The surface of the ice-age earth, *Science*, *191*(4232), 1131–1137, doi: 10.1126/science.191.4232.1131.

Comiso, J. C. (2012), Large decadal decline of the Arctic multiyear ice cover, *25*, 1176–1193.

Comiso, J. C., C. L. Parkinson, R. Gersten, and L. Stock (2008), Accelerated decline in the arctic sea ice cover, *Geophysical Research Letters*, *35*(1).

Corbett, J. J., P. S. Fischbeck, and S. N. Pandis (1999), Global nitrogen and sulfur inventories for oceangoing ships, *Journal of Geophysical Research-Atmospheres*, *104*(D3), 3457–3470.

Cosme, E., C. Genthon, P. Martinerie, O. Boucher, and M. Pham (2002), The sulfur cycle at high-southern latitudes in the lmd-zt general circulation model, *Journal of Geophysical Research-Atmospheres*, *107*(D23), 19.

Cosme, E., F. Hourdin, C. Genthon, and P. Martinerie (2005), Origin of dimethylsulfide, non-sea-salt sulfate, and methanesulfonic acid in eastern antarctica, *Journal of Geophysical Research-Atmospheres*, *110*(D3).

Cullather, R. I., D. H. Bromwich, and M. C. Serreze (2000), The atmospheric hydrologic cycle over the arctic basin from reanalyses. part i: Comparison with observations and previous studies, *Journal of Climate*, *13*(5), 923–937.

Curran, M. A. J., and G. B. Jones (2000), Dimethyl sulfide in the southern ocean: Seasonality and flux, *Journal of Geophysical Research-Atmospheres*, *105*(D16), 20,451–20,459.

Curran, M. A. J., T. D. van Ommen, V. I. Morgan, K. L. Phillips, and A. S. Palmer (2003), Ice core evidence for antarctic sea ice decline since the 1950s, *Science*, *302*(5648), 1203–1206.

de Boyer-Montegut, C., G. Madec, A. S. Fischer, A. Lazar, and D. Iudicone (2004), Mixed layer depth over the global ocean: An examination of profile data and a profile-based climatology, *Journal of Geophysical Research-Oceans*, *109*(C12).

de Vernal, A., et al. (2005), Reconstruction of sea-surface conditions at middle to high latitudes of the northern hemisphere during the last glacial maximum (lgm) based on dinoflagellate cyst assemblages, *Quaternary Science Reviews*, *24*(7-9), 897–924.

Delille, B., B. Jourdain, A. V. Borges, J. L. Tison, and D. Delille (2007), Biogas (co2, o-2, dimethylsulfide) dynamics in spring antarctic fast ice, *Limnology and Oceanography*, *52*(4), 1367–1379.

Dunbar, N. W., and A. V. Kurbatov (2011), Tephrochronology of the siple dome ice core, west antarctica: correlations and sources, *Quaternary Science Reviews*, *30*(13-14), 1602–1614.

Elliott, S. (2009), Dependence of dms global sea-air flux distribution on transfer velocity and concentration field type, *Journal of Geophysical Research-Biogeosciences*, *114*.

Faloona, I. (2009), Sulfur processing in the marine atmospheric boundary layer: A review and critical assessment of modeling uncertainties, *Atmospheric Environment*, *43*(18), 2841–2854.

Ferguson, S. H., I. Stirling, and P. McLoughlin (2005), Climate change and ringed seal *(Phoca hispida)* recruitment in western Hudson Bay, *Marine Mammal Science*, *21*, 121–135.

Fischer, H., et al. (2007), Reconstruction of millennial changes in dust emission, transport and regional sea ice coverage using the deep epica ice cores from the atlantic and indian ocean sector of antarctica, *Earth and Planetary Science Letters*, *260*(1-2), 340–354.

Foster, A. F., M. A. Curran, B. T. Smith, T. D. van Ommen, and V. I. Morgan (2006), Covariation of sea ice and methanesulphonic acid in wilhelm ii land, east antarctica, *Annals of Glaciology*, *44*, 429–432(4), doi:doi:10.3189/172756406781811394.

Fundel, F., H. Fischer, R. Weller, F. Traufetter, H. Oerter, and H. Miller (2006), Influence of large-scale teleconnection patterns on methane sulfonate ice core records in dronning maud land, *Journal of Geophysical Research-Atmospheres*, *111*(D4).

Gabric, A. J., J. M. Shephard, J. M. Knight, G. Jones, and A. J. Trevena (2005), Correlations between the satellite-derived seasonal cycles of phytoplankton biomass and aerosol optical depth in the southern ocean: Evidence for the influence of sea ice, *Global Biogeochemical Cycles*, *19*(4).

Gersonde, R., X. Crosta, A. Abelmann, and L. Armand (2005), Sea-surface temperature and sea ice distribution of the southern ocean at the epilog last glacial maximum - a circum-antarctic view based on siliceous microfossil records, *Quaternary Science Reviews*, *24*(7-9), 869–896.

Gondwe, M., M. Krol, W. Klaassen, W. Gieskes, and H. de Baar (2004), Comparison of modeled versus measured msa : nss so4= ratios: A global analysis, *Global Biogeochemical Cycles*, *18*(2).

Gosink, T. A., J. G. Pearson, and J. J. Kelley (1976), Gas movement through sea ice, *Nature*, *263*(5572), 41–42.

Guenther, A., T. Karl, P. Harley, C. Wiedinmyer, P. I. Palmer, and C. Geron (2006), Estimates of global terrestrial isoprene emissions using megan (model of emissions of gases and aerosols from nature), *Atmospheric Chemistry and Physics*, *6*, 3181–3210.

Hammill, M. O., and T. G. Smith (1991), The role of predation in the ecology of the ringed seal in barrow strait, northwest territories, canada, *Marine Mammal Science*, *7*(2), 123–135, doi:10.1111/j.1748-7692.1991.tb00559.x.

Hansen, J., et al. (2007), Climate simulations for 1880-2003 with giss modele, *Climate Dynamics*, *29*(7-8), 661–696.

Hezel, P. J., B. Alexander, C. M. Bitz, E. J. Steig, C. D. Holmes, X. Yang, and J. Sciare (2011), Modeled methanesulfonic acid (msa) deposition in antarctica and its relationship to sea ice, *Journal of Geophysical Research-Atmospheres*, *116*, doi:10.1029/2011JD016383.

Hezel, P. J., X. Zhang, C. M. Bitz, B. P. Kelly, and F. Massonnet (2012), Projected decline in spring snow depth on Arctic sea ice caused by progressively later autumn open ocean freeze-up this century, *Geophysical Research Letters*, doi:10.1029/2012GL052794.

Holmes, C. D., D. J. Jacob, E. S. Corbitt, J. Mao, X. Yang, R. Talbot, and F. Slemr (2010), Global atmospheric model for mercury including oxidation by bromine atoms, *Atmospheric Chemistry and Physics*, *10*(24), 12,037–12,057.

Huebert, B. J., B. W. Blomquist, M. X. Yang, S. D. Archer, P. D. Nightingale, M. J. Yelland, J. Stephens, R. W. Pascal, and B. I. Moat (2010), Linearity of dms transfer coefficient with both friction velocity and wind speed in the moderate wind speed range, *Geophysical Research Letters*, *37*, 5.

Huwald, H., L. Tremblay, and H. Blatter (2005), A multilayer sigma-coordinate thermodynamic sea ice model: Validation against Surface Heat Budget of the Arctic Ocean (SHEBA)/Sea Ice Model Intercomparison Project Part 2 (SIMIP2) data, *Journal of Geophysical Research-Oceans*, *110*(C5), doi:10.1029/2004JC002328.

IUPAC (2007), IUPAC Subcommittee for Gas Kinetic Data Evaluation – Data Sheet SOx76.

Jones, G., D. Fortescue, S. King, G. Williams, and S. Wright (2010), Dimethylsulphide and dimethylsulphoniopropionate in the south-west indian ocean sector of east antarctica from 30 degrees to 80 degrees e during broke-west, *Deep-Sea Research Part Ii-Topical Studies in Oceanography*, *57*(9-10), 863–876.

Kaplan, J. O., et al. (2003), Climate change and arctic ecosystems: 2. modeling, paleodata-model comparisons, and future projections, *Journal of Geophysical Research-Atmospheres*, *108*(D19).

Karl, M., A. Gross, C. Leck, and L. Pirjola (2007), Intercomparison of dimethylsulfide oxidation mechanisms for the marine boundary layer: Gaseous and particulate sulfur constituents, *Journal of Geophysical Research-Atmospheres*, *112*(D15), 20.

Kattsov, V. M., J. E. Walsh, W. Chapman, V. A. Govorkova, T. Pavlova, and X. Zhang (2007), Simulation and projection of arctic freshwater budget components by the ipcc ar4 global climate models, *J. Hydrometeor*, *8*, 571–589.

Kelly, B., et al. (2010), Status review of the ringed seal *Phoca hispida*, *Tech. Rep. NMFS-AFSC-212*, NOAA Technical Memorandum.

Kelly, B. P. (2001), Climate change and ice breeding pinnepeds, in *"Fingerprints" of Climate Change — Adapted Behavior and Shifting Species Ranges*, edited by G. Walther, C. A. Burga, and P. J. Edwards, pp. 43–55, Kluwer Academic/Plenum Publishers, New York, NY.

Kettle, A. J., and M. O. Andreae (2000), Flux of dimethylsulfide from the oceans: A comparison of updated data seas and flux models, *Journal of Geophysical Research-Atmospheres*, *105*(D22), 26,793–26,808.

Kettle, A. J., et al. (1999), A global database of sea surface dimethylsulfide (dms) measurements and a procedure to predict sea surface dms as a function of latitude, longitude, and month, *Global Biogeochemical Cycles*, *13*(2), 399–444.

Kurbatov, A. V., G. A. Zielinski, N. W. Dunbar, P. A. Mayewski, E. A. Meyerson, S. B. Sneed, and K. C. Taylor (2006), A 12,000 year record of explosive volcanism in the siple dome ice core, west antarctica, *Journal of Geophysical Research-Atmospheres*, *111*(D12).

Kurtz, N. T., and S. L. Farrell (2011), Large-scale surveys of snow depth on Arctic sea ice from Operation IceBridge, *Geophys. Res. Lett.*, *38*, L20,505, doi:10.1029/2011GL049,216.

Kwok, R., and D. Rothrock (2009), Decline in Arctic sea ice thickness from submarine and ICESat records: 1958–2008, *Geophys. Res. Lett.*, *36*, L15,501: doi:10.1029/2009GL039,035.

Kwok, R., B. Panzer, C. Leuschen, S. Pang, T. Markus, B. Holt, and S. Gogineni (2011), Airborne surveys of snow depth over arctic sea ice, *Journal of Geophysical Research-Oceans*, *116*.

Lana, A., et al. (2011), An updated climatology of surface dimethlysulfide concentrations and emission fluxes in the global ocean, *Global Biogeochemical Cycles*, *25*, 17.

Legrand, M., and C. Feniet-Saigne (1991), Methanesulfonic-acid in south polar snow layers - a record of strong el-nino, *Geophysical Research Letters*, *18*(2), 187–190.

Legrand, M., C. Feniet-Saigne, E. S. Saltzman, C. Germain, N. I. Barkov, and V. N. Petrov (1991), Ice-core record of oceanic emissions of dimethylsulfide during the last climate cycle, *Nature*, *350*(6314), 144–146.

Levasseur, M., M. Gosselin, and S. Michaud (1994), A new source of dimethylsulfide (dms) for the arctic atmosphere - ice diatoms, *Marine Biology*, *121*(2), 381–387.

Liss, P., and L. Merlivat (1986), Air-sea gas exchange rates: introduction and synthesis, in *The Role of Air-Sea Exchange in Geochemical Cycling*, edited by P. Buat-Menard, pp. 113–127, D Reidel, Norwell, Mass.

Liu, H. Y., D. J. Jacob, I. Bey, and R. M. Yantosca (2001), Constraints from pb-210 and be-7 on wet deposition and transport in a global three-dimensional chemical tracer model driven by assimilated meteorological fields, *Journal of Geophysical Research-Atmospheres*, *106*(D11), 12,109–12,128.

Loose, B., et al. (2011), Gas diffusion through columnar laboratory sea ice: implications for mixed-layer ventilation of co(2) in the seasonal ice zone, *Tellus Series B-Chemical and Physical Meteorology*, *63*(1), 23–39.

Lucas, D. D., and R. G. Prinn (2005), Parametric sensitivity and uncertainty analysis of dimethylsulfide oxidation in the clear-sky remote marine boundary layer, *Atmospheric Chemistry and Physics*, *5*, 1505–1525.

Lukin, L. P., G. N. Ognetov, and N. S. Boiko (2006), *Ecology of the ringed seal in the White Sea*, 165 pp. pp., UrO RAN, Ekaterinburg, Russia (Translated from Russian by the Baltic Fund for Nature, State University of St. Petersburg, Russia).

Lydersen, C., P. M. Jensen, and E. Lydersen (1990), A survey of the vanmijen fjord, svalbard, as habitat for ringed seals, phoca-hispida, *Holarctic Ecology*, *13*(2), 130–133.

Malin, G., and G. O. Kirst (1997), Algal production of dimethyl sulfide and its atmospheric role, *Journal of Phycology*, *33*(6), 889–896.

Mayewski, P. A., et al. (2009), State of the antarctic and southern ocean climate system, *Reviews of Geophysics*, *47*.

Maykut, G. A., and N. Untersteiner (1971), Some results from a time-dependent thermodynamic model of sea ice, *J. Geophys. Res.*, *76*, 1550–1575.

McLinden, C. A., S. C. Olsen, B. Hannegan, O. Wild, M. J. Prather, and J. Sundet (2000), Stratospheric ozone in 3-d models: A simple chemistry and the cross-tropopause flux, *Journal of Geophysical Research-Atmospheres*, *105*(D11), 14,653–14,665.

Minikin, A., M. Legrand, J. Hall, D. Wagenbach, C. Kleefeld, E. Wolff, E. C. Pasteur, and F. Ducroz (1998), Sulfur-containing species (sulfate and methanesulfonate) in coastal antarctic aerosol and precipitation, *Journal of Geophysical Research-Atmospheres*, *103*(D9), 10,975–10,990.

Monaghan, A. J., et al. (2006), Insignificant change in antarctic snowfall since the international geophysical year, *Science*, *313*(5788), 827–831.

Nightingale, P. D., G. Malin, C. S. Law, A. J. Watson, P. S. Liss, M. I. Liddicoat, J. Boutin, and R. C. Upstill-Goddard (2000), In situ evaluation of air-sea gas exchange parameterizations using novel conservative and volatile tracers, *Global Biogeochemical Cycles*, *14*(1), 373–387.

Notz, D. (2009), The future of ice sheets and sea ice: Between reversible retreat and unstoppable loss, *Proc. Nat. Acad. Sci. USA*, *106*, 20,590–20,595.

Otto-Bliesner, B. L., C. D. Hewitt, T. M. Marchitto, E. Brady, A. Abe-Ouchi, M. Crucifix, S. Murakami, and S. L. Weber (2007), Last glacial maximum ocean thermohaline circulation: Pmip2 model intercomparisons and data constraints, *Geophysical Research Letters*, *34*(12), 6.

Park, R. J., D. J. Jacob, B. D. Field, R. M. Yantosca, and M. Chin (2004), Natural and transboundary pollution influences on sulfate-nitrate-ammonium aerosols in the united states: Implications for policy, *Journal of Geophysical Research-Atmospheres*, *109*(D15).

Parrenin, F., et al. (2007), The edc3 chronology for the epica dome c ice core, *Climate of the Past*, *3*(3), 485–497.

Pasteur, E., R. Mulvaney, D. Peel, E. Saltzman, and P.-Y. Whung (1995), A 340 year record of biogenic sulphur from the weddell sea area, antarctica, *Annals of Glaciology*, *21*, 169–174(6).

Peltier, W. R. (2004), Global glacial isostasy and the surface of the ice-age earth: The ice-5g (vm2) model and grace, *Annual Review of Earth and Planetary Sciences*, *32*, 111–149.

Penner, J. E., et al. (2001), Aerosols, their direct and indirect effects, in *Climate Change 2001: The Scientific Basis. Contribution of Working Group I to the Third Assessment Report of the Intergovernmental Panel on Climate Change*, pp. 289–348, Cambridge University Press, Cambridge, UK, and New York, NY, USA.

Pham, M., J. F. Muller, G. P. Brasseur, C. Granier, and G. Megie (1995), A three-dimensional study of the tropospheric sulfur cycle, *Journal of Geophysical Research-Atmospheres*, *100*(D12), 26,061–26,092.

Powell, D., T. Markus, and A. Stossel (2005), Effects of snow depth forcing on Southern Ocean sea ice simulations, *JOURNAL OF GEOPHYSICAL RESEARCH-OCEANS*, *110*(C6), doi:10.1029/2003JC002212.

Preunkert, S., M. Legrand, B. Jourdain, C. Moulin, S. Belviso, N. Kasamatsu, M. Fukuchi, and T. Hirawake (2007), Interannual variability of dimethylsulfide in air and seawater and its atmospheric oxidation by-products (methanesulfonate and sulfate) at dumont d'urville, coastal antarctica (1999-2003), *Journal of Geophysical Research-Atmospheres*, *112*(D6).

Preunkert, S., B. Jourdain, M. Legrand, R. Udisti, S. Becagli, and O. Cerri (2008), Seasonality of sulfur species (dimethyl sulfide, sulfate, and methanesulfonate) in antarctica: Inland versus coastal regions, *Journal of Geophysical Research-Atmospheres*, *113*(D15).

Rawlins, M. A., et al. (2010), Analysis of the arctic system for freshwater cycle intensification: Observations and expectations, *23*, 5715–5737.

Rayner, N. A., D. E. Parker, E. B. Horton, C. K. Folland, L. V. Alexander, D. P. Rowell, E. C. Kent, and A. Kaplan (2003), Global analyses of sea surface temperature, sea ice, and night marine air temperature since the late nineteenth century, *Journal of Geophysical Research-Atmospheres*, *108*(D14).

Read, K. A., et al. (2008), Dms and msa measurements in the antarctic boundary layer: Impact of bro on msa production, *Atmospheric Chemistry and Physics*, *8*(11), 2985–2997.

Reynolds, R. W., N. A. Rayner, T. M. Smith, D. C. Stokes, and W. Q. Wang (2002), An improved in situ and satellite sst analysis for climate, *Journal of Climate*, *15*(13), 1609–1625.

Saigne, C., and M. Legrand (1987), Measurements of methanesulfonic-acid in antarctic ice, *Nature*, *330*(6145), 240–242.

Saltzman, E. S., I. Dioumaeva, and B. D. Finley (2006), Glacial/interglacial variations in methanesulfonate (msa) in the siple dome ice core, west antarctica, *Geophysical Research Letters*, *33*(11).

Savoie, D. I., J. M. Prospero, R. J. Larsen, F. Huang, M. A. Izaguirre, T. Huang, T. H. Snowdon, L. Custals, and C. G. Sanderson (1993), Nitrogen and sulfur species in antarctic aerosols at mawson, palmer station, and marsh (king george island), *Journal of Atmospheric Chemistry*, *17*(2), 95–122.

Schmidt, G. A., et al. (2006), Present-day atmospheric simulations using giss modele: Comparison to in situ, satellite, and reanalysis data, *Journal of Climate*, *19*(2), 153–192.

Sciare, J., N. Mihalopoulos, and F. J. Dentener (2000), Interannual variability of atmospheric dimethylsulfide in the southern indian ocean, *Journal of Geophysical Research-Atmospheres*, *105*(D21), 26,369–26,377.

Semiletov, I., A. Makshtas, S. I. Akasofu, and E. L. Andreas (2004), Atmospheric co2 balance: The role of arctic sea ice, *Geophysical Research Letters*, *31*(5), 4.

Silvente, E., and M. Legrand (1993), Ammonium to sulfate ratio in aerosol and snow of greenland and antarctic regions, *Geophysical Research Letters*, *20*(8), 687–690.

Simo, R., and J. Dachs (2002), Global ocean emission of dimethylsulfide predicted from biogeophysical data, *Global Biogeochemical Cycles*, *16*(4).

Simpson, W. R., D. Carlson, G. Honninger, T. A. Douglas, M. Sturm, D. Perovich, and U. Platt (2007), First-year sea-ice contact predicts bromine monoxide (bro) levels at barrow, alaska better than potential frost flower contact, *Atmospheric Chemistry and Physics*, *7*, 621–627.

Smith, T. G., and C. Lydersen (1991), Availability of suitable landfast ice and predation as factors limiting ringed seal populations, *Phoca hispida*, in Svalbard, *Polar Research*, *10*, 585–594.

Smith, T. G., and I. Stirling (1975), The breeding habitat of the ringed seal *(Phoca hispida)*. The birth lair and associated structures, *Canadian Journal of Zoology*, *53*, 1297–1305.

Spracklen, D. V., K. J. Pringle, K. S. Carslaw, M. P. Chipperfield, and G. W. Mann (2005), A global off-line model of size-resolved aerosol microphysics: I. model development and prediction of aerosol properties, *Atmospheric Chemistry and Physics*, *5*, 2227–2252.

Stefels, J., G. Carnat, J. W. H. Dacey, T. Goossens, J. T. M. Elzenga, and J.-L. Tison (2012), The analysis of dimethylsulfide and dimethylsulfoniopropionate in sea ice: Dry-crushing and melting using stable isotope additions, *Marine Chemistry*, *128*, 34–43.

Stirling, I., and T. G. Smith (2004), Implications of warm temperatures, and an unusual rain event for the survival of ringed seals on the coast of southeastern Baffin Island, *Arctic*, *57*, 59–67.

Sun, J. Y., J. W. Ren, and D. H. Qin (2002), 600 years record of biogenic sulfur from lambert glacier basin firn core, east antarctica, *Annals of Glaciology, Vol 35*, *35*, 362–367.

Taylor, K. E., R. J. Stouffer, and G. A. Meehl (2012a), An overview of cmip5 and the experiment design, *Bulletin of the American Meteorological Society*, *93*(4), 485–498.

Taylor, K. E., R. J. Stouffer, and G. A. Meehl (2012b), An overview of cmip5 and the experiment design, *Bull. Amer. Meteor. Soc.*, *93*(4), 485–498, doi:doi: 10.1175/BAMS-D-11-00094.1.

Theys, N., et al. (2011), Global observations of tropospheric BrO columns using GOME-2 satellite data, *Atmospheric Chemistry and Physics*, *11*(4), 1791–1811.

Tortell, P. D., and M. C. Long (2009), Spatial and temporal variability of biogenic gases during the southern ocean spring bloom, *Geophysical Research Letters*, *36*.

Trevena, A. J., and G. B. Jones (2006), Dimethylsulphide and dimethylsulphoniopropionate in antarctic sea ice and their release during sea ice melting, *Marine Chemistry*, *98*(2-4), 210–222.

Udisti, R., et al. (2004), Sensitivity of chemical species to climatic changes in the last 45 kyr as revealed by high-resolution dome c (east antarctica) ice-core analysis, *Annals of Glaciology, Vol 39, 2005*, *39*, 457–466.

von Glasow, R., and P. J. Crutzen (2004), Model study of multiphase dms oxidation with a focus on halogens, *Atmospheric Chemistry and Physics*, *4*, 589–608.

Wagner, T., O. Ibrahim, R. Sinreich, U. Friess, R. von Glasow, and U. Platt (2007), Enhanced tropospheric bro over antarctic sea ice in mid winter observed by max-doas on board the research vessel polarstern, *Atmospheric Chemistry and Physics*, *7*(12), 3129–3142.

Wagnon, P., R. J. Delmas, and M. Legrand (1999), Loss of volatile acid species from upper firn layers at vostok, antarctica, *Journal of Geophysical Research-Atmospheres*, *104*(D3), 3423–3431.

Wang, Y. H., D. J. Jacob, and J. A. Logan (1998), Global simulation of tropospheric o-3-nox-hydrocarbon chemistry 1. model formulation, *Journal of Geophysical Research-Atmospheres*, *103*(D9), 10,713–10,725.

Wanninkhof, R. (1992), Relationship between wind-speed and gas-exchange over the ocean, *Journal of Geophysical Research-Oceans*, *97*(C5), 7373–7382.

Warren, S. G., I. G. Rigor, N. Untersteiner, V. F. Radionov, N. N. Bryazgin, Y. I. Aleksandrov, and R. Colony (1999), Snow depth on Arctic sea ice, *12*, 1814–1829.

Webb, R. S., D. H. Rind, S. J. Lehman, R. J. Healy, and D. Sigman (1997), Influence of ocean heat transport on the climate of the last glacial maximum, *Nature*, *385*(6618), 695–699.

Welch, K. A., P. A. Mayewski, and S. I. Whitlow (1993), Methanesulfonic-acid in coastal antarctic snow related to sea-ice extent, *Geophysical Research Letters*, *20*(6), 443–446.

Weller, R., F. Traufetter, H. Fischer, H. Oerter, C. Piel, and H. Miller (2004), Postdepositional losses of methane sulfonate, nitrate, and chloride at the european project for ice coring in antarctica deep-drilling site in dronning maud land, antarctica, *Journal of Geophysical Research-Atmospheres*, *109*(D7).

Weller, R., D. Wagenbach, M. Legrand, C. Elsaesser, X. Tian-Kunze, and G. Koenig-Langlo (2011), Continuous 25-yr aerosol records at coastal antarctica - i: inter-annual variability of ionic compounds and links to climate indices, *Tellus Series B-Chemical and Physical Meteorology*, *63*(5), 901–919.

Wesely, M. L. (1989), Parameterization of surface resistances to gaseous dry deposition in regional-scale numerical-models, *Atmospheric Environment*, *23*(6), 1293–1304.

Wolff, E. W. (2006), The challenge from ice cores: Understanding the climate and atmospheric composition of the late quaternary, *Journal De Physique Iv*, *139*, 185–196.

Wolff, E. W., A. M. Rankin, and R. Rothlisberger (2003), An ice core indicator of antarctic sea ice production?, *Geophysical Research Letters*, *30*(22).

Wolff, E. W., et al. (2006), Southern ocean sea-ice extent, productivity and iron flux over the past eight glacial cycles (vol 440, pg 491, 2006), *Nature*, *449*(7163), 748–748.

Wolff, E. W., et al. (2010), Changes in environment over the last 800,000 years from chemical analysis of the epica dome c ice core, *Quaternary Science Reviews*, *29*(1-2), 285–295.

Yang, X., R. A. Cox, N. J. Warwick, J. A. Pyle, G. D. Carver, F. M. O'Connor, and N. H. Savage (2005), Tropospheric bromine chemistry and its impacts on ozone: A model study, *Journal of Geophysical Research-Atmospheres*, *110*(D23).

Yuan, X. J., J. Patoux, and C. H. Li (2009), Satellite-based midlatitude cyclone statistics over the southern ocean: 2. tracks and surface fluxes, *Journal of Geophysical Research-Atmospheres*, *114*.

Zemmelink, H. J., L. Houghton, J. W. H. Dacey, A. P. Worby, and P. S. Liss (2005), Emission of dimethylsulfide from weddell sea leads, *Geophysical Research Letters*, *32*(23).

Zemmelink, H. J., J. W. H. Dacey, L. Houghton, E. J. Hintsa, and P. S. Liss (2008), Dimethylsulfide emissions over the multi-year ice of the western weddell sea, *Geophysical Research Letters*, *35*(6).

Zhang, X., and J. Walsh (2006), Toward a seasonally ice-covered Arctic Ocean: Scenarios from the IPCC AR4 model simulations, *19*, 1730–1747.

Zwally, H. J., J. C. Comiso, C. L. Parkinson, D. J. Cavalieri, and P. Gloersen (2002), Variability of antarctic sea ice 1979-1998, *Journal of Geophysical Research-Oceans*, *107*(C5).

VITA

Paul J. Hezel is originally from upstate New York. He obtained his B.S. in Physics from Boston College in 1994 and taught for nearly three years as a Jesuit International Volunteer in Pohnpei, Micronesia, and Kathmandu, Nepal. Prior to joining the Department of Atmospheric Sciences at the University of Washington, he digitized Arctic submarine sonar data at the Polar Science Center at U.W. and was Laboratory Manager and instructor in the Physics Department at Seattle University. He obtained his Ph.D. in Atmospheric Sciences from the University of Washington in 2012.